DALHOUSIE UNIVERSITY

CHEMOSTRATIGRAPHY OF THE UPPER SILURIAN ARISAIG GROUP, NOVA SCOTIA.

Samantha Marie Hamilton

SUBMITTED IN PARTIAL FULFILLMENT OF THE REQUIREMENTS FOR
THE DEGREE OF BACHELOR OF SCIENCE, HONOURS
DEPARTMENT OF EARTH SCIENCES
DALHOUSIE UNIVERSITY, HALIFAX, NOVA SCOTIA

April 2017

Distribution License

DalSpace requires agreement to this non-exclusive distribution license before your item can appear on DalSpace.

NON-EXCLUSIVE DISTRIBUTION LICENSE

You (the author(s) or copyright owner) grant to Dalhousie University the non-exclusive right to reproduce and distribute your submission worldwide in any medium.

You agree that Dalhousie University may, without changing the content, reformat the submission for the purpose of preservation.

You also agree that Dalhousie University may keep more than one copy of this submission for purposes of security, back-up and preservation.

You agree that the submission is your original work, and that you have the right to grant the rights contained in this license. You also agree that your submission does not, to the best of your knowledge, infringe upon anyone's copyright.

If the submission contains material for which you do not hold copyright, you agree that you have obtained the unrestricted permission of the copyright owner to grant Dalhousie University the rights required by this license, and that such third-party owned material is clearly identified and acknowledged within the text or content of the submission.

If the submission is based upon work that has been sponsored or supported by an agency or organization other than Dalhousie University, you assert that you have fulfilled any right of review or other obligations required by such contract or agreement.

Dalhousie University will clearly identify your name(s) as the author(s) or owner(s) of the submission, and will not make any alteration to the content of the files that you have submitted.

If you have questions regarding this license please contact the repository manager at dalspace@dal.ca.

Grant the distribution license by signing and dating below.

_____ _____

Name of signatory Date

DALHOUSIE UNIVERSITY

Department of Earth Sciences
Halifax, Nova Scotia
Canada B3H 4R2
(902) 494-2358

DATE: 28 April 2017

AUTHOR: Samantha Marie Hamilton

TITLE: Chemostratigraphy of the Upper Silurian Arisaig Group, Nova Scotia.

Degree: B. Sc. Honours Earth Sciences Convocation: May Year: 2017

Abstract

Silurian Carbon Isotope Excursions (SCIE) are characterized by extreme spikes in the positive stable isotope of carbon-13. These events are marked across the globe and are unvarying in their instance of appearance, making them an easily traceable event in the rock record. Although they are well documented, it remains unknown as to why there would be climactic variation to the degree that we observe with SCIE. Because of the relatively unaltered fossiliferous carbonate rocks found in the Arisaig Group, Nova Scotia, as well as their dating to known SCIE at the Wenlock/ Ludlow boundary as well as the Silurian/ Devonian boundary, this may provide an ideal study location for SCIE to add to the database of geographic locations in which they are observed. These rocks are also suitable for environmental analysis to provide an approximation of the conditions that might have given rise to SCIE. In this study, samples were taken across a section of the Upper Silurian of the Arisaig Group spanning from the Ludfordian Green member of the Moydart Formation to the Pridolian Stonehouse Formation. Electron Microprobe analysis was conducted to establish a complete chemical stratigraphy of the study location. A model was proposed to simulate paleoenvironmental conditions throughout the section, focusing on paleothermometry. Additionally, microtextural and Mn, Mg, Sr and Fe elemental concentrations were used to determine the degree of diagenetic effects in the section. Major environmental differences were observed across the section in locations we would expect to observe SCIE and that are consistent with global ∂O^{18} data . These rocks also display minimal amounts of diagenesis, and are therefore well suited for future stable isotope work.

Keywords: Silurian Arisaig Group, Calcite, Coquinite, Electron Microprobe, Chemostratigraphy

Table of Contents

List of Figures

List of Tables

Acknowledgements

I would like to express my sincerest thanks to Dr. Richard Cox for providing me with outstanding instruction in geochemistry and guidance throughout my research project. I would also like to thank Dr. Djordje Grujic for his encouragement and teaching. My greatest thanks also go to Dan MacDonald for his unceasing helpfulness and extensive knowledge in Electron Microprobe analysis. A big thank you to Dr. James Brenan, Sergei Ratchinski, Dr. Yana Fedortchouk and Roman Kislitsyn for allowing me to use their equipment and facilities. Finally, a big thank you to the ERTH 3000 field school team, Isabelle Coutand and Thomas Duffet, as well as the wonderful people at Camp Geddie who allowed me to share accommodations while conducting my field work.

Chapter 1: Introduction

1.1 Scope of this Study

Silurian Carbon Isotope Excursions (SCIE) are characterized by extreme spikes in the positive stable isotope of carbon-13. These events are marked across the globe and are unvarying in their instance of appearance, making them an easily traceable event in the rock record. Although they are well documented, it remains unknown as to why there would be climactic variation to the degree that we observe with SCIE. Clearly, some major global environmental event is occurring during the Silurian to produce these isotopic excursions which in some cases, are accompanied by mass extinction events (Cramer and Saltzman 2005). Therefore, it is imperative that we understand these excursions to properly evaluate and understand the environmental conditions during the Silurian and how they affected the conditions for life on Earth.

Previous studies done on SCIE have been done in Baltica and Laurentia (Fig 1.1). However, this work has yet to be done in Avalonia. Fortunately, the fossiliferous limestones of Nova Scotia's Arisaig Group may yield an ideal Avalonian study location for Silurian Carbon Isotope Excursions. The Arisaig Group is comprised of easily accessible and well preserved strata spanning the entire Silurian Period and into the lower Devonian. The abundance of fossil material including brachiopods, bivalves and crinoids offers an excellent selection of carbonate material that can be used for environmental and stable isotope analysis. This could lead to a much better understanding of SCIE overall. However, isotopic analyses and elemental ratios are sensitive to diagenetic affects and alteration. Nearby intrusions and local orogeny may have caused some or all the Arisaig Group limestones to have been diagenetically altered. In this study, we address this possibility by analyzing samples from the Arisaig Group for evidence of diagenesis. Additionally, elemental ratios were used to estimate environmental conditions at the time of deposition. These data provide information that is crucial to establishing the Arisaig Group as a valid study site for Silurian Carbon Isotope Excursions.

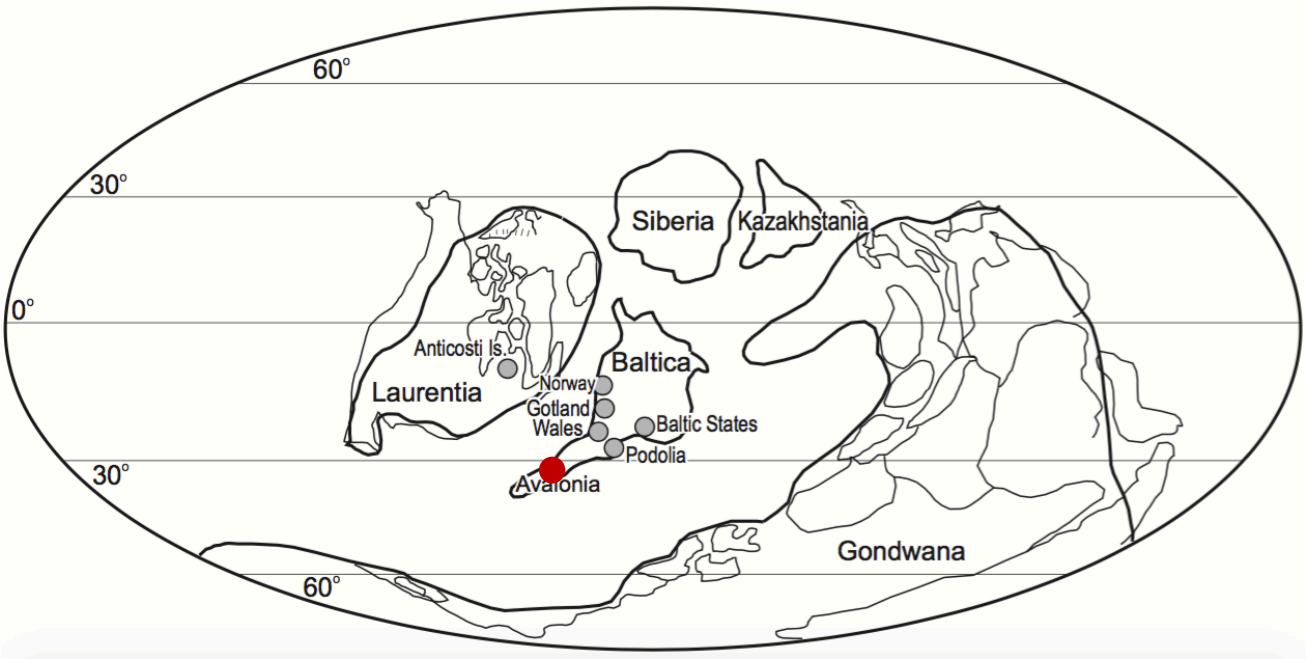

Fig. 1.1. Paleogeographic map of the Earth during the early Silurian, Llandovery Epoch. Approximate locations of previous SCIE studies are marked by grey circles. A red dot shows the approximate location of the Arisaig Group rocks. Position of paleocontinents from Cocks and Scotese, 1991. Figure from Azmy et al. 1998.

Chapter 2: Geological Background

2.1 The Arisaig Group

Located along the Northumberland Strait of Northern Nova Scotia (Fig. 2.1) the Arisaig Group is an extensive succession of shallow marine carbonates that are rich in fossil material. The Group was deposited during the Appalachian accretionary events (Murphy et al. 2004) and consists of a continuous span from the lowermost Silurian Beechhill Cove Formation to the Early Devonian Knoydart Formation (Fig. 2.2). However, this study focuses on strata ranging from the mid-Llandoverian Middle Ross Brook Formation to the Upper Silurian Stonehouse Formation. The strata of the Arisaig Group is comprised typically of finely laminated siltstone, highly bioturbated mudstone, very-fine grained sandstone and fossiliferous coquina limestone beds (Lane and Jensen 1975). The relatively unaltered nature of these rocks has made them the target of many paleontological studies in the past. However, these limestones have been considerably faulted and folded during the Middle Devonian Acadian orogeny as well as during the late Paleozoic (Boucot et al. 1974), raising the possibility of recrystallization.

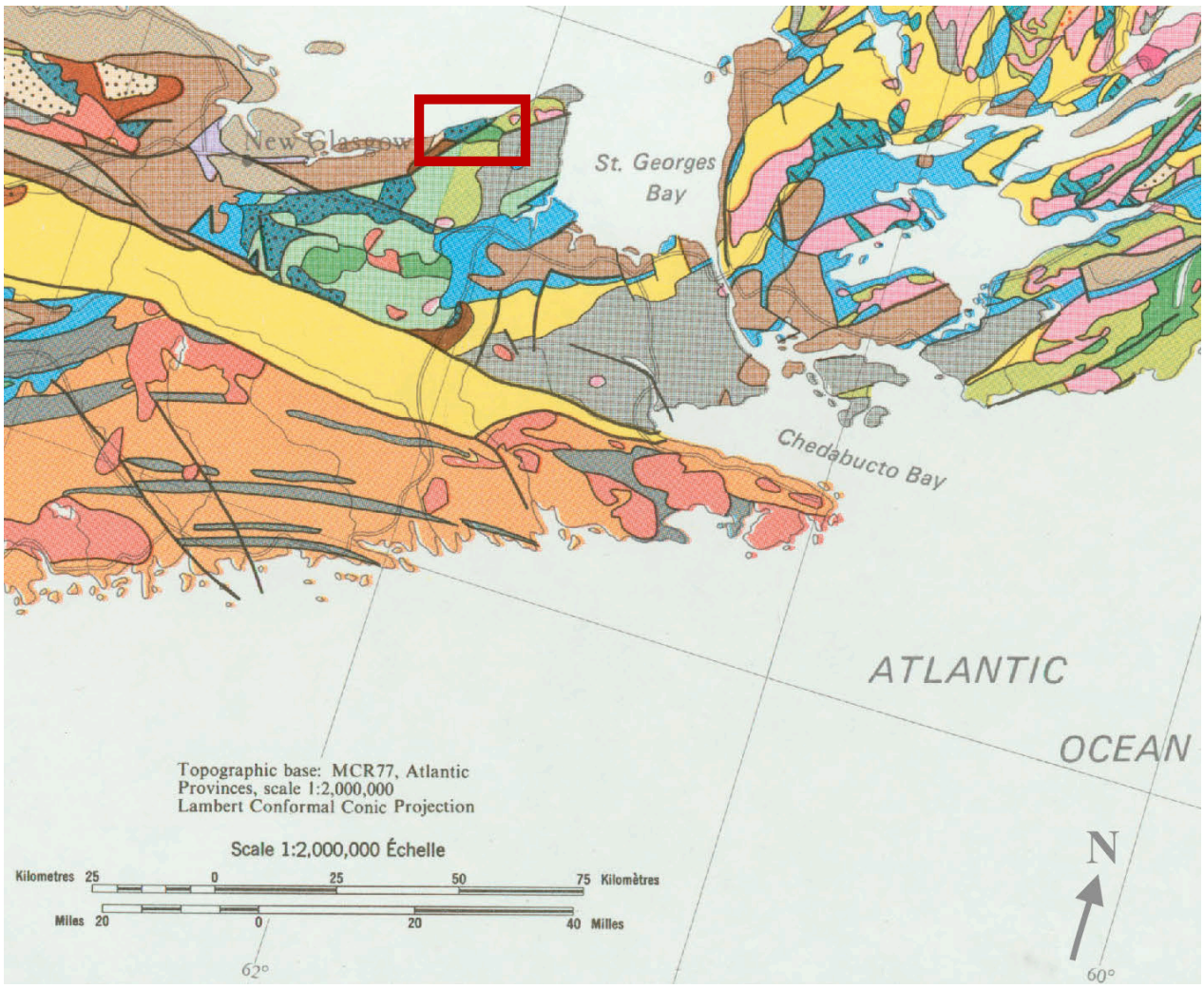

Fig. 2.1. A. Geological map of NorthWestern Nova Scotia, Canada, A red box encases the location of the Arisaig Group rocks. Map from Keppie (1979).

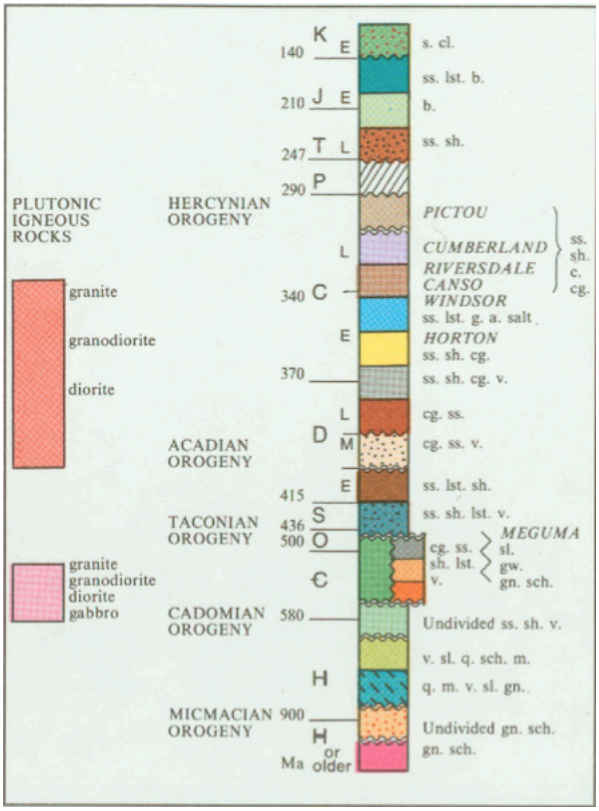

Fig. 2.1.B. Legend to the Map of NorthWestern Nova Scotia, Canada (Fig. 2.1.A). From Keppie (1979).

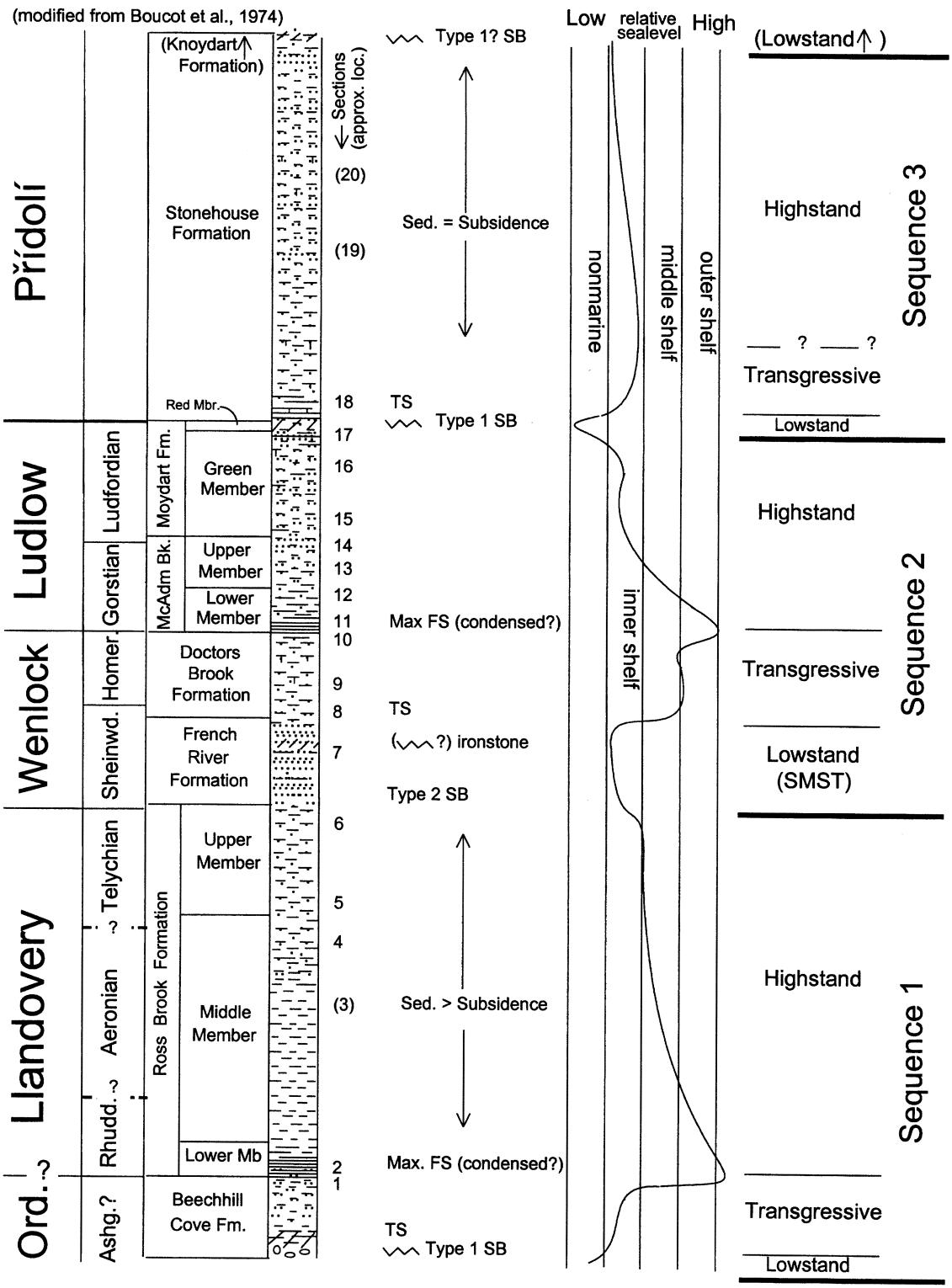

Fig. 2.2. Stratigraphic column to scale of the Arisaig Group. Slash marks indicate redbeds, FS indicates a flooding surface, TS for transgressive surface and SB denotes a sequence boundary. From Beck and Strother (2001), modified from Boucot et al. (1974).

2.1.1 Ross Brook Formation

The Ross Brook Formation lies above the Beechhill Cove Formation and is Mid to Upper Llandoverian in age (Boucot et al. 1974). The Formation was divided by Boucot et al (1974) into lower, middle and upper members. The lower member is composed of 25m of fissile black shale with micro laminations and contains graptolites and some brachiopod fossils. The middle member is approximately 180m thick and is a zone of transition from the lower to the upper member. The top section of the middle member is characterized by green-grey mudstone and thin beds of siltstone. The mudstone tends to be massive and contains many casts of burrows, indicating a high degree of life and periods of calm waters. The upper member is composed predominantly of siltstones ranging in size from small laminations and lenses to 1m thick, massive beds. The siltstone deposits are the result of seasonal storms, as indicated by ripples and cross laminations at the top of beds. These periods of high energy likely caused organisms living on the bottom of the shallow waters to die and accumulate in coquina lenses within scour depressions. These coquina beds are limestone, being mainly composed of shell fragments within a calcite matrix (Lane and Jensen 1975). The Formation can be interpreted as three facies. These are mottled silty mudstone facies on which organisms lived, laminated shale facies that were anoxic and harboured little to no life and laminated siltstone facies induced by storm activity (Hurst and Pierill 1986). In general, this represents a shallowing upwards (Boucot et al. 1974).

2.1.2 French River Formation

The French River formation lies conformably over the Ross Brook Formation and is Lower Wenlockian in age. Approximately 85% of the beds are a green siltstone that contain graded beds, ripple cross lamination and burrowing traces. There is evidently much more siltstone present within the French River Formation than in the Ross Brook Formation or the underlying Doctor's Brook Formation. The other 15% of the Formation is composed of fissile, thinly laminated shales that display some microlaminations and burrows. Lenses of highly fossiliferous limestone are also present along with an oolitic ironstone bed (Boucot et al. 1974, Waldron et al. 1996).

2.1.3 Doctor's Brook Formation

The Doctor's Brook Formation dates to the Upper Wenlock. Approximately half of its volume is composed of laminated shale beds that contain phosphatic nodules. It also contains calcareous siltstones and arenaceous limestones that contain laminations, cross-laminations, some grading and channel fill. Lenses and channel deposits of coquinite limestone occur as calcite-filled molds of shells within a silty matrix. These beds contain predominantly brachiopod and crinoid fragments (Boucot et al. 1974, Waldron et al. 1996).

2.1.4 McAdam Brook Formation

The McAdam Brook Formation dates to the Early Ludlovian and is comprised of a lower and an upper member. The bottom of the lower member contains very fissile silty shale with some interbedding of quartz-rich shale beds up to 2 inches in thickness. The upper part of the lower member contains dark grey shale interbedded with thin beds of laminated and cross laminated siltstone as well as thin beds of massive or occasionally microlaminated arenaceous limestone beds that contain septarian nodules. The lower member also contains calcareous nodules and lenses of shelly coquinite in depressions and scours. The upper member of the McAdam Brook Formation contains layers of much thicker siltstone and shales. These siltstones become increasingly thicker and lighter in colour towards the top of the section (Boucot et al. 1974, Waldron et al. 1996).

2.1.5 Moydart Formation

The Moydart Formation is Upper Ludlovian in age (Boucot et al. 1974). It is divided into a lower green member and an upper red member. The lower green member begins with approximately 9m dominated by siltstone that contains interference ripple marks and parallel as well as cross lamination. This area also contains coquina limestone beds as well as beds of mudstone that display characteristics of a shallow, low energy environment. The presence of organisms buried in their life positions indicates occasional strong currents bringing rapid burial.

Above this are mainly massive mudstone beds with several thin layers of siltstone. The mudstones represent life surfaces and ichnofossils such as burrows and trails are common. The uppermost green member is comprised of laminated siltstones and coquina limestone beds. Structures such as megaripples and cross laminations along with the lack of trace fossils indicate a higher current with a greater influx of sediment (Lane and Jensen 1975).

The upper red member of the Moydart Formation contains some green siltstones in the lowermost section but grades upwards into red terrestrial mudstones. This member also holds pedogenic carbonate. Overall, the Moydart Formation represents progressive shallowing and transitioning into a terrestrial environment (Fig. 2.3), marked by fossils of fresh water organisms in the uppermost section. Indeed, the Moydart and the overlying Stonehouse Formation both display some subaerial characteristics (Lane and Jensen 1975, Boucot et al. 1974).

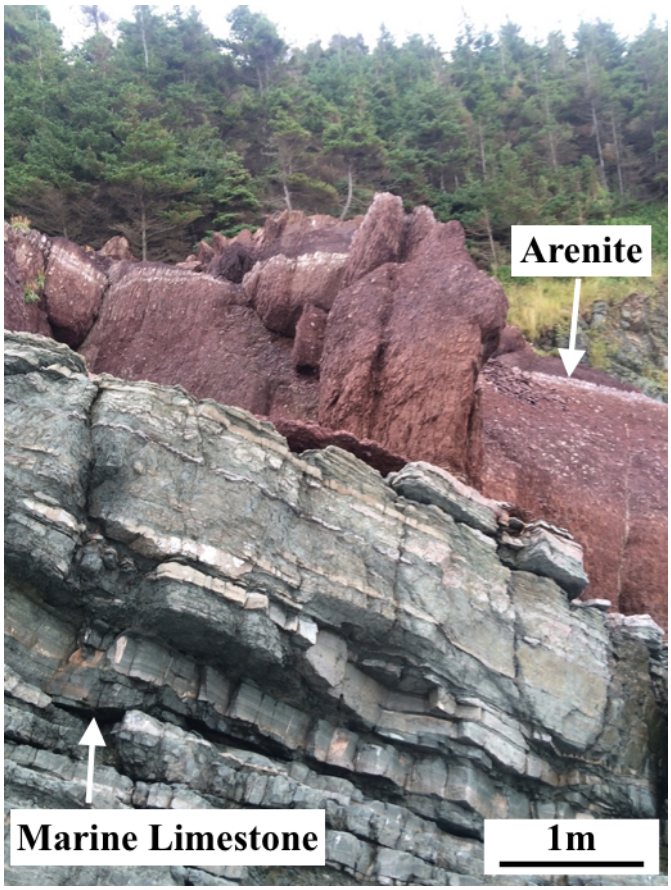

Fig. 2.3. Photograph showing a terrestrial arenite conformably overlying marine limestones in the Uppermost Moydart Formation. Photographed August 2016, Arisaig, Nova Scotia.

2.1.6 Stonehouse Formation

The Stonehouse Formation (Fig. 2.4) is Pridolian in age and lies conformably over the Moydart Formation and has a similar configuration (Boucot et al. 1974). Like the Moydart Formation, it has a high concentration of calcareous materials such as coquinite beds and the upper sequence is terrestrial with a brackish water setting. The Stonehouse Formation is divided into two members. The lower member is dominantly composed of mudstone and contains some thin beds of siltstone. Coquina beds are common throughout the section. The presence of interference ripples and the lack of benthic fauna indicates a nearshore environment with low salinity. The upper member of the Stonehouse Formation contains siltstone beds that are continuous, retaining their shape and thickness, as well as some that taper off in lenses. It also contains beds of mudstone that are highly bioturbated in the top portions of bedding. Here, coquinite is also common especially in scour depressions. These scour depressions as well as megaripples, interference ripples and convolute lamination indicate an abundance of erosion and deposition in a high energy environment (Lane and Jensen 1975).

Fig. 2.4. Photograph of the Upper Stonehouse Formation from the Arisaig Group, Arisaig, Nova Scotia. Photographed August 2016.

2.2 Silurian Paleoclimate Proxies

2.2.1 Elemental Ratios and Stable Isotopes

It is well understood that certain elemental ratios and isotopes within rock strata can provide reliable approximations of paleo-climate (Urey et al. 1951, Epstein et al. 1953, Elderfield et al. 1996, lear et al. 2000, Hoogakketet al. 2009). Perhaps the most useful and the most utilized of these is the ability to calculate paleo-temperature. Marine limestones and shell material can record ocean temperature from the time of deposition or precipitation respectively. The ratio in sea water of the heavier oxygen-18 isotope to the lighter oxygen-16 isotope is highly temperature dependent. This is because during times of increased temperature, the lighter oxygen-16 isotope is preferentially evaporated out of water and enters the atmosphere. The now heavier water then becomes recorded in calcium carbonate deposits. Additionally, the lighter oxygen-16 isotope is favored by shell-constructing organisms. Consequently, this allows the material to be used as a thermometer of paleo-temperature (Urey at al. 1951, Epstein et al. 1953).

Mg/Ca ratios have also been shown to be a useful determinant for paleo-temperature and even depth-specific temperature. This is especially the case when applied to benthic foraminifera (Lear et al. 2000, Hoogakker et al. 2009). Until recently, it was also widely believed that Mg/Ca provided an approximation for ocean salinity (Rosenthal et al. 1997). However, it has recently been shown that multiple factors may contribute to an increase in the magnesium proportion (Hoogakker et al. 2009). Past water depth can also be approximated using the Sr/Ca ratio in foraminifera as it tends to decrease with increasing water depth (Elderfield et al. 1996). Sr/Ca is also a popular tool for use in paleo temperature studies. The partition coefficient of strontium has been shown to decrease with increasing temperature and is regulated by biological or kinetic influences (Gabitov and Watson 2006).

Additionally, Barium is considered a good paleoclimate proxy for several reasons. Studies have shown that Barium has a close association with organic productivity in the deep oceans. Therefore, the burial rate of Ba can be used to predict paleo-productivity of the ocean, which is typically measured as a ratio with Calcium (Dymond et al. 1992). Additionally, there is much interest in applying the Ba/Ca ratio in determination of paleoalkalinity. This is due to a strong correlation between Ba concentration and alkalinity that is observed in modern sea water.

(McMannus et al. 1999).

The above ratios are, in fact, so accurate that it is possible to produce monthly readings of ocean temperature using U/Ca, Ba/Ca and Sr/Ca ratios from the calcium carbonate growth of corals (Hilldebrand 1998). What's more, C, O and Sr isotope changes in sea water that is recorded in carbonates can record events such as glaciation, volcanic activity and plate tectonics (Bruckshen et al. 1995). These global processes will be considered in subsequent sections of this text. It follows that, using these techniques, researchers are easily able to produce extremely well-defined models of changing ocean environments and climate solely based on chemo-stratigraphic analysis.

2.2.2 Diagenetic effects on carbonates

Although analytical tools utilizing the above elemental ratios and isotopes are extremely useful and convenient, carbonate rocks are susceptible to diagenetic effects through the exchange of elements with pore fluids (Richter and DePaolo 1987,). The effects of diagenesis on isotopic and trace element data understandably increase with increasing diagenetic alteration. Transition metals move into calcium carbonates during diagenesis. Simultaneously, the lighter oxygen-16 isotope is preferentially assimilated by pore fluids, skewing any oxygen isotope data post-diagenesis. The effects of diagenesis on isotopic and trace element data understandably increase with increasing diagenetic alteration. The result of this is that only unaltered rocks, or those with very minor diagenetic effects are suitable for this kind of testing (Bruckschen et al. 1995). We can recognize diagenesis in samples by first looking at the concentrations of Fe, Mn and Sr. Fe and Mn concentrations increase after diagenesis has occurred. Unaltered Fe and Mn in calcitic fossil shells typically have concentrations of 20- 800ppm and 5- 500ppm respectively. Alternatively, Sr becomes depleted during diagenesis and unaltered Sr concentrations should be 800- 2000ppm (Bruckschen et al. 1995, Morrison and Brand 1986). These are important to recognize in rocks that are to be analyzed for oxygen isotopes since, as previously mentioned, these isotopes are prone to changing during diagenesis. Conversely, diagenesis has no effect on the stable carbon isotope value.

2.3 Silurian Carbon Isotope Excursions

Silurian Carbon Isotope Excursions (SCIE) are recognized global events marked by extreme spikes in the stable carbon-13 isotope that endure for periods of millions of years (Cramer and Saltzman, 2005). These have not only been observed throughout the Silurian but have also been remarked in the late Ordovician Hirnantian and at the Silurian/ Devonian boundary. There are four excursions within the Silurian. These occur during the eary Sheinwoodian (Ireviken), the late Homerian, the late Gorstian and the late Ludfordian (Fig. 2.5) (Munnecke et al 2003). These excusions have been observed and studied across the Earth (Azmy et al. 1998, Bickert et al 1997, Saltzman 2002, Cramer and Saltzman 2005), reflecting events relating to the carbon cycle that have global significance. One model suggests that these spikes in carbon are due to rapid organic carbon burial related to epi-continental black shale deposition in epeiric seas, assisted by conditions created during glaciation leading to increased primary productivity (Bickert et al. 1997, Cramer and Saltzman 2007). Athough this model may apply to very few single peak carbon events, it is not acceptable overall since the majority of SCIE for which this explanation has been used, displays carbon excursions much later than the black shale deposition events (Cramer and Saltzman 2007). Additionally, many carbon excursion events have been documented to coincide with massive carbonate deposition and production during times of major reef development (Amzy et al. 1998, Calner et al. 2006, Bickert et al. 1997). It is also noted that the oxygen-18 isotope curve shows extremely similar trends to the carbon-13 curve in the Silurian (Fig. 2.6) (Amzy et al. 1998). Regardless of extensive work done on brachiopods and foraminifera to investigate why the oxygen follows such a trend, the interpretations have been highly contradictive. As it stands, there is no satisfying explanation, though it is generally accepted that a portion of the isotopic signature is due to the increased carbonate production and the remainder due to a combination of environmental factors such as temperature, salinity and glacial extent (Cramer and Saltzman 2007). What we can infer, however, is that these excursions are the result of a global process during the Silurian. Sill, no conclusive model has been given to explain their occurrence. Furthermore, there is still much debate as to what initiated each individual SCIE event. Clearly, SCIE represents an area of paleo-climatology that although many researchers have contributed to its understanding, remains somewhat of a mystery.

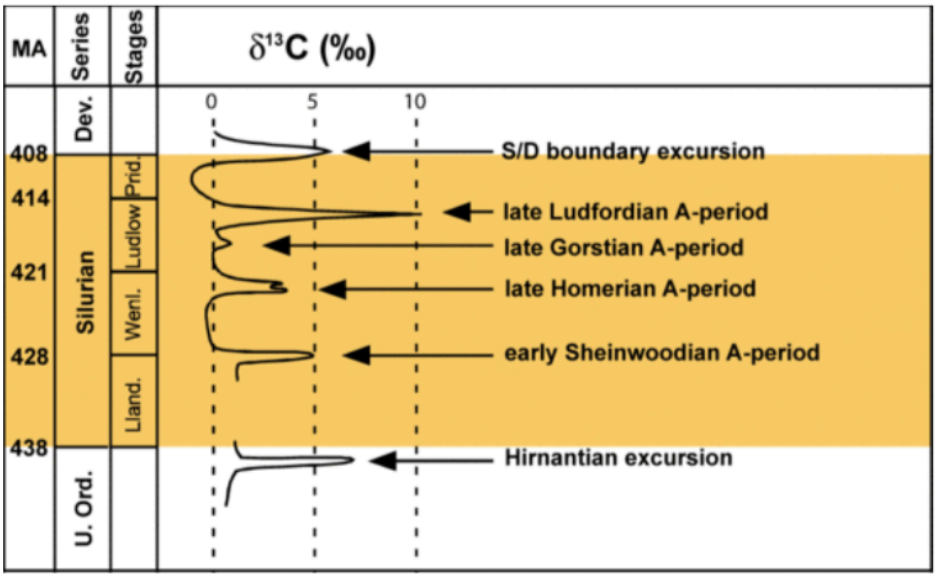

Fig. 2.5. The occurrence of Silurian Carbon Isotope Excursion events. From Munnecke et al. (2003).

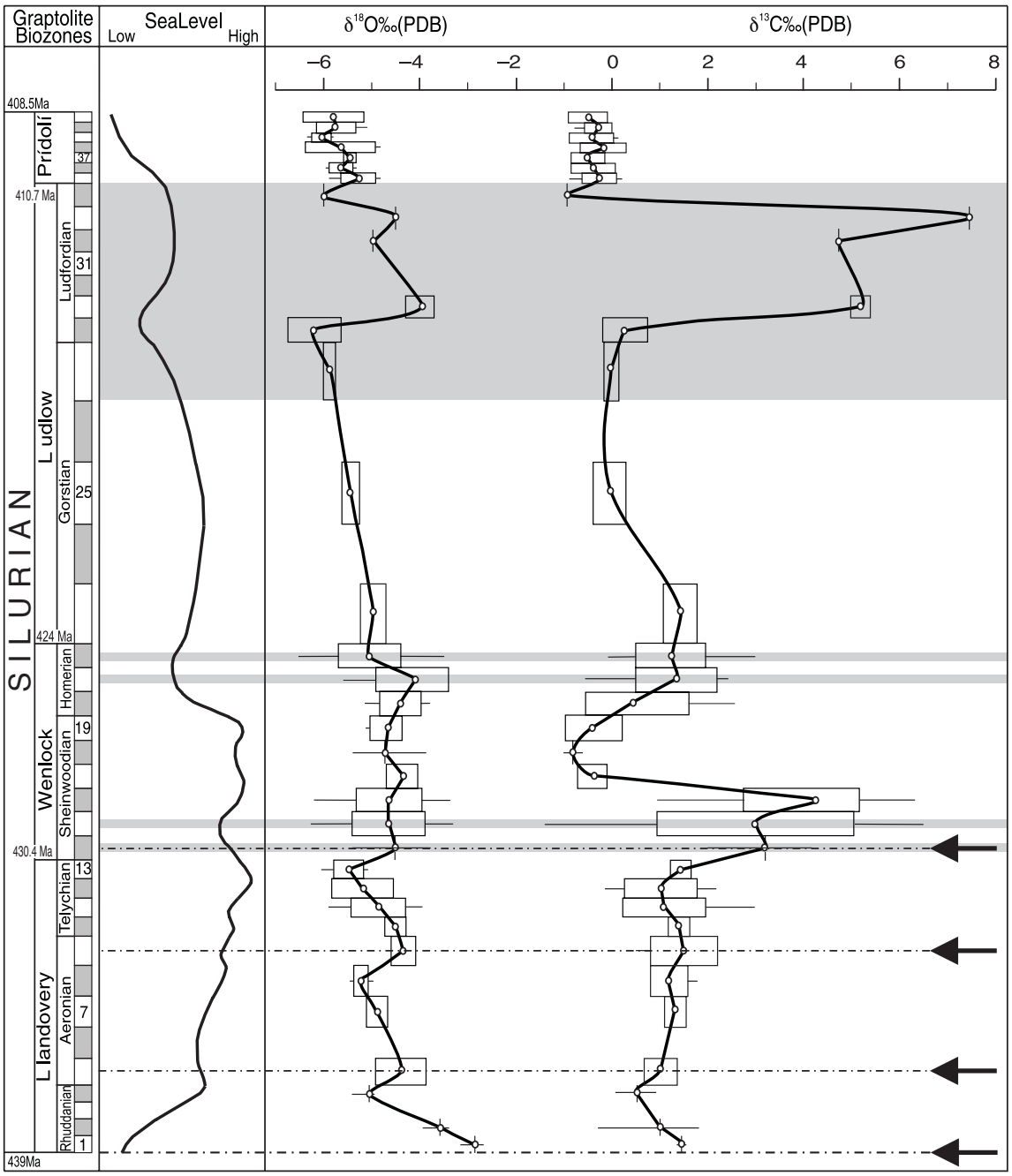

Fig. 2.6. Silurian carbon-13 and oxygen-18 isotope curves for brachiopods. Sea level data from Johnson et al (1991). Black arrows point to glacial episodes (Grahn and Caputo 1992). Figure from Azmy et al. (1998).

Chapter 3: Methods

3.1 Sample Collection

Forty samples were collected along the Arisaig shore (Fig. 3.1) in a section spanning from the Upper Ross Brook Formation to the Stonehouse Formation. In total, twenty-seven samples were collected from the Stonehouse Formation, one sample from the red member of the Moydart Formation, seven from the green member of the Moydart Formation, one from the lower McAdam Brook Formation, two from the Doctor's Brook Formation, one from the French River Formation and one from the upper member of the Ross Brook Formation. Since the bedding was dipping at 53 degrees, the stratigraphic orientation was measured and the vertical distance was calculated with respect to horizontal distance (Fig 3.2). This allowed for precise recognition of where the samples were taken within the stratigraphy. These samples were collected from coquinite beds (Fig. 3.3) that contained a significant amount of fossiliferous material. A geologic map (Fig. 3.1) from Boucot et al. (1974) and modified by Beck and Strother (2001), along with field observations, was followed along the shoreline to recognize stratigraphic location of the samples collected. This same map is shown in Figure 3.1 but has been modified to show our sample locations. Identification of sample numbers from the locations can be found in table 3.1.

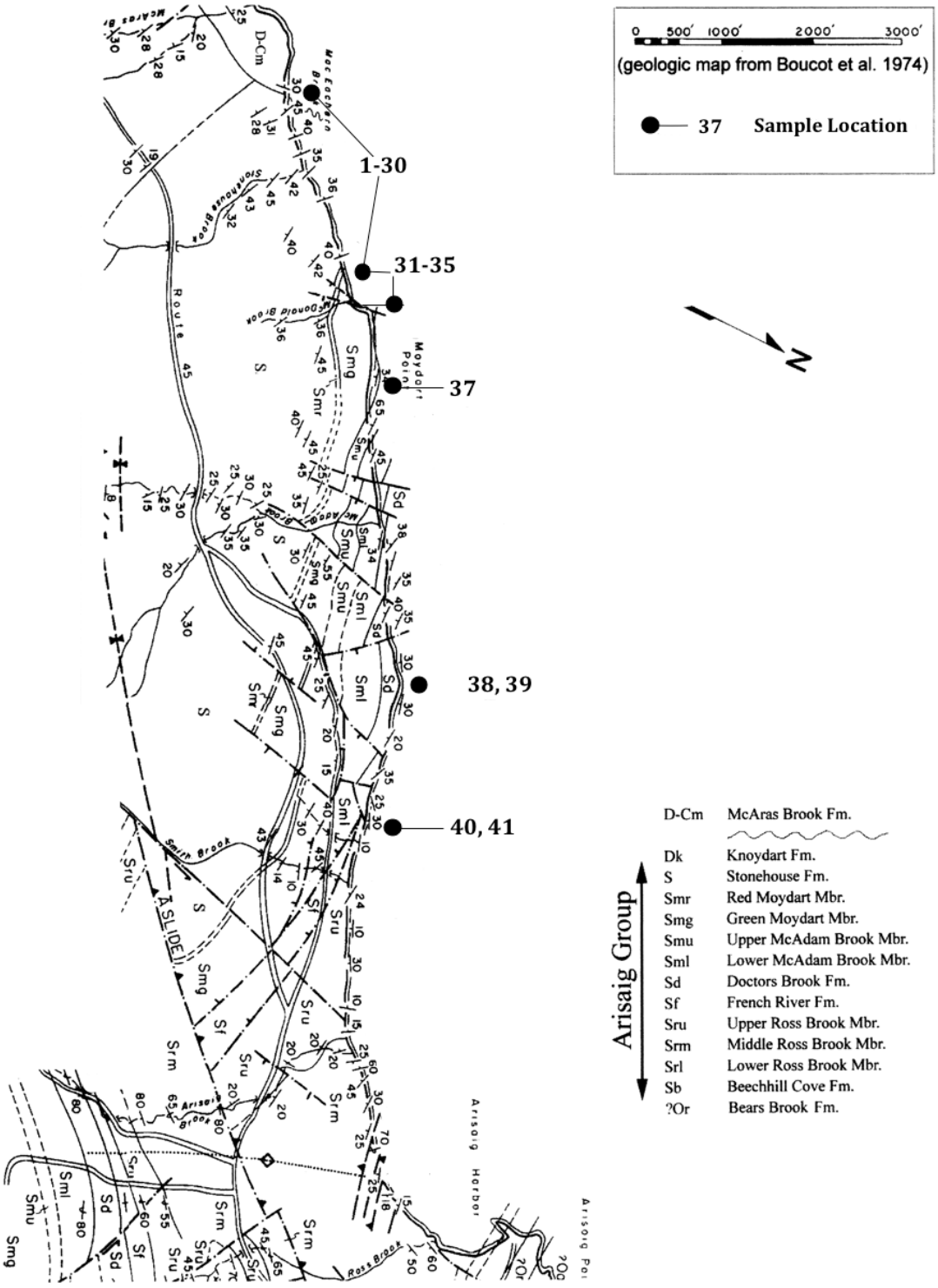

Fig. 3.1. Geologic map of the Arisaig shore in Nova Scotia modified Beck and Strother (2001), originally from Boucot et al. (1974). This figure has been altered to include our sample locations along the Arisaig Group. Sample numbers can be found in table 1. Stratigraphic column based on Murphy et al. (1991).

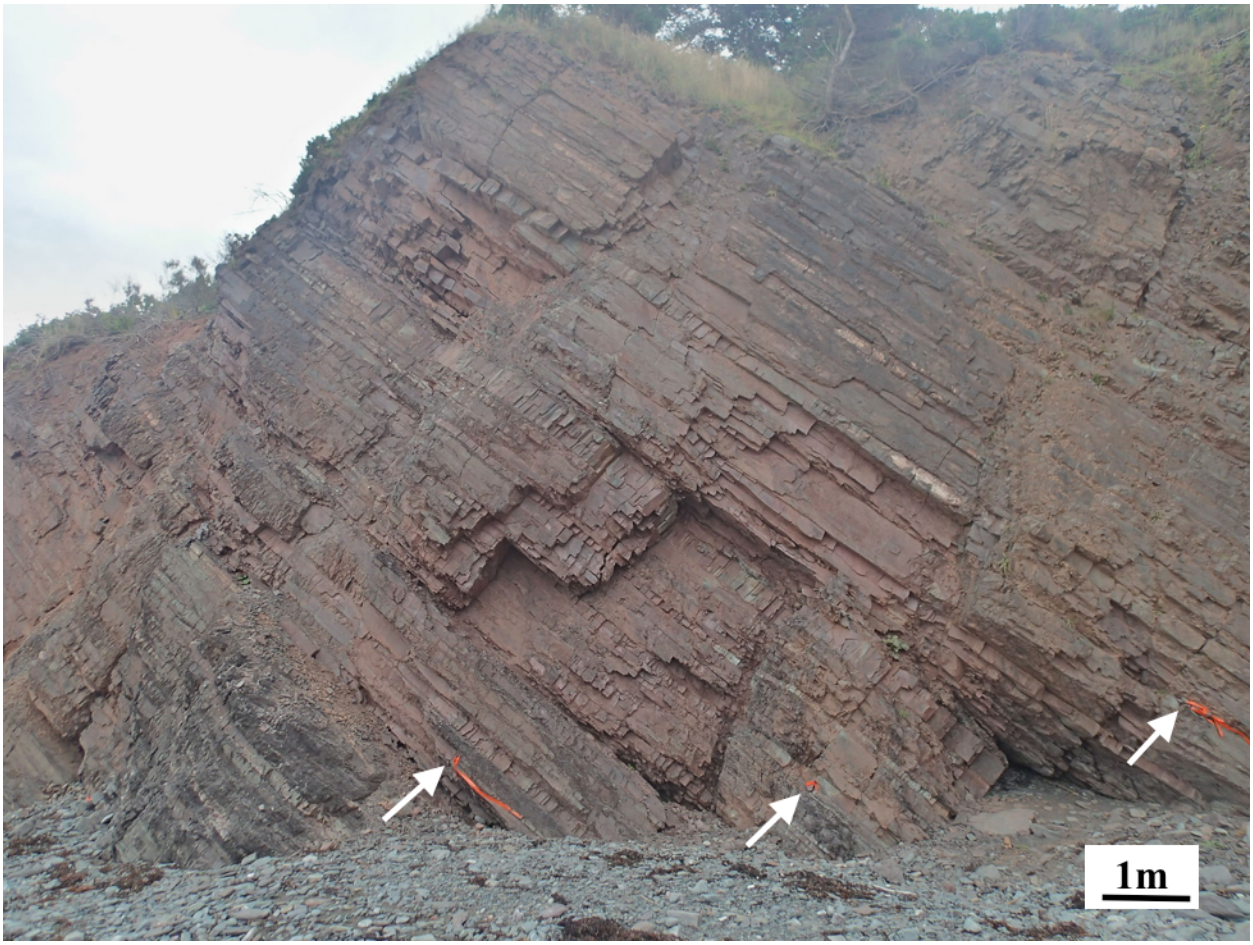

Fig. 3.2. Photograph of the Upper Stonehouse Formation from the Arisaig Group, Arisaig, Nova Scotia. White arrows in the picture point to flagging tape used to mark sample locations and measure distance to allow for stratigraphic orientation. Photographed August 2016.

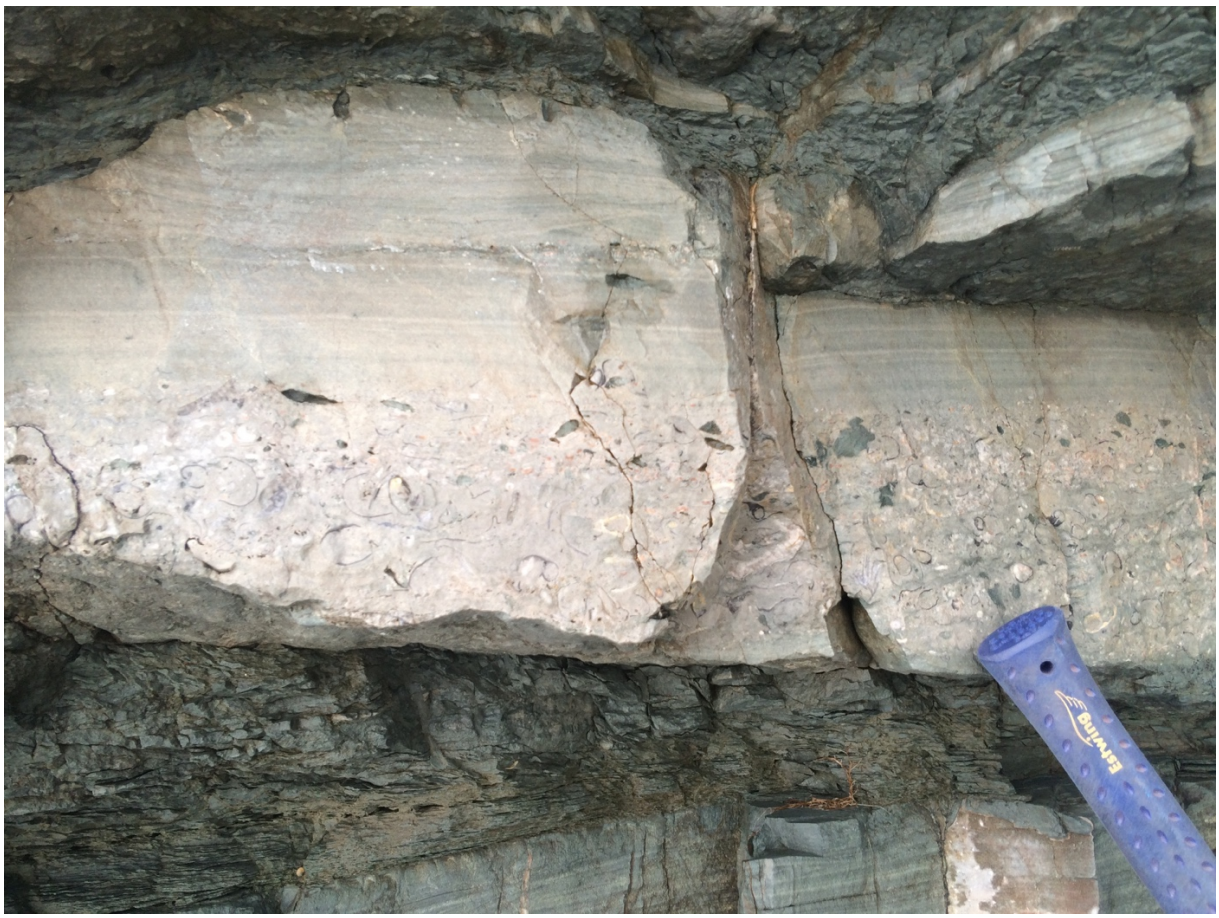

Fig. 3.3. Coquinite bed in the Stonehouse Formation. A geologic hammer is provided in the bottom right corner for scale. Photographed August 2016, Arisaig Nova Scotia.

Table 3.1. Sample numbers that coincide with the location numbers in figure 3.1. The units shown are the Stonehouse Formation (S), the red member of the Moydart Formation (Smr), the green member of the Moydart formation (Smg), the lower member of the McAdam Brook Formation (Sml), the Doctors Brook Formation (Sd), the French River Formation (Sf) and the upper member of the Ross Brook Formation (Sru).

Location ID	Sample	Unit	Location ID	Sample	Unit
1	SH08/31/16-01	S	22	SH09/01/16-10	S
2	SH08/31/16-02 & 03	S	23	SH09/01/16-09	S
3	SH08/31/16-04	S	24	SH09/01/16-08	S
4	SH08/31/16-05	S	25	SH09/01/16-07	S
5	SH08/31/16-06	S	26	SH09/01/16-06	S
6	SH08/31/16-07	S	27	SH09/01/16-05	S
7	SH08/31/16-08	S	28	SH09/01/16-02	Smr
8	SH08/31/16-09	S	29	SH09/01/16-04	Smg
9	SH08/31/16-10	S	30	SH09/01/16-03	Smg
10	SH08/31/16-11	S	31	SH09/02/16-09	Smg
11	SH08/31/16-12	S	32	SH09/01/16-01	Smg
12	SH08/31/16-13	S	33	SH09/02/16-10	Smg
13	SH08/31/16-14	S	34	SH09/02/16-08	Smg
14	SH08/31/16-15	S	35	SH09/02/16-07	Smg
15	SH08/31/16-16	S	36	SH09/02/16-06	Smg
16	SH08/31/16-17	S	37	SH09/02/16-05	Sml
17	SH09/01/16-15	S	38	SH09/02/16-03	Sd
18	SH09/01/16-14	S	39	SH09/02/16-04	Sd
19	SH09/01/16-13	S	40	SH09/02/16-01	Sf
20	SH09/01/16-12	S	41	SH09/02/16-02	Sru
21	SH09/01/16-11	S			

3.2 Sample Preparation

Sample preparation was performed in the Earth Sciences Department of Dalhousie University. Samples were first cut with an abrasive saw, then sliced to ~1mm thicknesses using a low speed saw. These fragments were then mounted onto slides (Fig. 3.4) polished and carbon coated to the standard required for electron microprobe analysis. Scans of all pre-coated slides may be found in appendix A.

Fig. 3.4. An example of a polished standard size slide with samples collected from the upper Stonehouse Formation, Arisaig, Nova Scotia. Sample numbers are written above and below the samples. Various shelled organisms are visible in the specimens.

3.3 Petrographic Microscopy

All forty samples were observed under a petrographic microscope to search for small structures within the fossils and matrix that could indicate primary growth or secondary crystallization, should diagenesis have taken place. Photographs were taken of every sample and can be found in appendix B.

3.4 Electron Microprobe Analysis

Following carbon coating, 36 of the samples, ranging from the uppermost Stonehouse Formation into the Green Member of the Moydart Formation, were analyzed in Dalhousie university's Robert M. MacKay Electron Microprobe Lab. This was done with a JEOL JXA-8200 Election Microprobe Superprobe using an accelerating voltage of 15-kV, beam current of 10 nA and a spot size of 1 μm. All samples were analyzed for Ca, Mg, Fe, Mn, P, Si, Ba and Sr. A photograph was also taken of every analysis location (Fig. 3.5) (appendix C). Analyses included several points in the matrix as well as in fossils for each sample. The acquired data were used firstly, to re-calculate mineral formulas to discern the carbonate end-members present in the samples. These data were also used to calculate distribution coefficients and to plot the elements and their ratios along the stratigraphy in a bulk plot for matrix and fossil specimens separately for comparison across the stratigraphy. Additionally, the elemental ratios and concentrations were examined as indicators of diagenetic effects as well as paleoclimate variation.

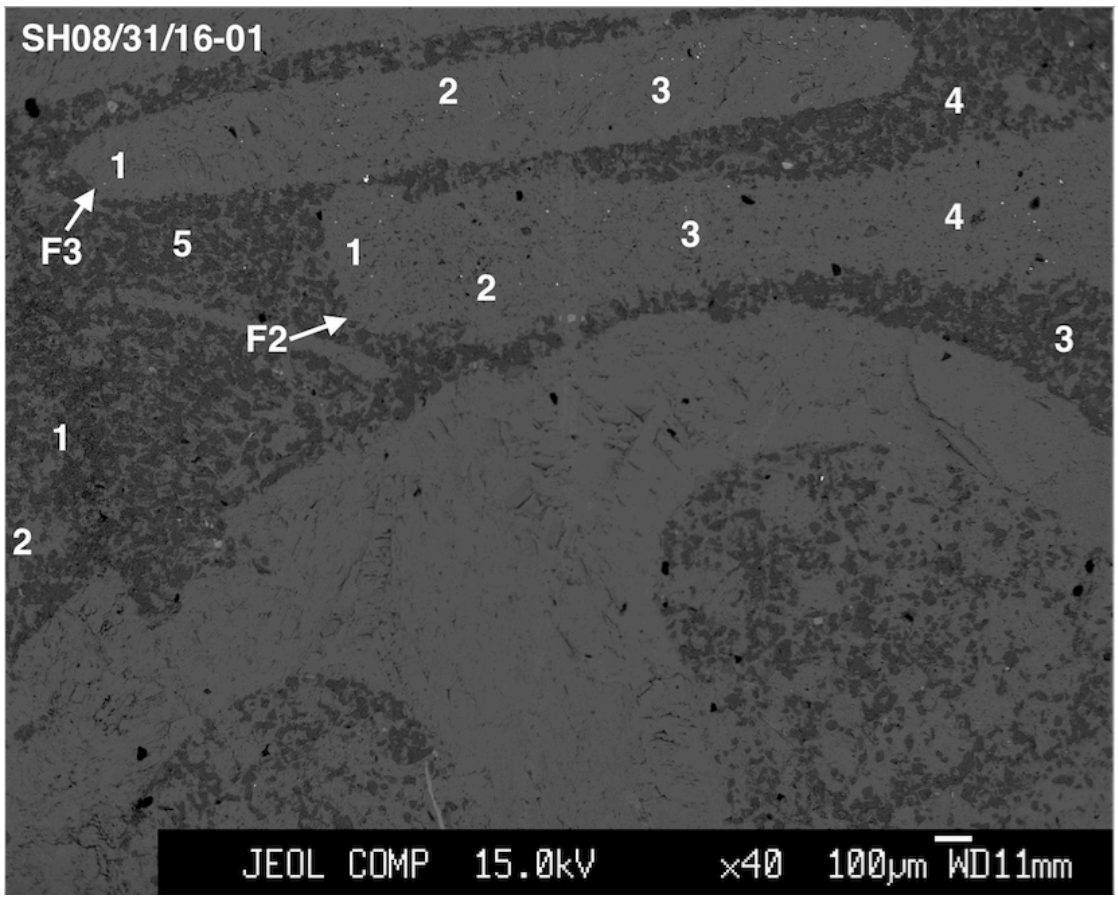

Fig. 3.5. Example of a back scattered electron image taken with the electron microprobe showing location of analysis points. Arrows point to fossil material within the picture.

3.5 Modeling

Sr/Ca and Mg/Ca ratios were plotted against stratigraphy to model the conditions at the time of deposition as well as the changes through time. In addition, paleotemperatures were calculated using the distribution coefficients for Mg partitioning between calcareous organisms (forams) and seawater (Raitzsch et al. 2010). Using these data, and assuming a linear relationship between seawater temperature and Mg partitioning into calcite shell structures, a formula can be presented as:

$$T = \frac{T}{D_{Mg}} * D_{Mg} + K$$

Where; T is temperature in degrees Celcius, T/D_{Mg} is the slope of the linear relationship between seawater temperature and Mg partitioning into calcite shell structures equal to 2.8, D_{Mg} is the distribution coefficient for Mg in calcite fluid and K is the temperature value of the y-intercept of the linear relationship between seawater temperature and Mg partitioning into calcite shell structures, equal to 16.7 °C.

The minimum temperatures defined by the experiments of Raitzsch et al. are around 16 oC where the partitioning of Mg into calcite would be negligible. From this, the Mg uptake of shelled organisms was calculated based on a Silurian seawater concentration of 1295 ppm which, as defined by Brennen and Lowenstein (2002), which is nearly identical to modern day Mg seawater concentrations. The Mg/Ca ratios for modern (3.15) versus Silurian (1.4) sea water were then used to convert these values into a function of the concentration in parts per million. The calculated distribution coefficients, Mg contents and apparent temperatures determined using this formula are show in table 4.1. Finally, this data was used to constrain the temperature conditions of the studied stratigraphic section. This method was also applied to examine the behavior of Sr in the samples. The distribution coefficients describing the partitioning of Sr into calcite organisms from seawater are also from Raitzsch (2010). The formula describing the apparent linear relationship between Sr partitioning and temperature can be given as:

$$\mathbf{T= \frac{T}{D_{Sr}} * D_{Sr} + K}$$

Where; T is temperature in degrees Celcius, T/D_{Sr} is the slope of the linear relationship between seawater temperature and Sr partitioning into calcite shell structures equal to 45.3, D_{Sr} is the distribution coefficient for Sr in calcite fluid and K is the temperature value of the y-intercept of the linear relationship between seawater temperature and Sr partitioning into calcite shell structures, equal to 10.5 °C.

For this calculation, modern sea water was taken to have a Sr content of 8.1ppm. However, as will be discussed below, these calculations suggest that Silurian seawater Sr concentrations would have to be significantly higher and that it is likely other factors beyond seawater temperatures contribute to the Sr uptake and variations recorded by the calcite fossils analyzed in this study.

Chapter 4: Results

4.1 Composition and Structure

Photographs from the petrographic microscope showed that all the samples displayed secondary growth in their fossils, indicative of diagenetic alteration (Fig. 4.1, 4.2). However, many of the samples also displayed primary growth structures relict from biological precipitation (Fig. 4.3). This primary growth occurred across entire fossil shells or, in a couple cases, the same shell contained both primary and secondary growth phases (Fig. 4.4). Nonetheless, every sample displayed some form of secondary carbonate crystal growth signifying that some form of diagenetic change has taken place to produce this re-growth. There is no systematic variation across the stratigraphy. However, during analysis of the polished sections with the electron microprobe, only five samples with fossils containing strictly primary growth structures were directly observed. These were spread moderately evenly throughout the lower Stonehouse Formation.

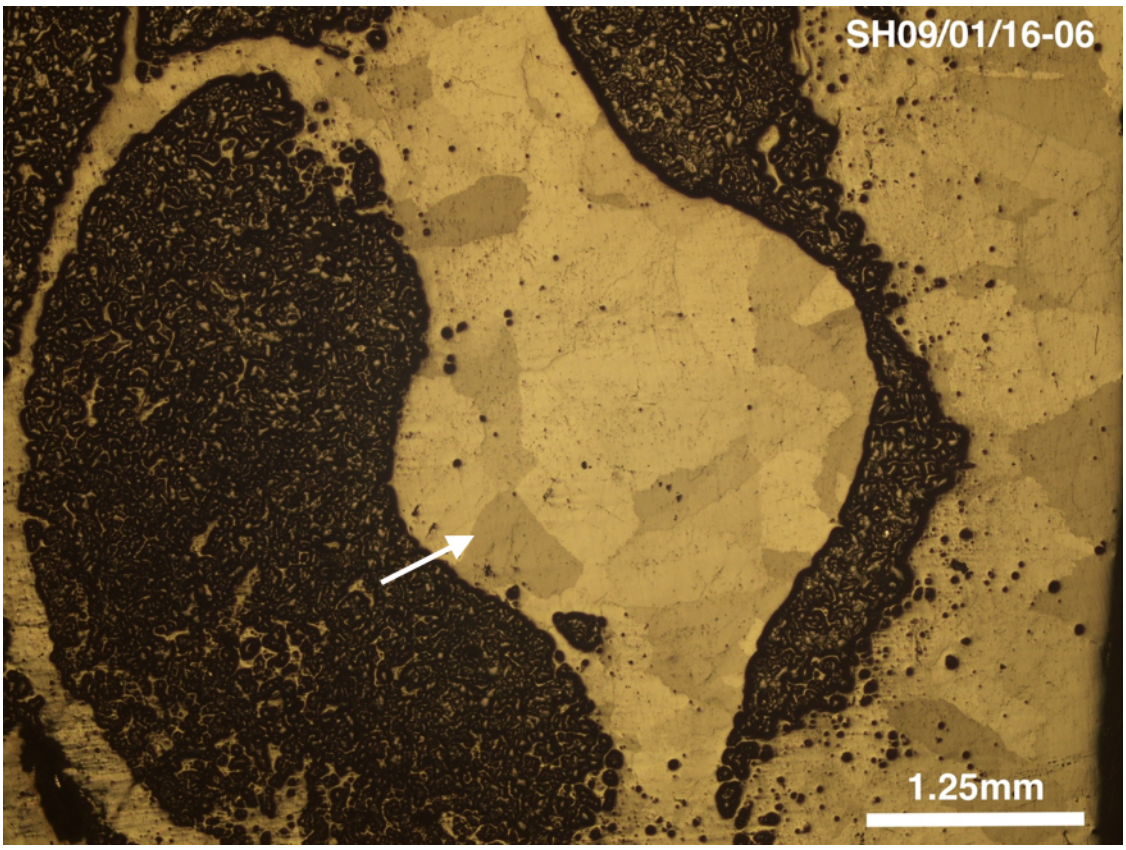

Fig. 4.1. Photomicrograph of sample SH09/01/16-06 from the lower Stonehouse Formation. The fossil here displays a crystalline structure associated with secondary crystallization after diagenesis, shown by an arrow.

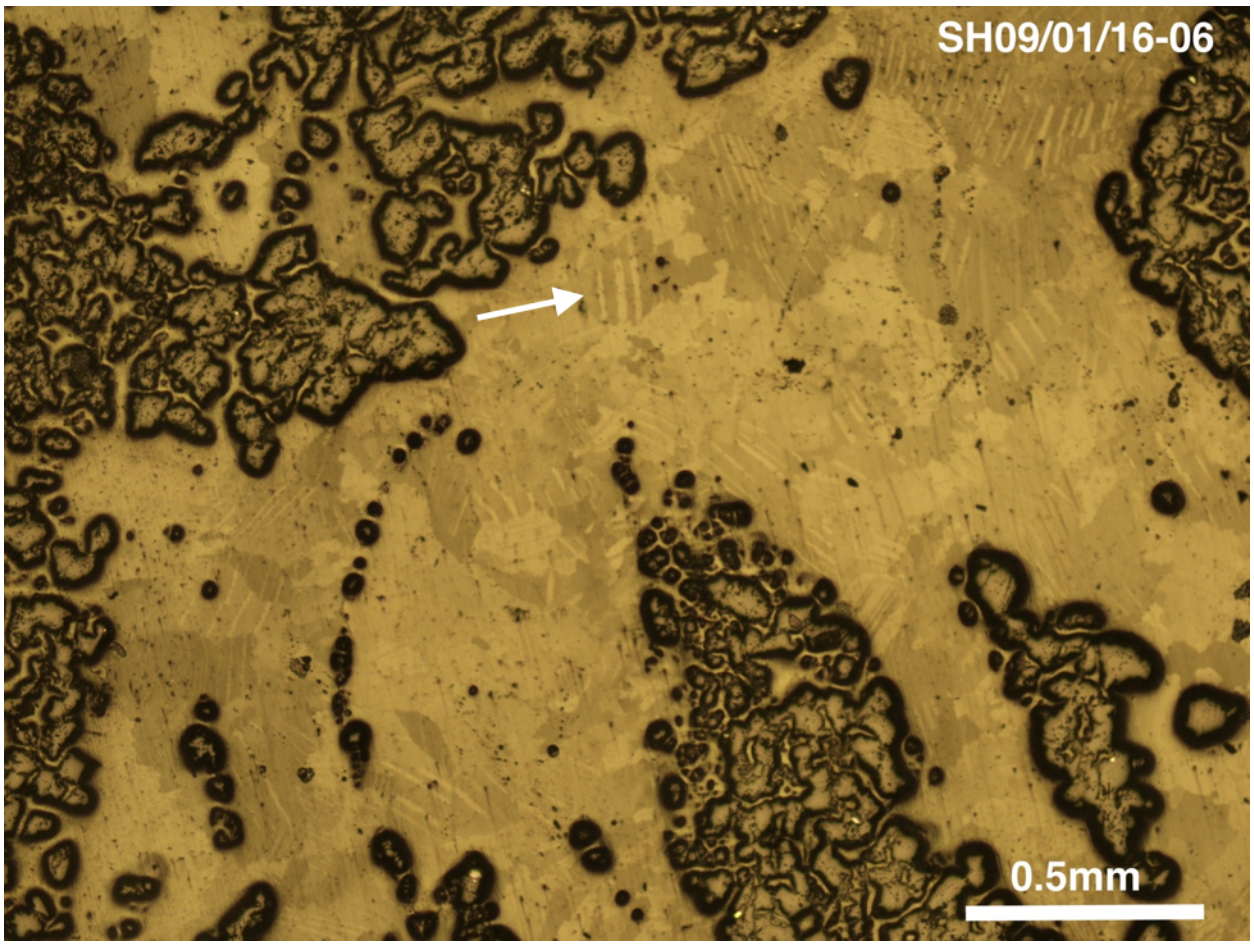

Fig. 4.2. Photomicrograph of sample SH09/01/16-06 from the lower Stonehouse Formation. Calcite twins can be seen where a fossil was once located, as shown by an arrow.

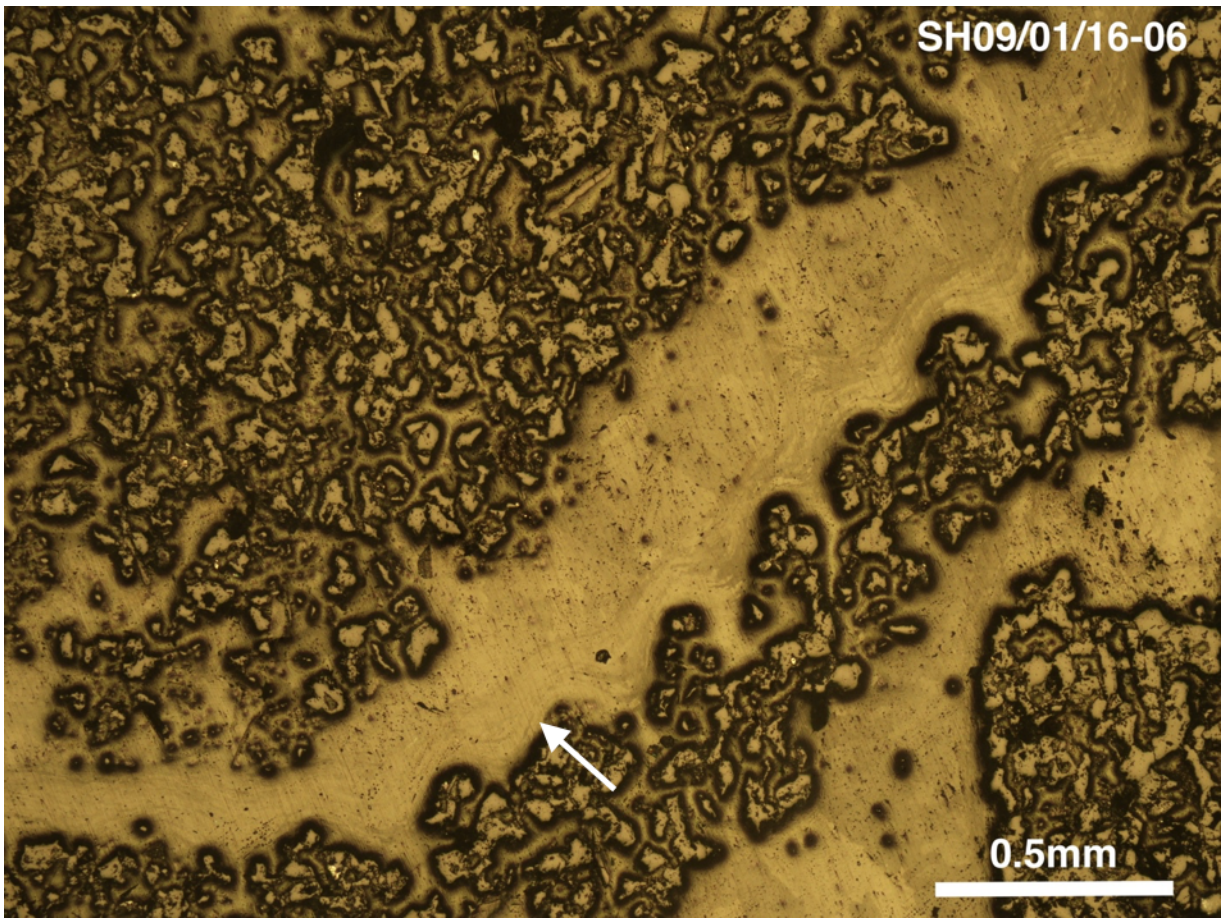

Fig. 4.3. Photomicrograph of sample SH09/01/16-06 from the lower Stonehouse Formation. Primary growth lines, indicated by an arrow, can be seen associated with primary precipitation by the organism.

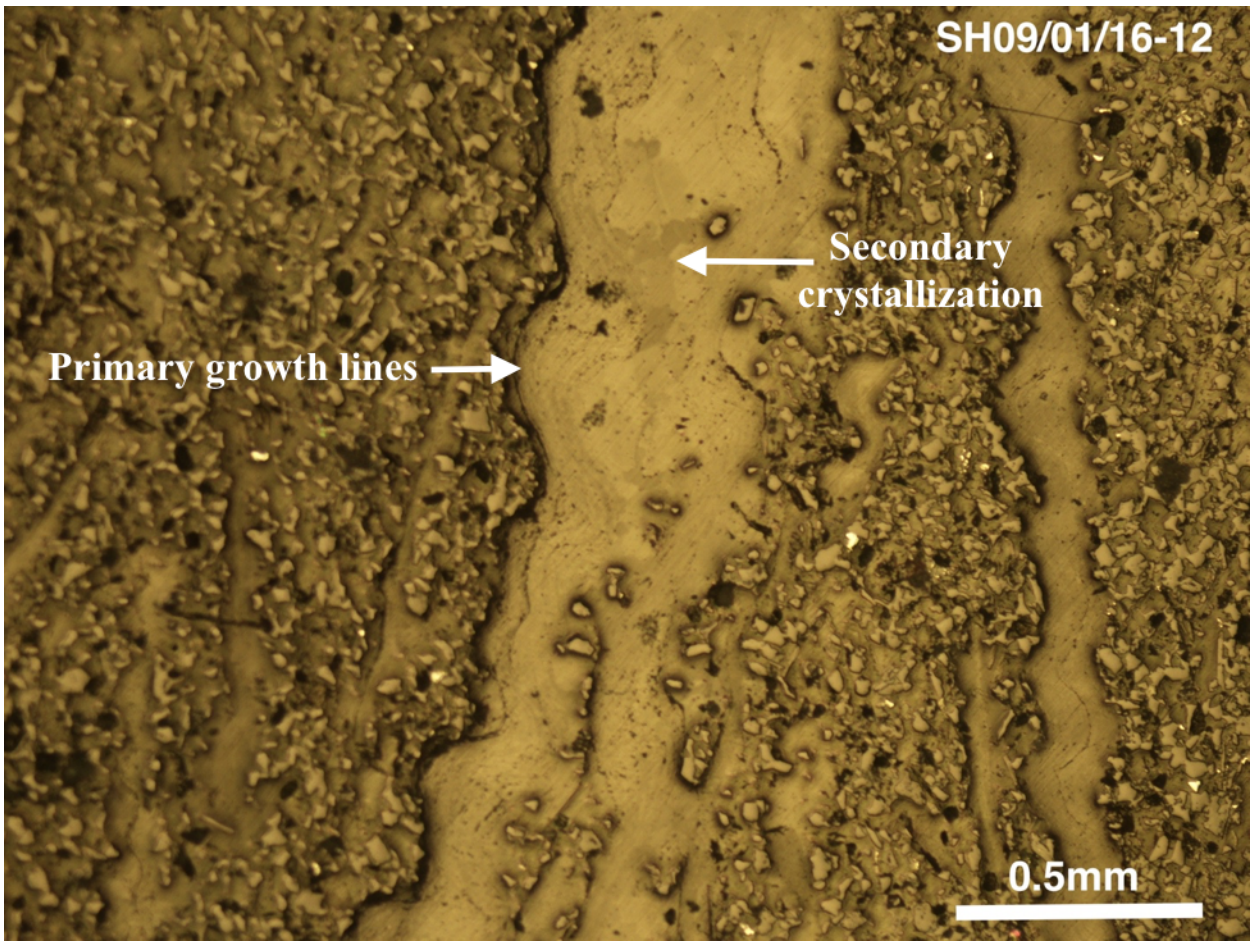

Fig. 4.4. Photomicrograph of sample SH09/01/16-12 Stonehouse Formation. In this fossil, primary growth lines as well as secondary crystallization are indicated by arrows.

In addition to petrographic microscopy, backscattered images produced using the Electron Microprobe show that all thirty-six samples were predominantly comprised of a micritic mud with calcite cement. This mud makes up about 50% of the matrix in all observed samples, the remainder being the carbonate cement. The dulled fluorescent glow of the rock matrix under a UV lamp compared to the more intense light radiating from the fossil material confirmed this. Several samples displayed a more mud-based matrix as well as a lack of fossils (SH09/01/16-05, SH09/01/16-11, SH09/02/16-02). These samples typically also yielded outlying data during microprobe analysis. This was attributed to the uneven polish caused by the muddy matrix material in contrast to the soft carbonate cement, leading to pitting in the samples. This difference in composition and texture is easily observed in figures 4.5 and 4.6, as they show that

analyses of fossil material generated an overwhelming lack of silicon concentration while analyses of the matrix continuously displayed the presence of silicon with very large standard deviations. These large errors are attributed to the uneven surface of the sample matrix and contamination with silicate mud minerals. Therefore, analyses of fossil material are much more accurate for geochemical analysis and are prioritized over matrix material for these rocks.

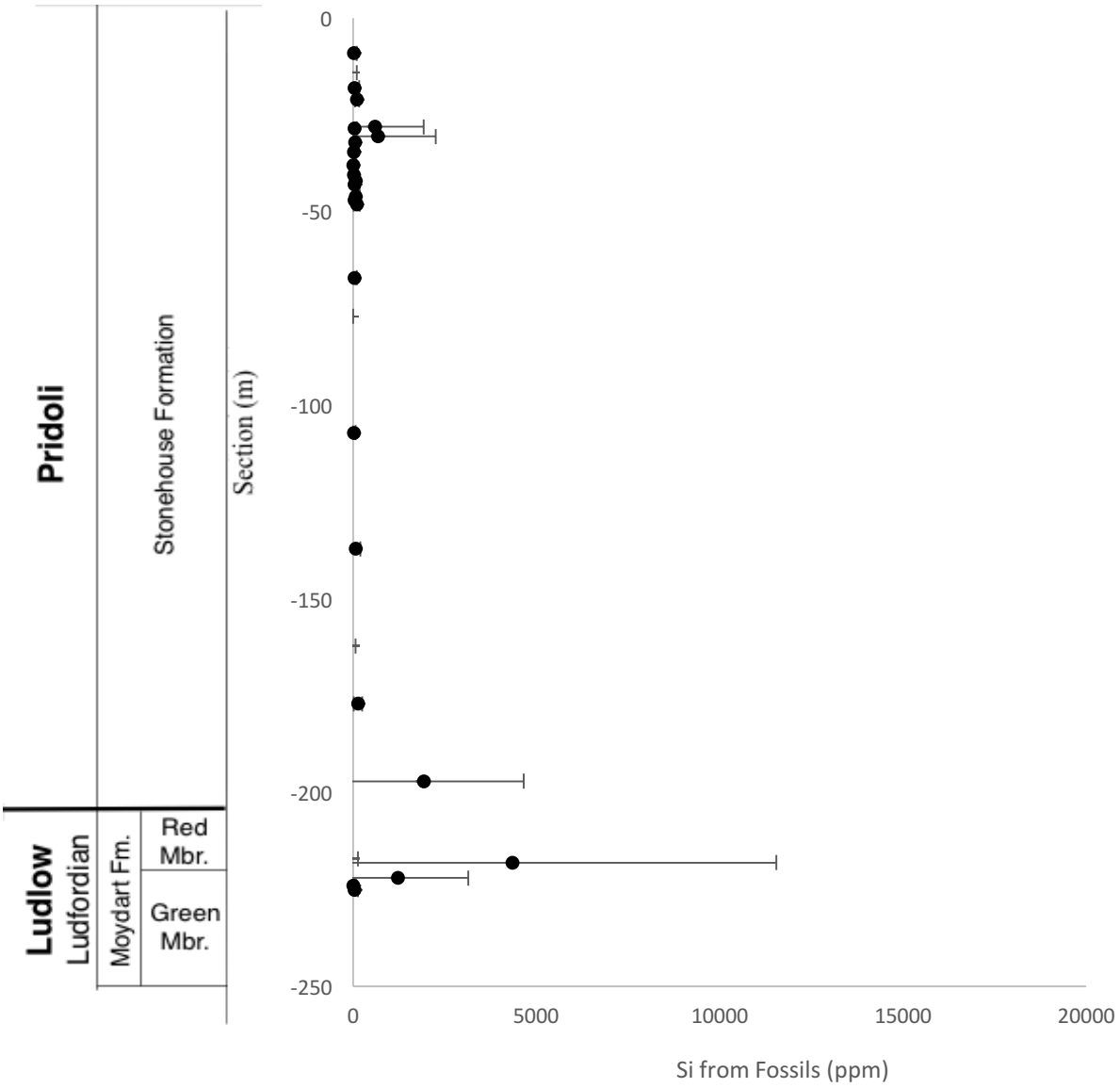

Fig. 4.5. Graph showing the concentration of silicon in parts per million of fossil material plotted against the stratigraphic location of samples from the Arisaig Group, Arisaig Nova Scotia, Canada. 0m corresponds to the top of the Stonehouse Formation. Error bars correspond to one standard deviation.

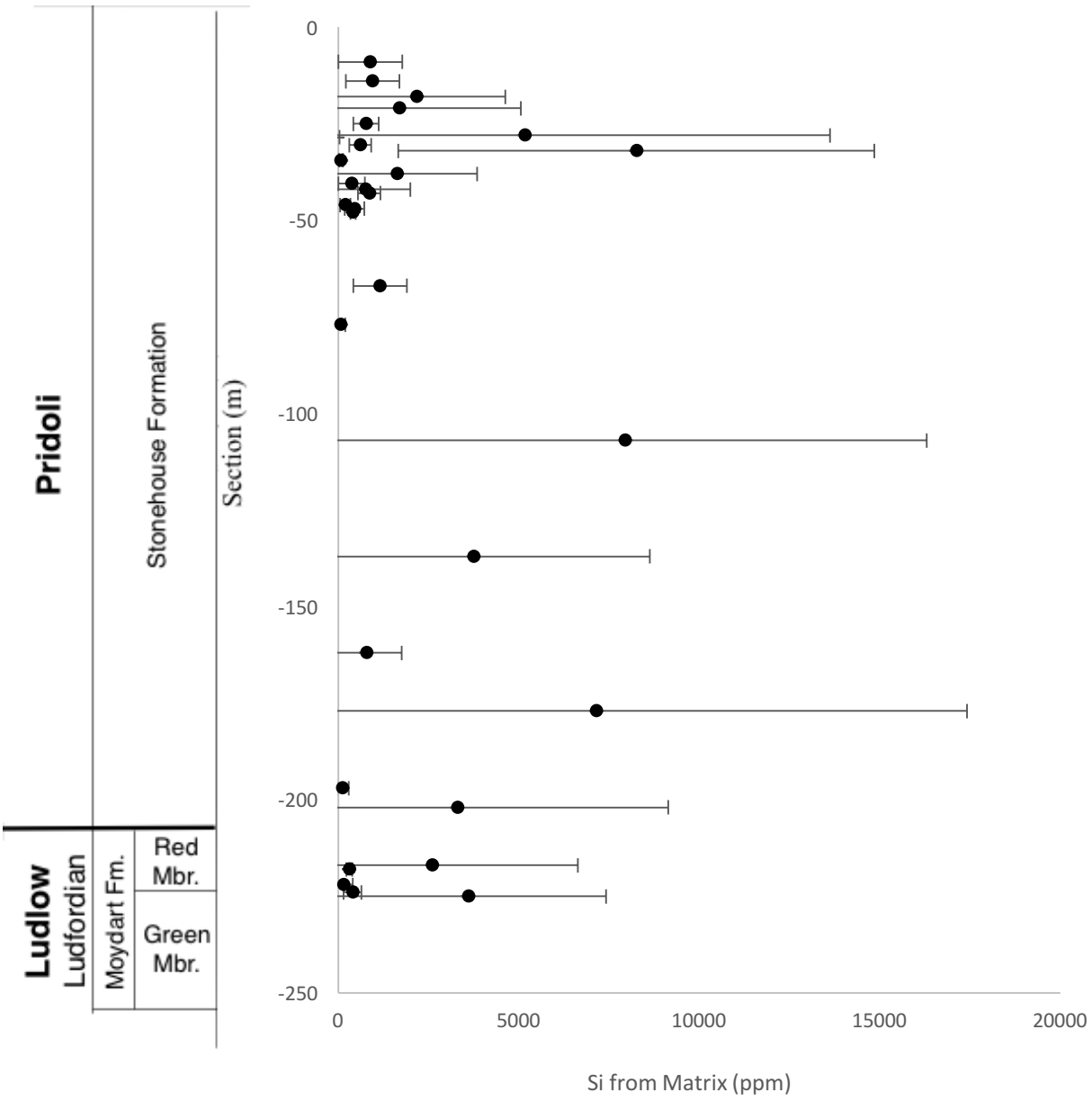

Fig. 4.6. Graph showing the concentration of silicon in parts per million of matrix material plotted against the stratigraphic location of samples from the Arisaig Group, Arisaig Nova Scotia, Canada. 0m corresponds to the top of the Stonehouse Formation. Error bars correspond to one standard deviation.

End-member calculations based on microprobe data showed that the carbonate material for both the matrix and the fossils is overwhelmingly calcitic (Fig. 4.7). Here, we have considered rhodochrosite to be the Mn end-member which is present in small amounts.

Calculations were also completed for siderite and strontianite, representing Fe and Sr concentration respectively. However, Fe and Sr were only minimally present in the samples.

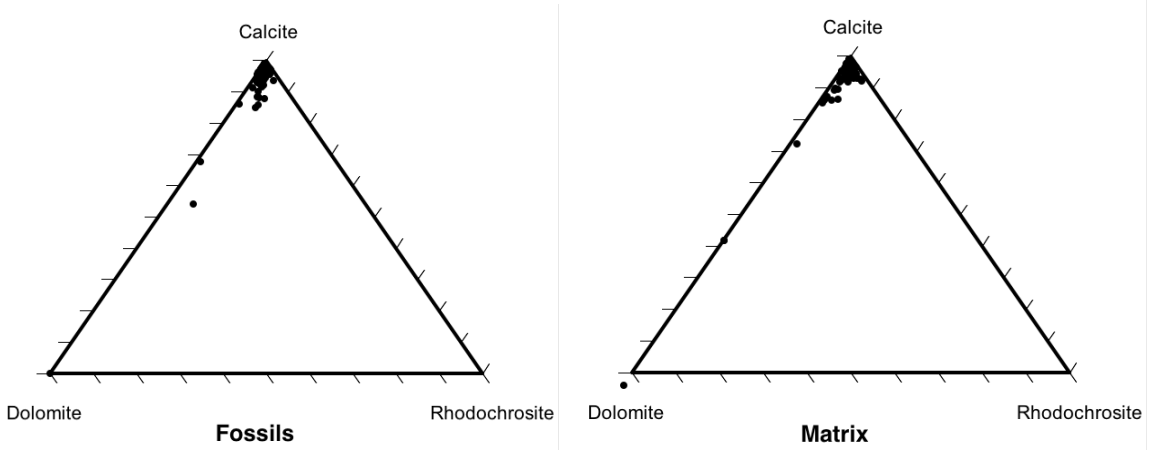

Fig. 4.7. Ternary plots showing the composition of the fossil material (left) and matrix material (right) of samples as a function of the calcite, dolomite and rhodochrosite end-members.

4.2 Chemical Stratigraphy

From microprobe analysis, Ba was found to be below the detection limit in all samples. This element is therefore not considered further in the geochemical analysis. Figures 4.8 to 4.17 show the chemical variation in the fossil and matrix material across the stratigraphy of the section. The Ca concentration does not vary much across the stratigraphy (Fig. 4.8, 4.9), with large standard deviations negating any apparent trend in the plots. The iron content of fossils (Fig. 4.10) has higher values in the Green Member and Upper Red Member. This is faintly reflected in the matrix material, as well as an additional increase in the middle Stonehouse Formation. The Mg concentrations of both the fossil (Fig. 4.12) and matrix (Fig. 13) materials show an overall trend of low values in the Upper Stonehouse Formation (~2000 ppm) and gradual peaks (3000-4000 ppm) in the middle Stonehouse Formation and Moydart Formation. A trend can also be observed in the Mn (Fig. 4.14, 4.15) concentrations with a minimum in the Middle Stonehouse Formation and peaks in the Upper and Lower Stonehouse Formations as well as throughout the Moydart Formation. This is especially

prominent in the data generated from fossil material (Fig. 4.14). The Sr values so do not fluctuate significantly across the stratigraphy for the matrix material (Fig. 4.16) but have a definite decrease within the Green Member of the Moydart Formation. The remainder of the data contains deviations that do not allow for a reliable conclusion to be drawn. However, the fossil material provides a much more pronounced trend (Fig. 4.17). These data show low values in the Upper Stonehouse Formation from approximately 0 to 2000 ppm, mostly clustered below 1000 ppm. Further down the stratigraphy is a gentle slope to a maximum of about 2000 ppm in the Middle Stonehouse Formation which then follows another gentle slope to an additional minimum in the Moydart Formation with values mostly below 1000 ppm. Samples which showed primary growth structures are marked by open circles in the figures for Mg (Fig.4.12), Mn (Fig. 4.14) and Sr (Fig. 4.16). These data points all show the same trends already mentioned and in every case, show an even more prominent curve. A complete table of raw data in the form of weight percent oxides as well as well as metal cations used to determine end-members and the resulting end-member proportions can be found in appendix D.

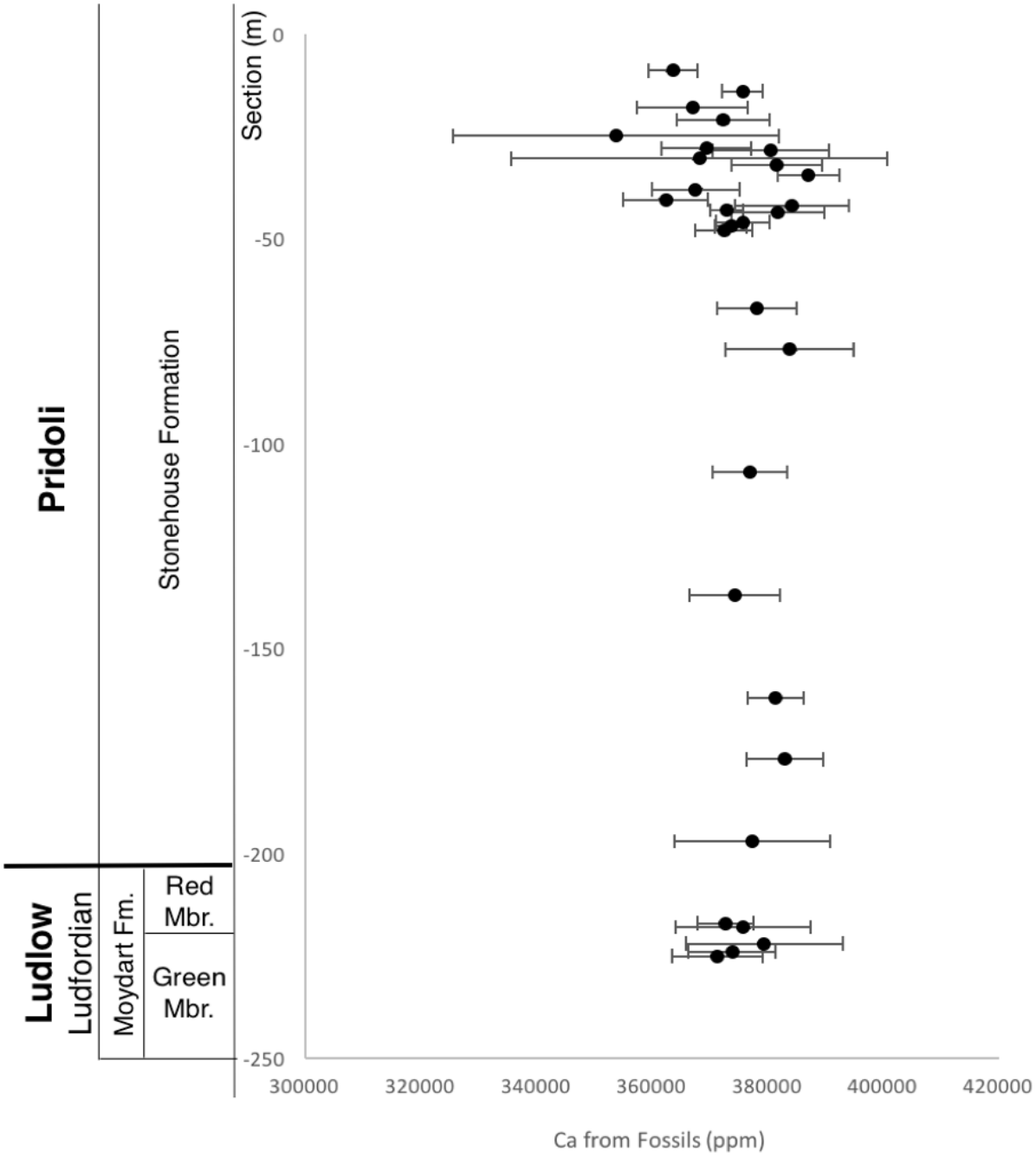

Fig. 4.8. Graph showing the concentration of calcium in parts per million of fossil material plotted against the stratigraphic location of samples from the Arisaig Group, Arisaig Nova Scotia, Canada. 0m corresponds to the top of the Stonehouse Formation. Error bars correspond to one standard deviation.

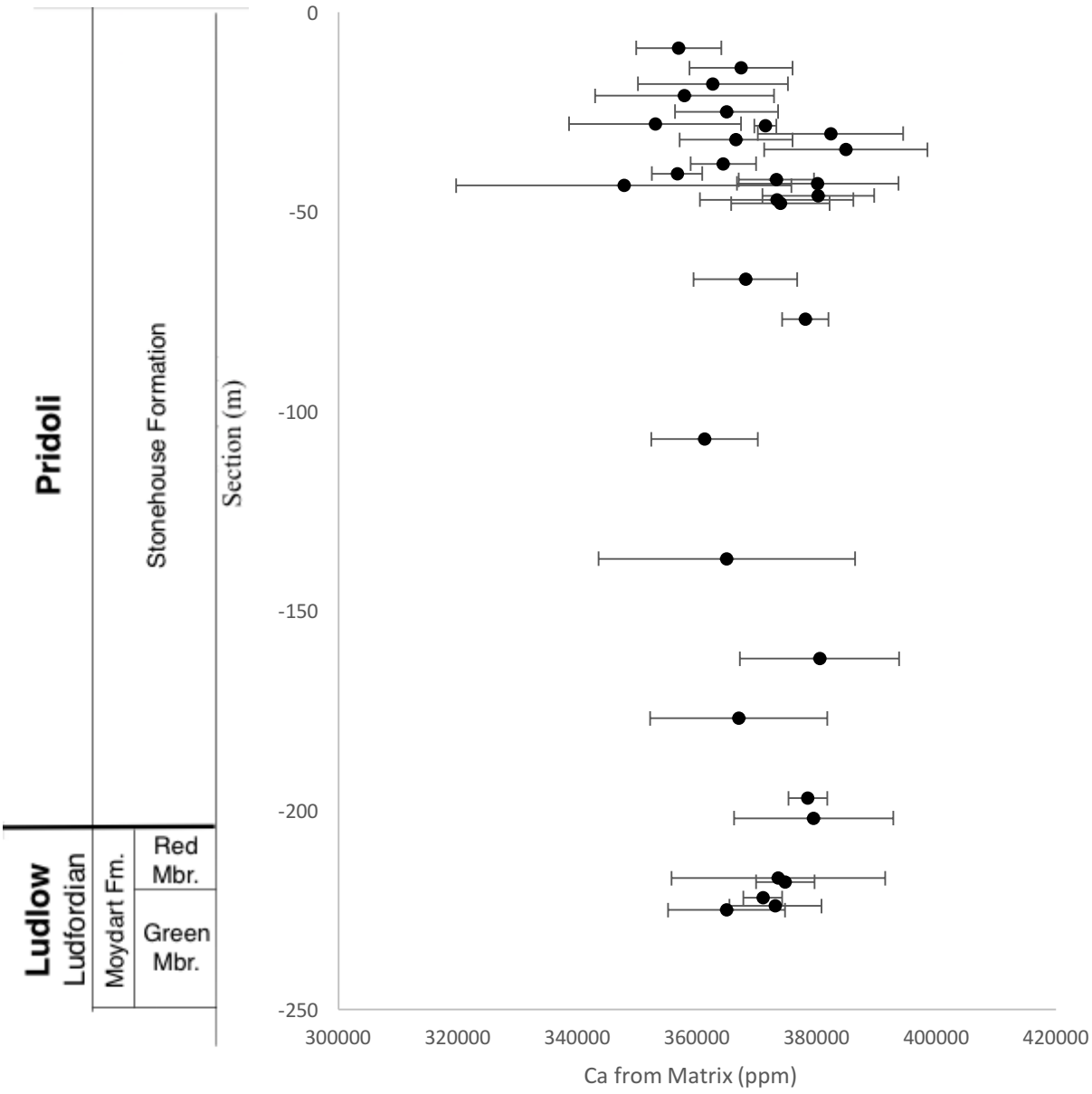

Fig. 4.9. Graph showing the concentration of calcium in parts per million of matrix material plotted against the stratigraphic location of samples from the Arisaig Group, Arisaig Nova Scotia, Canada. 0m corresponds to the top of the Stonehouse Formation. Error bars correspond to one standard deviation.

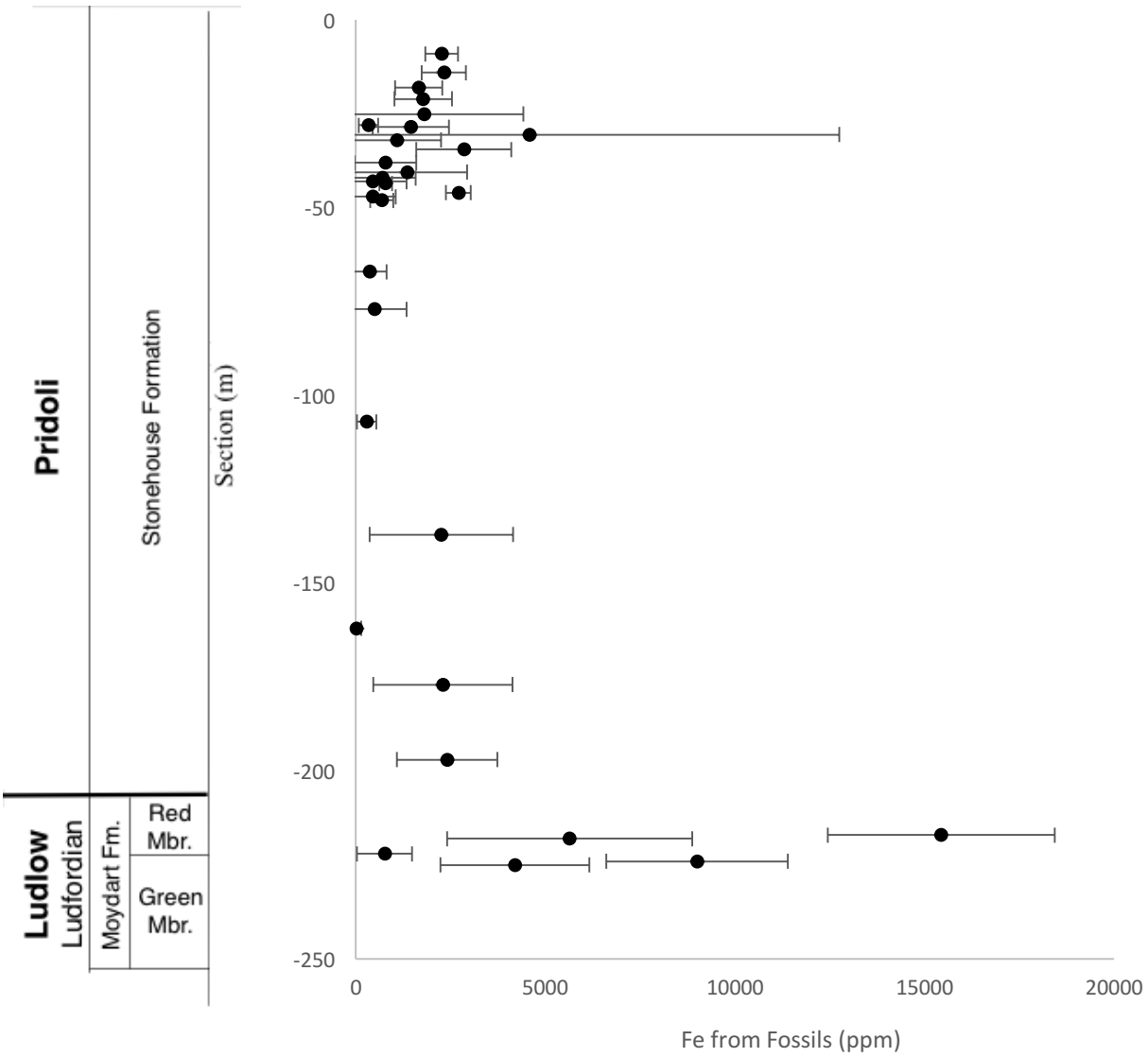

Fig. 4.10. Graph showing the concentration of iron in parts per million of fossil material plotted against the stratigraphic location of samples from the Arisaig Group, Arisaig Nova Scotia, Canada. 0m corresponds to the top of the Stonehouse Formation. Error bars correspond to one standard deviation.

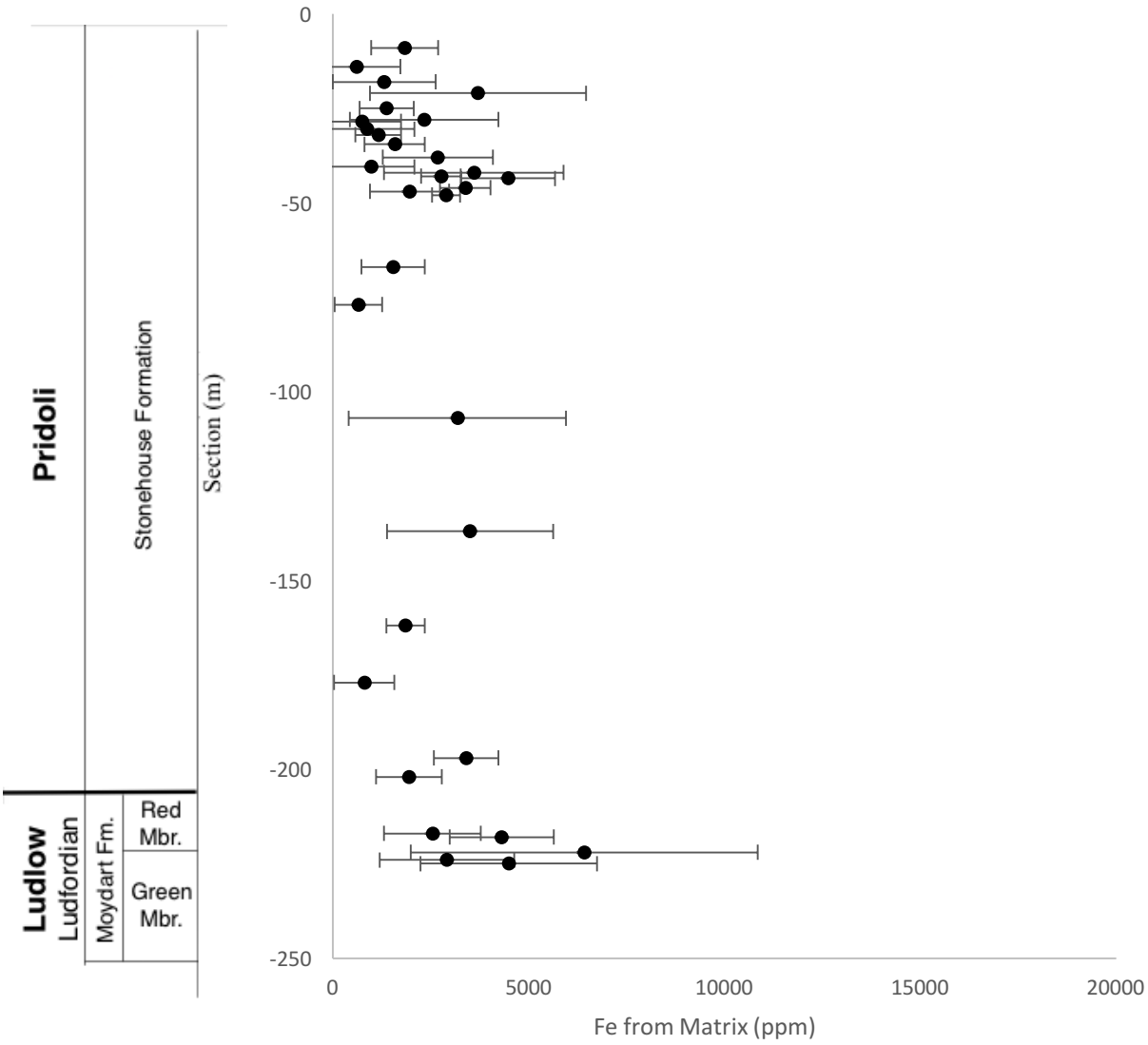

Fig. 4.11. Graph showing the concentration of iron in parts per million of matrix material plotted against the stratigraphic location of samples from the Arisaig Group, Arisaig Nova Scotia, Canada. 0m corresponds to the top of the Stonehouse Formation. Error bars correspond to one standard deviation.

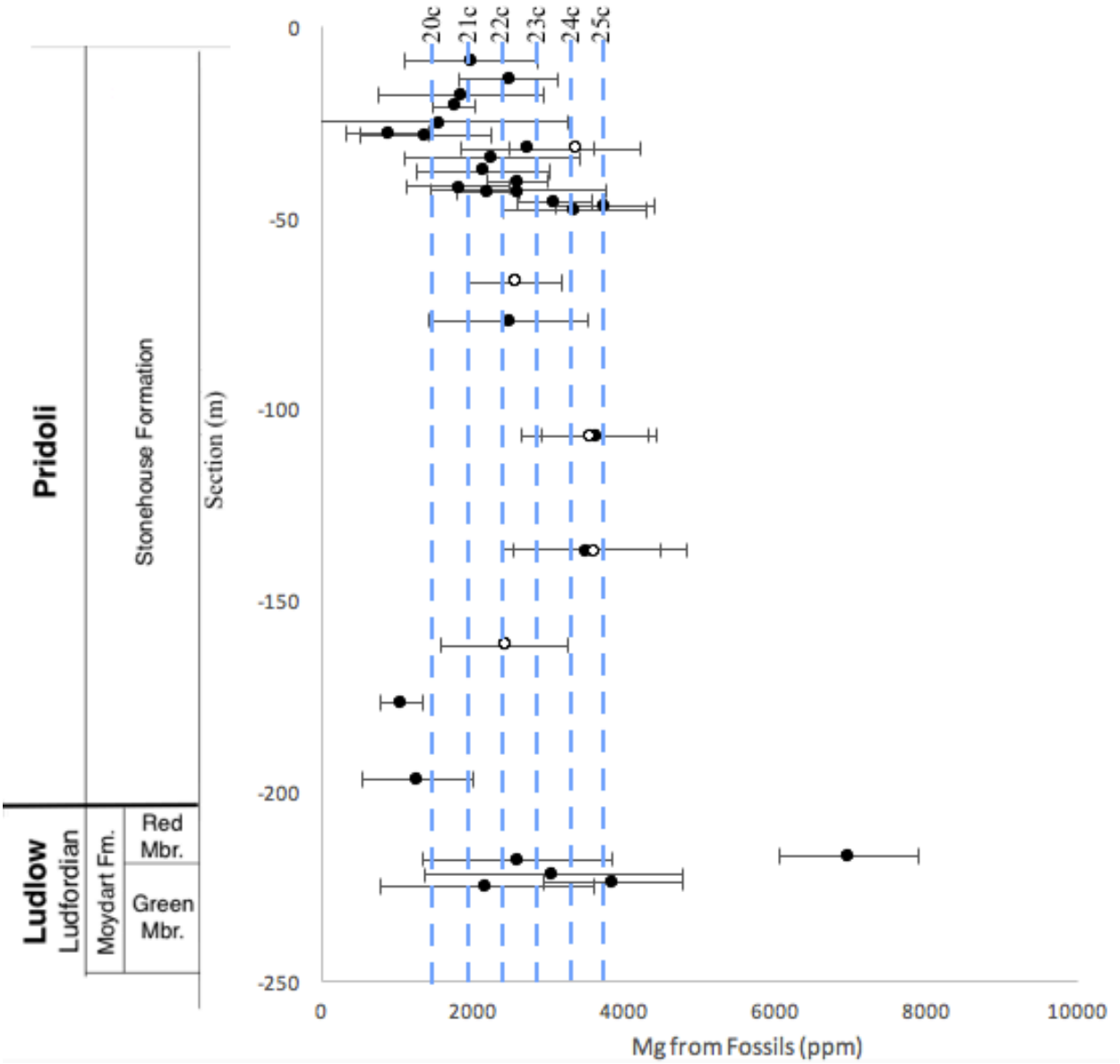

Fig. 4.12. Graph showing the concentration of Magnesium in parts per million of fossil material plotted against the stratigraphic location of samples from the Arisaig Group, Arisaig Nova Scotia, Canada. 0m corresponds to the top of the Stonehouse Formation. Error bars correspond to one standard deviation. Open circles identify samples that show only primary growth structures and are therefore considered not to have undergone diagenesis. Blue dashed lines represent temperature gradients in degrees Celsius based on Mg distribution coefficients (Table 4.1).

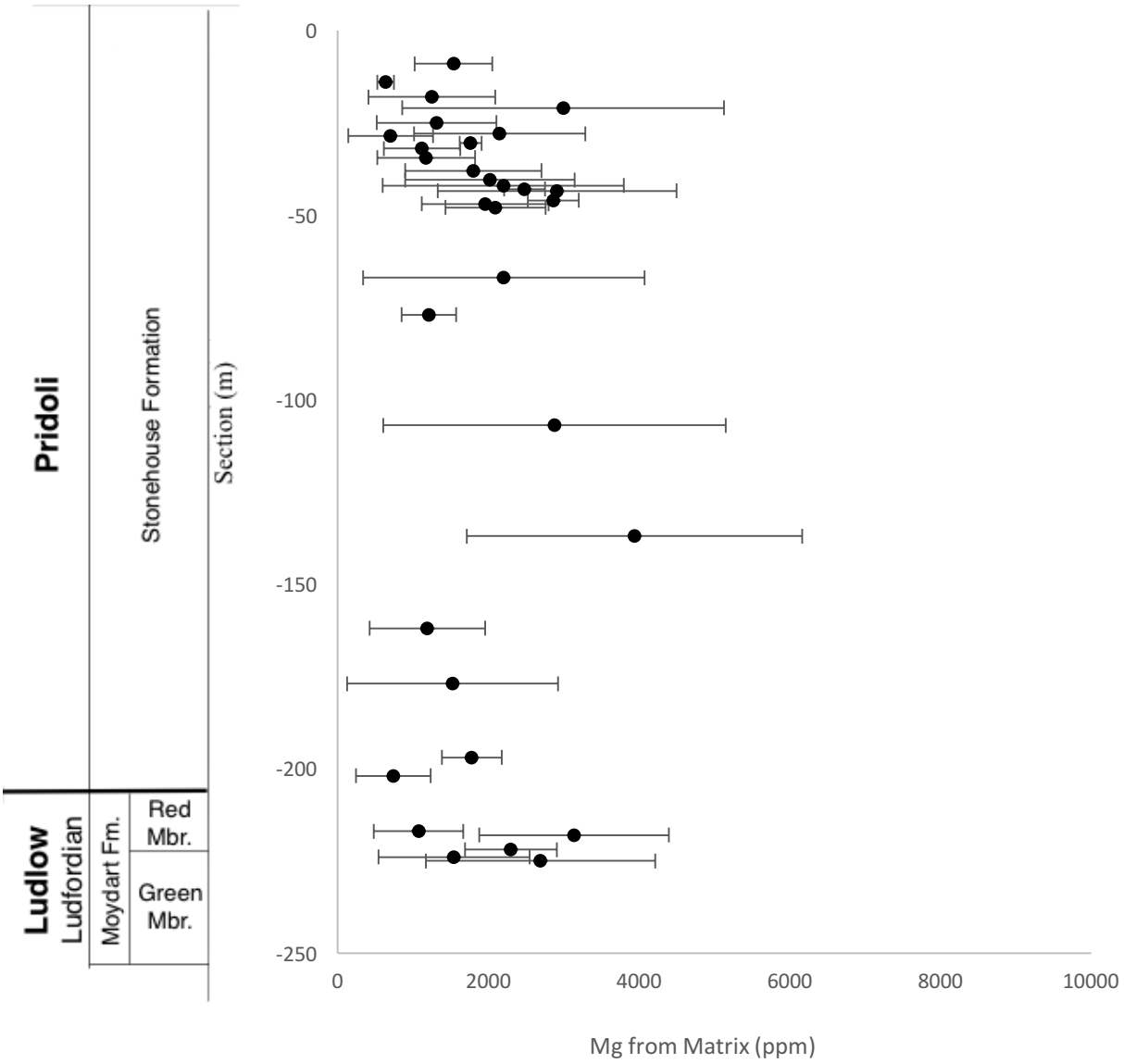

Fig. 4.13. Graph showing the concentration of Magnesium in parts per million of matrix material plotted against the stratigraphic location of samples from the Arisaig Group, Arisaig Nova Scotia, Canada. 0m corresponds to the top of the Stonehouse Formation. Error bars correspond to one standard deviation. Temperature gradients were not calculated for matrix materials.

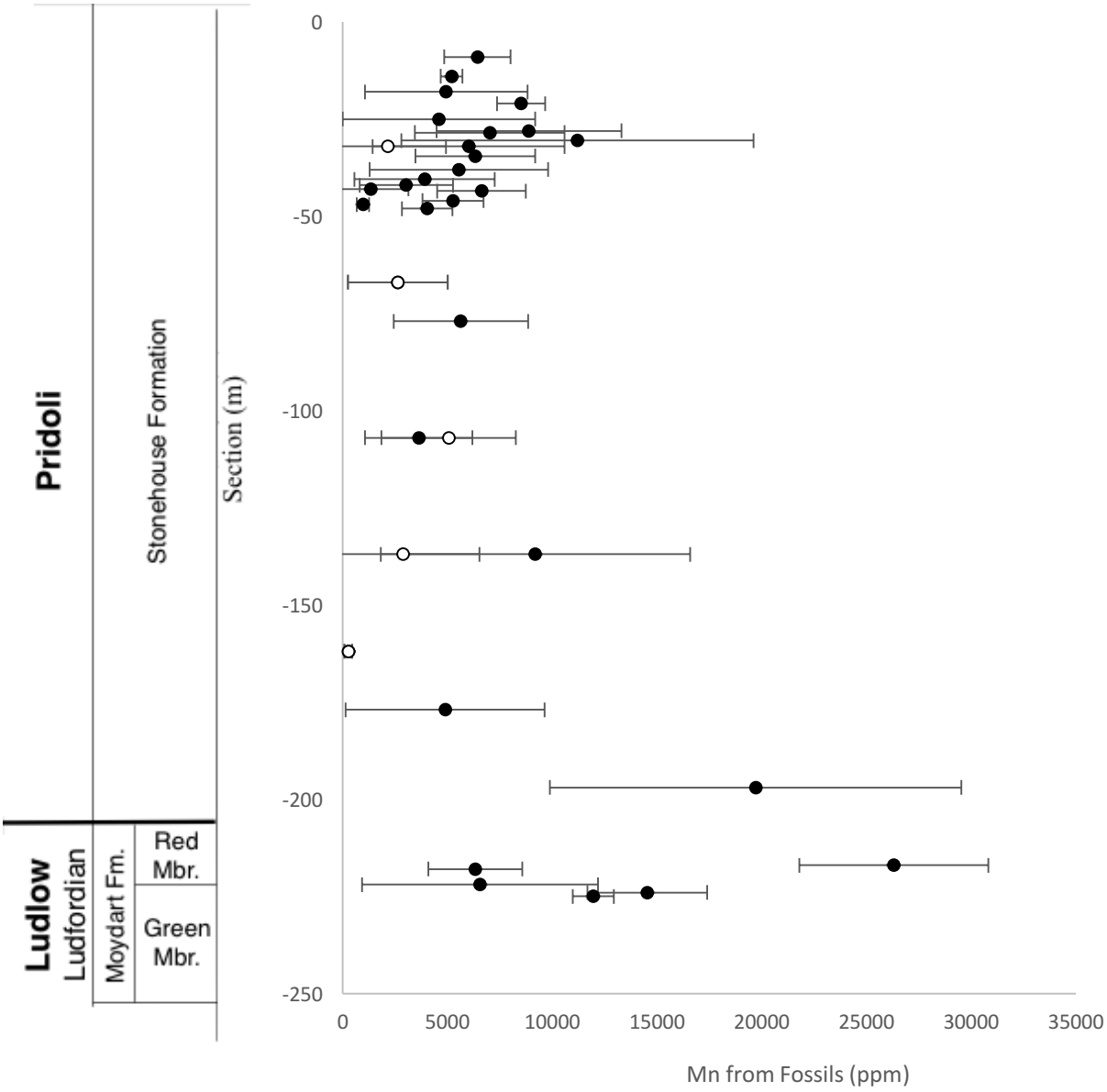

Fig. 4.14. Graph showing the concentration of manganese in parts per million of fossil material plotted against the stratigraphic location of samples from the Arisaig Group, Arisaig Nova Scotia, Canada. 0m corresponds to the top of the Stonehouse Formation. Error bars correspond to one standard deviation. Open circles identify samples that display only primary growth structures and therefore have not undergone diagenesis.

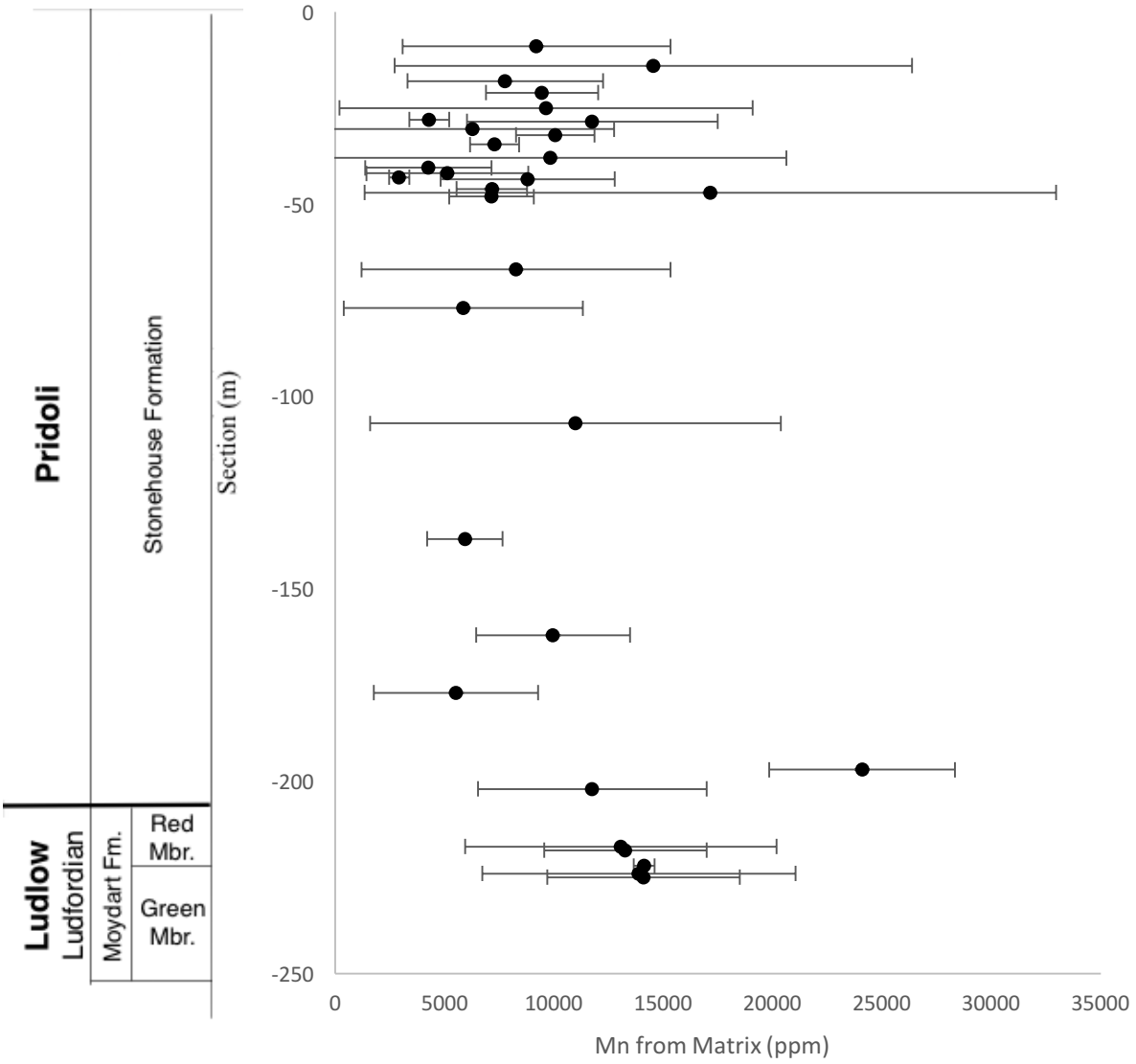

Fig. 4.15. Graph showing the concentration of manganese in parts per million of matrix material plotted against the stratigraphic location of samples from the Arisaig Group, Arisaig Nova Scotia, Canada. 0m corresponds to the top of the Stonehouse Formation. Error bars correspond to one standard deviation.

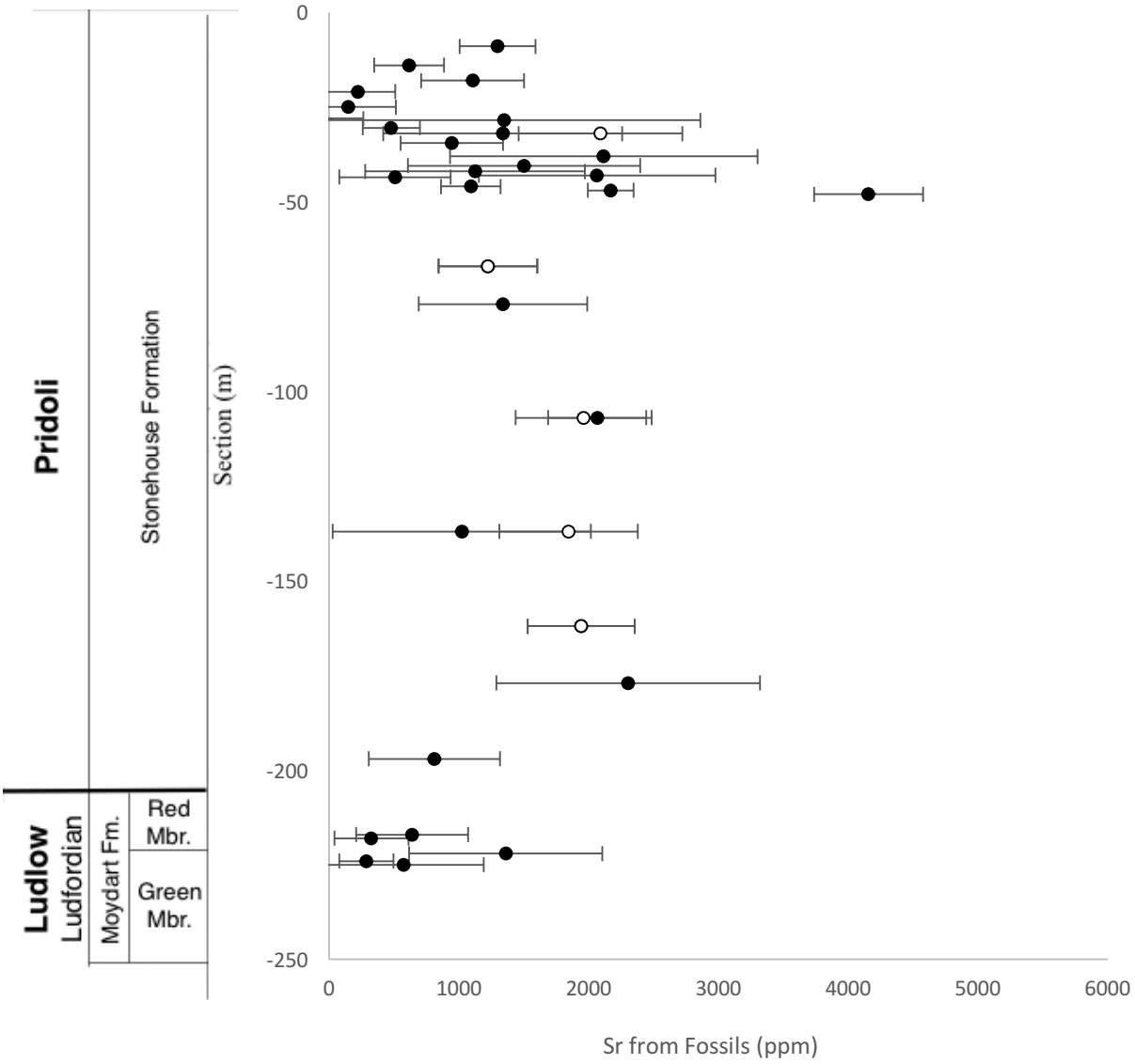

Fig. 4.16. Graph showing the concentration of strontium in parts per million of fossil material plotted against the stratigraphic location of samples from the Arisaig Group, Arisaig Nova Scotia, Canada. 0m corresponds to the top of the Stonehouse Formation. Error bars correspond to one standard deviation. Open circles identify samples that display only primary growth structures and therefore have not undergone diagenesis.

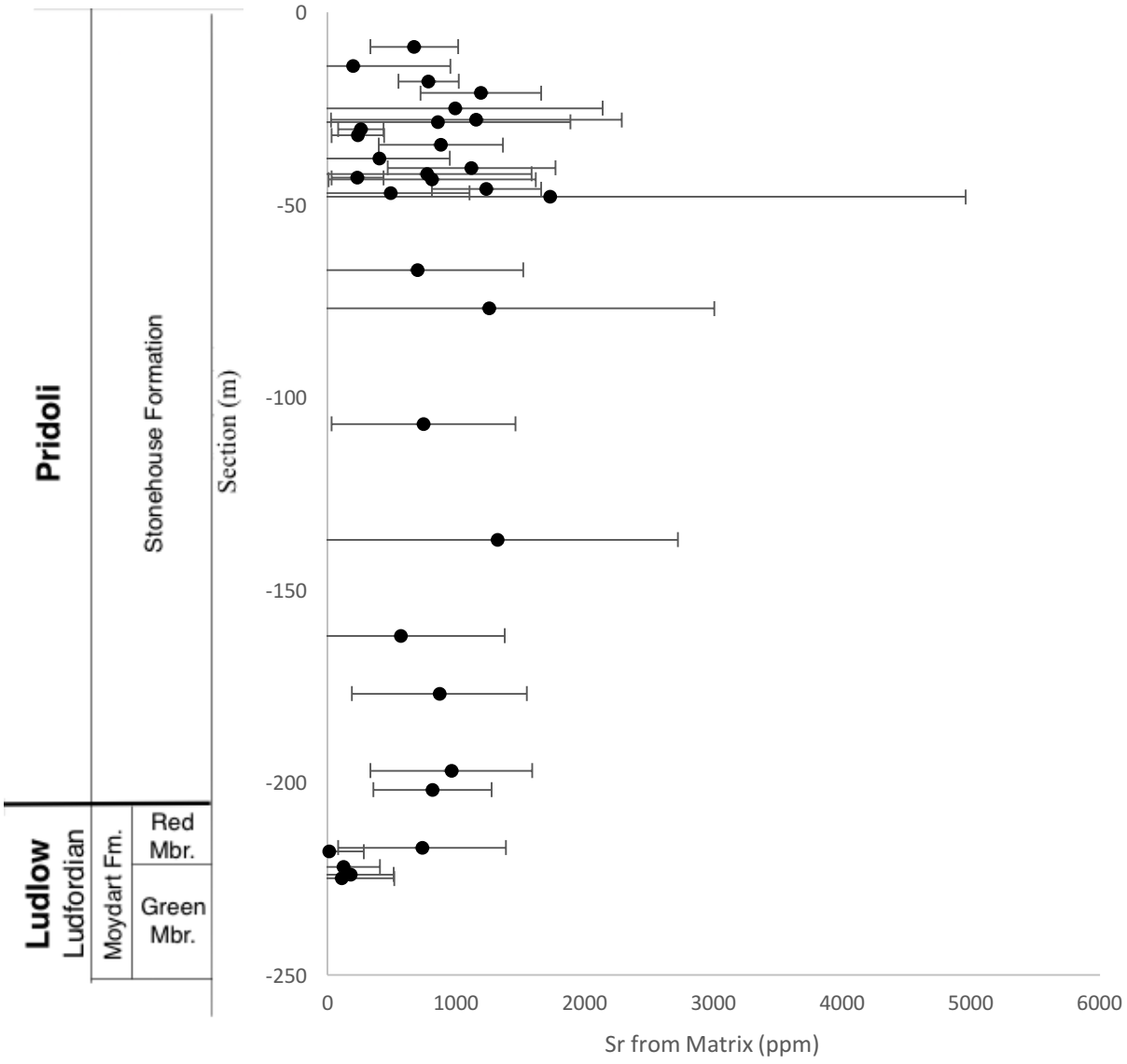

Fig. 4.17. Graph showing the concentration of strontium in parts per million of matrix material plotted against the stratigraphic location of samples from the Arisaig Group, Arisaig Nova Scotia, Canada. 0m corresponds to the top of the Stonehouse Formation. Error bars correspond to one standard deviation.

4.3 Modeling

Sr/Ca ratios (Fig. 4.18) display low values in the middle Moydart Formation with an observable increase near the Stonehouse/ Moydart boundary. Data at the top of the Stonehouse formation are extremely scattered, possibly due to the relatively high concentration of samples in this area. The Mg/Ca ratio (Fig. 4.19) is much more positive and shows indisputably of high values in the Moydart formation, decreasing sharply just above the Stonehouse/ Moydart boundary, followed by a positive slope to the middle Stonehouse Formation where it reaches a peak value only to decrease once more near the top of the Stonehouse Formation. As will be discussed later, these peaks and minimums can be attributed to maximum and minimum paleo temperature values, respectively.

The calculated data for temperature with respect to magnesium concentration are summarized in table 4.1. As expected, the concentration of magnesium in fossil material was found to increase significantly with increased paleotemperature. These results are shown with respect to stratigraphy in figure 4.12. The trend observed shows a temperature near 24 degrees Celsius within the Moydart Formation, decreasing by about five degrees at the Moydart/ Stonehouse boundary in the late Ludfordian. This is followed by another increase to a peak of approximately 25 degrees Celsius in the middle Stonehouse Formation. Finally, there is a temperature decrease near the top of the Stonehouse Formation in the Late Pridoli to about twenty degrees Celcius once more.

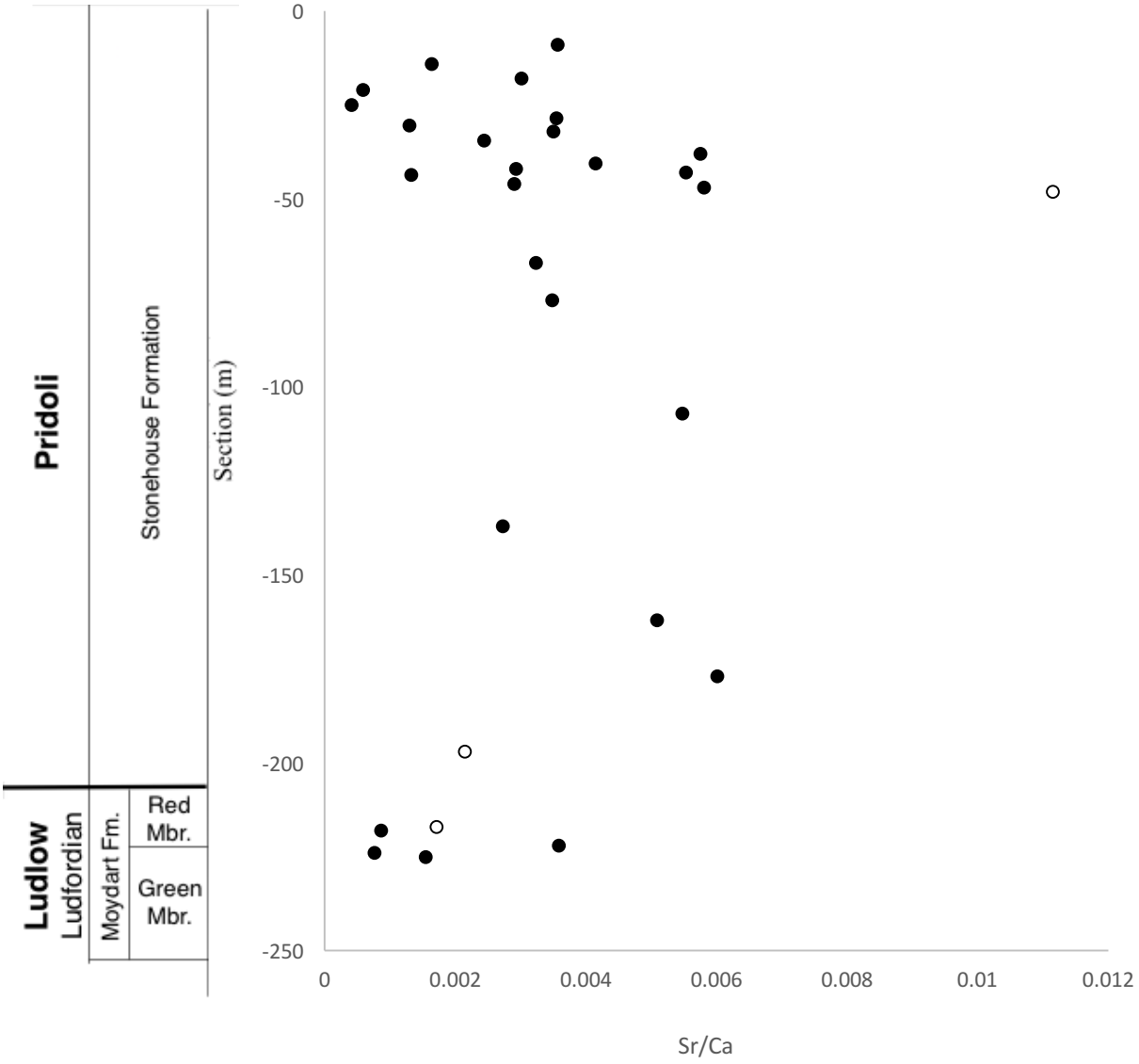

Fig. 4.18. Plot of Sr/Ca ratio from fossil material versus stratigraphic location of samples from the Arisaig Group, Nova Scotia. Open circles correspond to samples that are not pure calcite as seen in Figure 4.7.

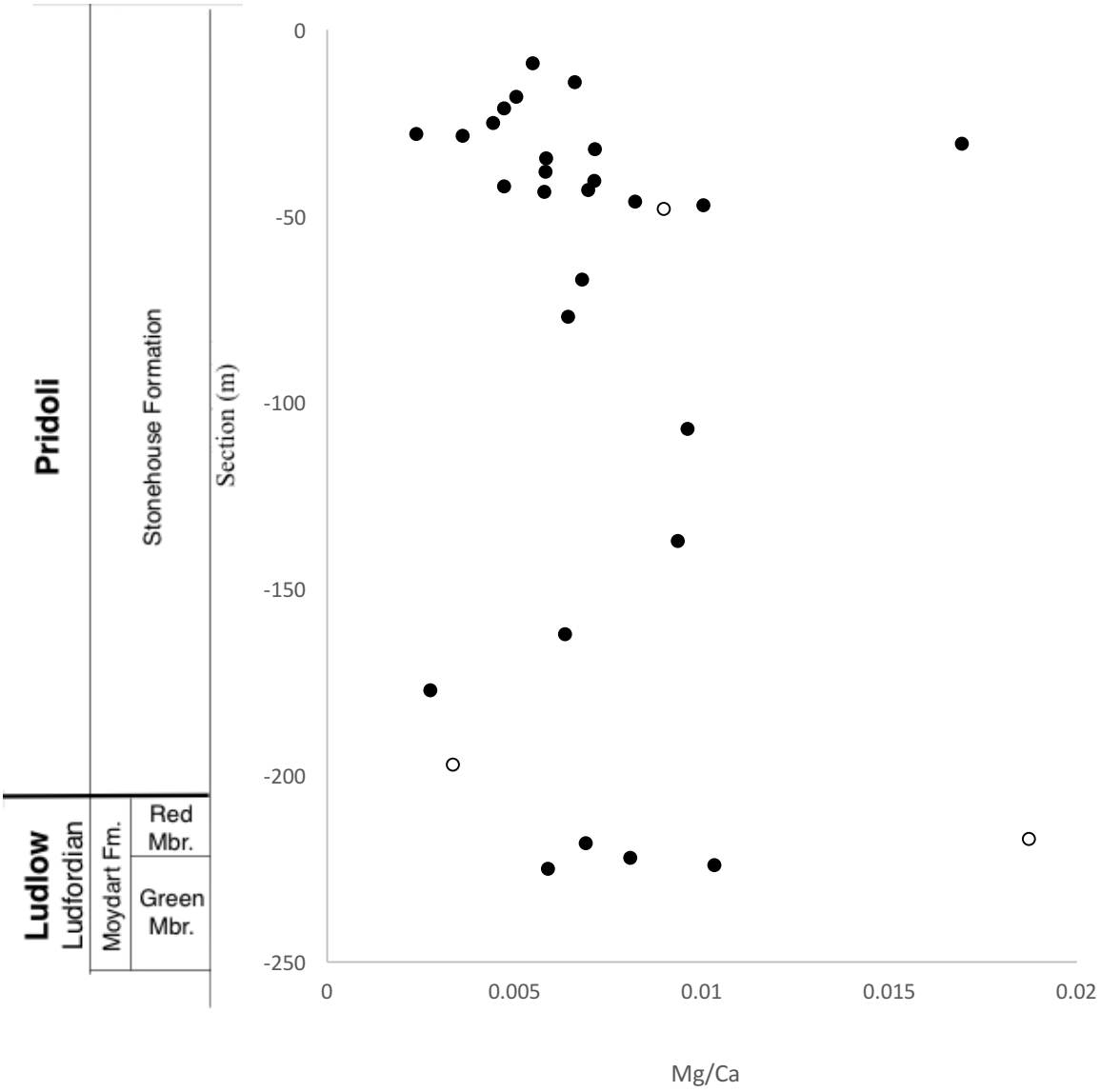

Fig. 4.19. Plot of Mg/Ca ratio from fossil material versus stratigraphic location of samples from the Arisaig Group, Nova Scotia. Open circles correspond to samples that are not pure calcite as seen in Figure 4.7.

Table 4.1. Table showing the results of Mg distribution coefficient calculations with corresponding temperatures and Mg concentrations. These were used to assign paleotemperature values to Mg concentrations observed in samples from the Arisaig Group, Nova Scotia.

Temperature (◦c)	KD Mg	Mg in Fossils (ppm)
17	0.001	135
18	0.005	599
19	0.008	1062
20	0.012	1526
21	0.015	1989
22	0.019	2452
23	0.023	2916
24	0.026	3379
25	0.030	3842
26	0.033	4306
27	0.037	4769
28	0.040	5233
29	0.044	5696
30	0.048	6159

Chapter 5: Discussion

5.1 Chemical Stratigraphy

The data generated from samples with observed primary growth are considered to be the least likely diagenetically altered and therefore the most precise. These unaltered samples are shown in the Mg (Fig. 4.12), Mn (Fig. 4.14) and Sr (Fig. 4.16) as open circles and strongly follow the trends shown by all other sample points. It is therefore assumed that these plots provide an accurate representation of the geochemical signatures that would be present before diagenesis throughout this section. Thus, figures 4.18 and 4.19 showing plots of Sr/Ca and Mg/Ca from fossil material revealing observable trends can be presumed to display valid paleoenvironmental fluctuations. Since Sr/Ca has been shown to decrease with increasing water depth in benthic foraminifera (Elderfield et al. 1996), we can conclude from the trend in figure 4.18 that there is a local shallowing of water located towards the top of the Stonehouse formation and then again at the bottom of the Stonehoue Formation and uppermost Moydart Formation. This is consistent with known sedimentological studies (Lane and Jensen 1975, Boucot et al. 1974) as well as our own field observations that indicate a regression sequence in the Uppermost Moydart Formation and lower Stonehouse Formation. This is followed by a transgression into the middle Stonehouse Formation. Finally, this transitions to another regression in the upper Stonehouse Formation.

The Mg/Ca ratio provides a proxy for paleotemperature and it is evident from figure 4.19 alone that there have been pronounced fluctuations in temperature over geologic time in this section. Mg uptake in fossil shells increases with temperature (Hoogakker et al. 2009). Therefore, it follows that there was a relatively warm climate during the Ludlow followed by a cooling as marine regression took place at the uppermost Moydart Formation into the lower Stonehouse Formation in the Early Pridoli. The climate warms again in the Middle Pridoli then cools slightly towards the Upper Stonehouse Formation. This prediction agrees with the quantitative data produced for the paleotemperature of the section (Fig. 4.12). From figure 4.12, we can clearly see a five-degree fluctuation in temperature accompanying the marine transgression and regression cycles. Since none of the samples show structural or compositional evidence for dolomitization, which would indicate a diagenetic increase in Mg, we assume that

these Mg data yield accurate paleotemperature approximations.

Distribution coefficients for Sr did not yield data in the range that we would expect if we were to apply it as a temperature indicator for the Silurian and did not correlate with the data generated from the Mg concentrations. The distribution coefficients that arose for Sr varied much less than those for Mg, only by a factor of four. This indicates that for our calculations, an extremely high Sr concentration would have been needed to produce the temperatures produced from our Mg calculations. The required Sr concentrations would be on the order of about 1000-2000 ppm which is very unlikely to have occurred in our study area. Although Silurian seawater has much lower Mg/Ca ratios since it is more calcic, this still would not account for the dramatic increase in Sr that we see here. It is therefore presumed that Sr uptake in these samples in controlled by factors other than temperature. There are several influences that could be contributors to this. Growth rate, salinity, organism type and pH a few examples (Bond et al. 2005, Gabitov and Watson 2006). Additionally, even minor diagenetic alteration can produce significant shifts in the Sr content of calcite (Vahrenkamp and swart 1990, Al-Aasm and Packard 2000). As will be discussed below, there is minor diagenetic alteration in our samples which could be contributing to the high Sr content observed.

5.2 Relevance to Silurian Carbon Isotope Excursions

Mg/Ca ratios (Fig. 4.19) as well as Sr/Ca data (Fig. 4.18) indicating local environmental change show significant changes in the top 50m of the Stonehouse Formation (Pridoli) and the Moydart Formation (Ludlow). It is possible that these conditions of marine regression and cooling followed by and transgression and warming could contribute to the onset of Silurian Carbon Isotope Excursion (SCIE) events. One known SCIE occurs at the Silurian/ Devonian boundary. The decrease in concentration of Mg and Sr in the uppermost Stonehouse Formation, located at the end of the Pridoli, reflects some manner of environmental shift that may have contributed to the onset of SCIE in this area. These same lower levels of Mg and Sr occurs once again within the Ludfordian Moydart Formation. This is dated to the upper Ludlow Epoch, in which another SCIE is located. The Late Ludfordian excursion event is nearly twice as large as that of the S/D boundary, $\partial^{13}C$ being about 10‰ as opposed to approximately 6‰ at the S/D

boundary (Munnecke et al. 2003). Therefore, we may expect to see stronger signals in these areas. However, only five samples were taken from the Moydart Formation as opposed to almost twenty from the Upper Stonehouse Formation alone. Because of this, our results may lack a thorough description of the Ludlow conditions.

5.3 Diagenesis

From experiments, dolomite is known to form under higher temperatures than calcite and is rarely produced at ambient temperatures (Montes-Hernandez et al. 2016). Since dolomite is minor compared to calcite in these samples, it is very likely that the small amount of dolomite observed is the result of minor diagenetic alteration. Dolomitization of calcite occurs in the presence of fluids rich in magnesium (Jacquemyn et al. 2014). The marine setting of the Arisaig Group with its abundant shelled fossils provides a wealth of Mg-rich material which can undergo dissolution and be incorporated into fluid during diagenesis (Montes-Hernandez et al. 2016).

In addition to the secondary crystallization textures observed under microscopy, the elevated elemental concentrations of Fe and Mn further indicate that diagenesis has taken place in these samples. Nearly every sample had concentrations of Fe and Mn well above the limit of unaltered material suggested by Bruckschen et al. (1995). However, the numerical limits provided by Bruckschen et al. (1995) were established for modern brachiopods. Because of the comparatively elevated Fe and Mn concentrations in Silurian seawater, higher values are expected in the Silurian samples from Arisaig. Instead, it is more useful to contrast the Sr and Mn contents of the material such as in figure 5.1. Since we can observe primary growth textures in most samples, we assume that any diagenesis taken place has been minimal. Samples that display only primary growth structures are shown in figure 5.1 as open circles. These are clustered around low Mn values, ~0-5000 ppm, and high Sr values, ~1250-2000 ppm. This provides us with a minimum standard area on the Mn vs Sr plot for where we would expect unaltered material from the Arisaig group to plot. As we can see in Figure 5.1, most samples plot very close to this standard minimum area. However, there are several samples that plot at very low Sr values and high Mn values. These samples are undoubtedly altered. From this, it is indisputable that there have been diagenetic effects in the Arisaig area to some extent. However,

most of the data plots near or within the range expected for unaltered material. Additionally, observable primary growth features are in many of the samples and the discussed geochemical trends are consistent with known paleoenvironmental conditions in the area. This suggests that the extent of diagenesis is minimal and is likely limited to zones of diagenetic alteration within rock strata. Additionally, when the geochemical data of the bulk samples are compared with samples that are known to have not undergone diagenesis, as indicated by the presence of only primary growth textures(Fig. 4.12, 4.14, 4.16), the unaltered data lies comfortably within the overall trends of the bulk data. This suggests that the influence of diagenesis on the composition of the fossil material is minimal.

Additionally, the Stonehouse Formation is overlain by basaltic flows which could have generated the elemental concentrations we observe. However, no evidence of contact with igneous material was noted in the study area. From this, we conclude that the minor diagenetic effects observed in many of our samples can likely be attributed to diagenesis due to the overlying igneous intrusions that has caused a very minor effect on the rocks, concentrated in limited zones of diagenetic changes. Consequently, any future studies regarding the $\partial^{18}O$ stable isotope analysis of the Arisaig Group should provide reliable data, provided the selected study material displays textural and geochemical characteristics indicating that diagenesis has not occurred, following the results mentioned above.

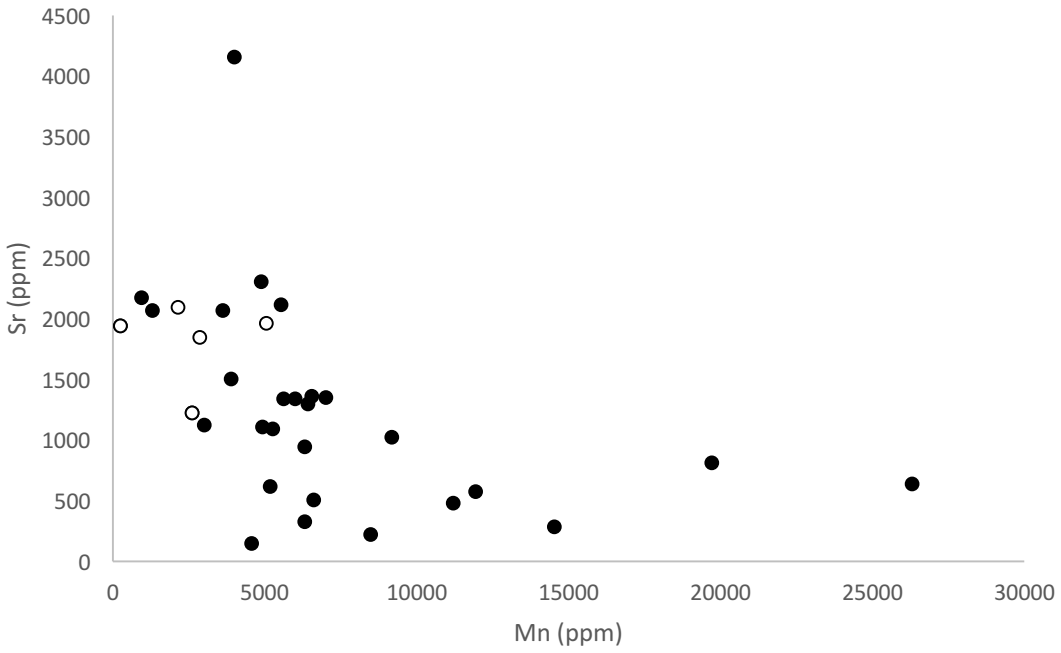

Fig. 5.1. Plot of Mn vs Sr from fossil material from the Arisaig Group, Nova Scotia. Open circles correspond to samples that display only primary growth structures and therefore have not been subject to diagenesis. Relatively much lower Sr and much higher Mn values thus indicate the presence of diagenetic alteration in the samples.

Chapter 6: Conclusions and Suggestions

The Arisaig Group of North Western Nova Scotia has had a significant amount of climactic variation through the late Ludlow and the Pridoli epochs of the Silurian. Chemical stratigraphy and modelling have shown that there is a marine regression in the Landoverian Moydart Formation, followed by a transgression and warming in the middle Pridoli of the Stonehouse Formation. Then, another regression along with cooling occurs near the end of the Pridoli. Additionally, analysis of elemental concentrations as well as micro textural examination has shown that the rocks of the Arisaig Group are slightly altered and have undergone recrystallization throughout the stratigraphic section. However, data suggest that diagenesis is very minor and is limited to zones of diagenetic alteration. There remains an abundance of material within the section that has not been diagenetically altered to an extent that would skew geochemical paleoenvironmental indicators.

The observed regression and cooling episodes occur in stratigraphy in the locations where two Silurian Carbon Isotope Excursions (SCIE) are known to occur elsewhere on Earth. What's more, our Mg/Ca data matches the global ∂O^{18} data (Azmy et al. 1998). Furthermore, the very low degree of diagenesis in the samples indicates that the Arisaig Group would be an idea study location for future research regarding the stable carbon-13 and Oxygen-18 isotope analysis. An elemental analysis of foraminifera throughout the studied section would also be beneficial. This would help to reinforce paleoclimate data and to add well-defined constraints and robust data to the observed environmental changes in the Arisaig Group. This information would provide essential insights into local environmental conditions during the occurrence of Silurian Carbon Isotope Excursions.

References

Al-Aasm IS, Packard JJ. 2000. Stabilization of early-formed dolomite: a tale of divergence from two Mississippian dolomites. Sediment Geol. 131: 97-108.

Azmy K, Veizer J, Bassett MG, Coper P. 1998. Oxygen and carbon isotopic composition of Silurian brachiopods: Implications for coeval seawater and glaciations. Geol Soc Am Bull. 110(11): 1499-1512.

Beck JH, Strother PK. 2001. Silurian Spores and Crytprospores from the Arisaig Group, Nova Scotia, Canada. Palynology. 25: 127-177.

Bickert T, Pätzold, Samtleben C, Munnecke A. 1997. Paleoenvironmental changes in the Silurian indicated by stable isotopes in brachiopod shells from Gotland, Sweden. Geochim Cosmochim Ac. 61(13): 2717-2730.

Bond ZA, Cohen AL, Smith SR, Jenkins WJ. 2005. Growth and composition of high-Mg calcite in the skeleton of a Bermudian gorgonian (*Plexaurella dichotoma*): Potential for paleothermometry. Geochem Geophy Geosy. 6(8): 10p.

Boucot AJ, Dewey JF, Dineley DL, Fletcher R, Fyson WK, Griffin JG, Hickox CJ, McKerrow WS, Zeigler AM. 1974. Geology of the Arisaig area, Antigonish County, Nova Scotia. Geol Soc Am Spec Pap. 139: 191p.

Brennan ST, Lowenstein TK. 2002. The major-ion composition of Silurian seawater. Geochim Cosmochim Ac. 66(15): 2683-2700.

Bruckschen P, Bruhn F, Meijer J, Stephan A, Veizer J. 1995. Diagenetic alteration of calcitic fossil shells: Proton microprobe (PIXE) as a trace element tool. Nucl Instrum Meth B. 104: 427-431.

Calner M, Kozlowska A, Masiak M, Schmitz B. 2006. A Shoreline to deep basin correlation chart for the middle Silurian coupled extinction-stable isotopic event. GFF. 128: 79-84.

Cocks LRM, Scotese CR. 1991. The global biogeography of the Silurian Period: Spec Pap Palaeontol. 44: 109-122.

Cramer BD, Saltzman MR. 2005. Sequestration of ^{12}C in the deep ocean during the early Wenlock (Silurian) positive carbon isotope excursion. Palaeogeogr Palaeocl. 219: 333-349.

Cramer BD, Saltzman MR. 2007. Fluctuations in epeiric sea carbonate production during Silurian positive carbon isotope excursions: A review of proposed paleooceanographic models. Palaeogeogr Palaeocl. 245: 37-45.

Dymond J, Suess E, Lyle M. 1992. Barium in deep-sea sediment: a geochemical proxy for paleoproductivity. Paleoceanography. 7(2): 163-181.

Elderfield H, Bertram CJ, Erez J. 1996. A biomineralization model for the incorporation of trace elements into foraminiferal calcium carbonate. Earth Planet Sc Lett. 142: 409-423.

Epstein S, Buchsbaum R, Lowenstam HA, Urey HC. 1953. Revised carbonate-water isotopic temperature scale. Bull Geol Soc Am. 64: 1315-1326.

Gabitov RI, Watson EB. 2006. Partitioning of strontium between calcite and fluid. Geochem Geophy Geosy. 7(11): 12p.

Grahn YG, Caputo MV. 1992. Early Silurian glaciation in Brazil. Palaeogeogr Palaeocl. 99: 9-15.

Hilldebrand DC. 1998. Elemental ratio determination via ICP-MS and DCP-AES: methodology to extract climate records from coral aragonite [Master's Thesis]. [Tampa, Florida]: University of South Florida.

Hoogakker BAA, Klinkhammer GP, Elderfield H, Rohling EJ, Hayward C. 2009. Mg/Ca paleothermometry in high salinity environments. Earth Planet Sc Lett. 284: 583-589.

Hurst JM, Pickerill RK. 1986. The relationship between sedimentary facies and faunal associations in the Llandovery siliciclastic Ross Brook Formation, Arisaig, Nova Scotia. Can J Earth Sci. 23: 705-726.

Jacquemyn C, Desouky HE, Hunt D, Casini G, Swennen R. 2014. Dolomitization of the Latemar platform: Fluid flow and dolomite evolution. Mar Petrol Geol. 55: 43-67.

Johnson ME, Kaljo D, Rong JY. 1991. Silurian eustasy. Spec Pap Paleontol. 44: 145-163.

Keppie JD. 1979. Geological Map of Nova Scotia, 1979. (1:2,000,000). Map ME 1979-4. Nova Scotia, Canada: Nova Scotia Department of Mines and Energy.

Lane TE, Jensen LR. 1975. Stratigraphy of the Arisaig Group. Atl Geol. 11(3): 119-140.

Lear CH, Wilson PA, Shackleton NJ, Elderfield H. 2000. Palaeotemperature and ocean chemistry record for the Palaeogene from Mg/Ca and Sr/ Ca in benthic foraminiferal calcite. GFF, 122:1, 93-93, DOI: 10.1080/11035890001221093

Montes-Hernandez G, Findling N, Renard F. 2016. Dissolution-precipitation reactions controlling fast formation of dolomite under hydrothermal conditions. Appl Geochem. 73: 169-177.

Morrison JO, Brand U. 1986. Geochemistry of Recent Marine Invertebrates. Geosci Can. 13(4): 237-254.

Munnecke A, Samtleben C, Bickert T. 2003. The Ireviken Event in the lower Silurian of Gotland, Sweden- relation to similar Palaeozoic and Proterozoic events. Palaeogeogr Palaeocl. 195(1-2): 99-124.

Murphy JB, Fernández-Suárez J, Jeffries TE. 2004. Lithogeochemical and Sm-Nd and U-Pb isotope data from the Silurian-Lower Devonian Arisaig Group clastic rocks, Avalon terrane, Nova Scotia: A record of terrane accretion in the Appalachian-Caledonide orogen. Geol Soc Am Bull. 116(9/10): 1183-1201.

Murphy JB, Keppie JD, Hynes AJ. 1991. The geology of the Antigonish Highlands, Nova Scotia. Geol Surv Canada Paper. 89-10: 115p.

Raitzsch M, Dueñas-Bórquez A, Reichart AJ, de Nooijer LJ, Bickert T. 2010. Incorporation of Mg and Sr in calcite of cultured benthic foraminifera: impact of calcium concentration and associated calcite saturation state. Biogeosciences. 7: 869-881.

Richter FM, DePaolo DJ. 1987. Numerical models for diagenesis and the Neogene Sr isotopic evolution of seawater from DSDP Site 590B. Earth Planet Sc Lett. 83(1-4): 27-38.

Rosenthal Y, Boyle A, Slowey N. 1997. Temperature control on the incorportaiton of magnesium, strontium, fluorine, and cadmium into benthic foraminiferal shells from Little Bahama Bank: Prospects for thermocline paleoceanography. Geochim Cosmochim Ac. 61(17): 3633-3643.

Saltzman MR. 2002. Carbon isotope ($\delta^{13}C$) stratigraphy across the Silurian-Devonian transition in North America: evidence for a perturbation of the global carbon cycle. Palaeogeogr Palaeocl. 187: 83-100.

Urey HC, Lowenstam HA, Epstein S, McKinney CR. 1951. Measurement of Paleotemperatures and temperatures of the upper Cretaceous of England, Denmark, and the Southeastern United States. Bull Geol Soc Am. 62: 399-416.

Vahrenkamp VC, Swart PK. 1990. New distribution coefficient for the incorporation of strontium into dolomite and its implications for the formation of ancient dolomites. Geology. 18: 387-391.

Waldron JWF, Murphy JB, Melchin MJ, Davis G. 1996. Silurian Tectonics of Western Avalonia: Strain-Corrected Subsidence History of the Arisaig Group, Nova Scotia. J Geol. 104: 677-694.

Appendices

Appendix A

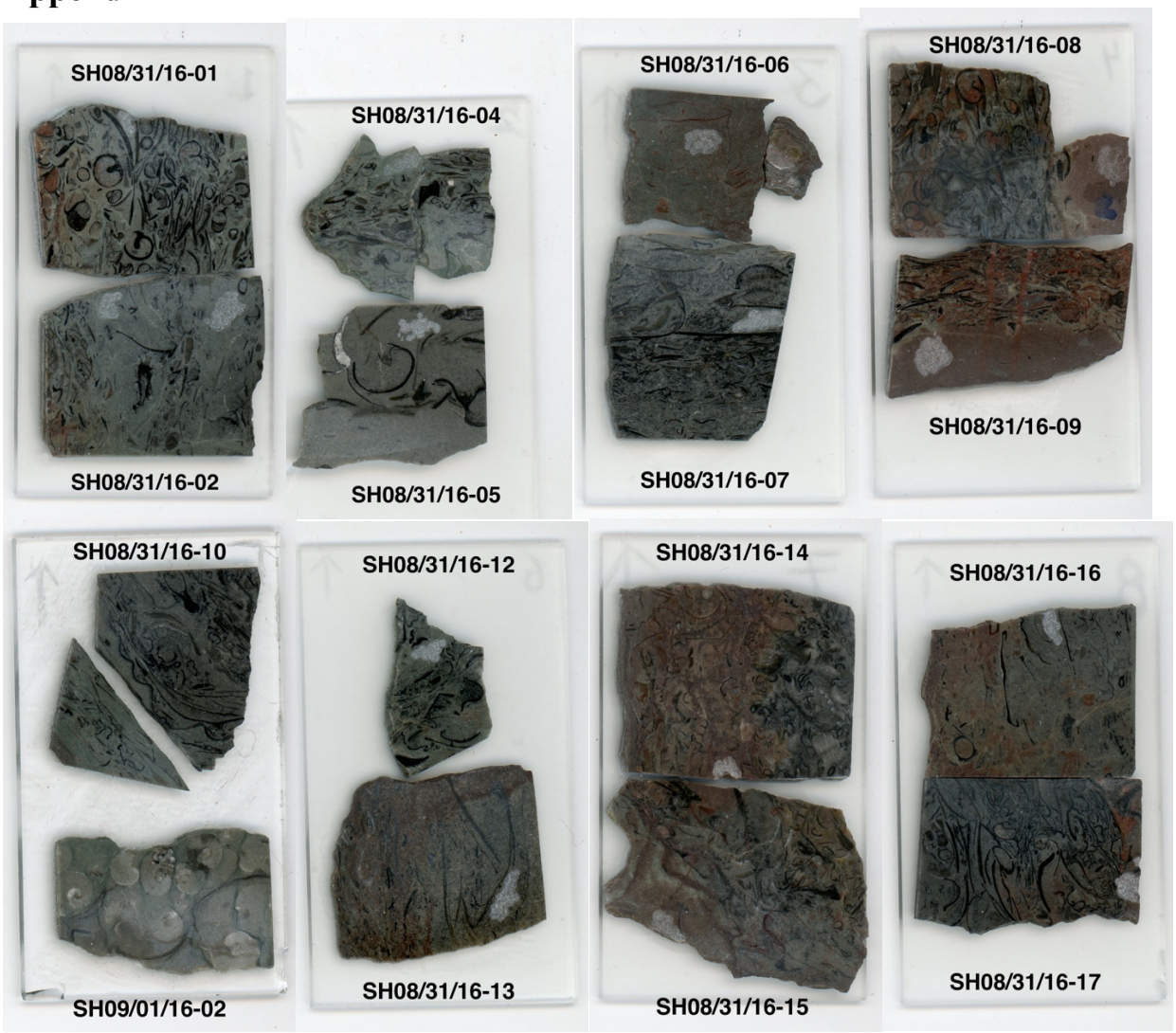


SH09/01/16-15
SH09/01/16-14


SH09/01/16-13
SH09/01/16-12


SH09/01/16-07
SH09/01/16-06


SH08/31/16-11
SH09/01/16-05


SH09/01/16-04
SH09/01/16-03


SH09/02/16-09
SH09/01/16-01


SH09/02/16-08
SH09/02/16-07


SH09/02/16-06
SH09/02/16-05

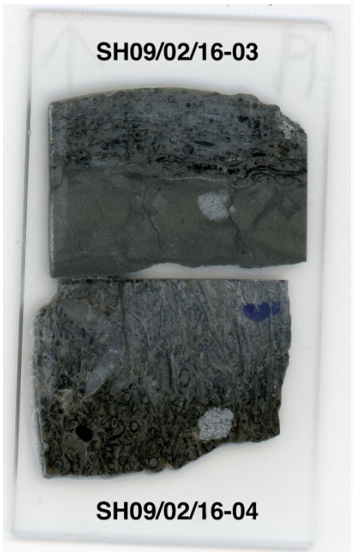
SH09/02/16-03
SH09/02/16-04


SH09/02/16-01
SH09/02/16-02

Appendix B

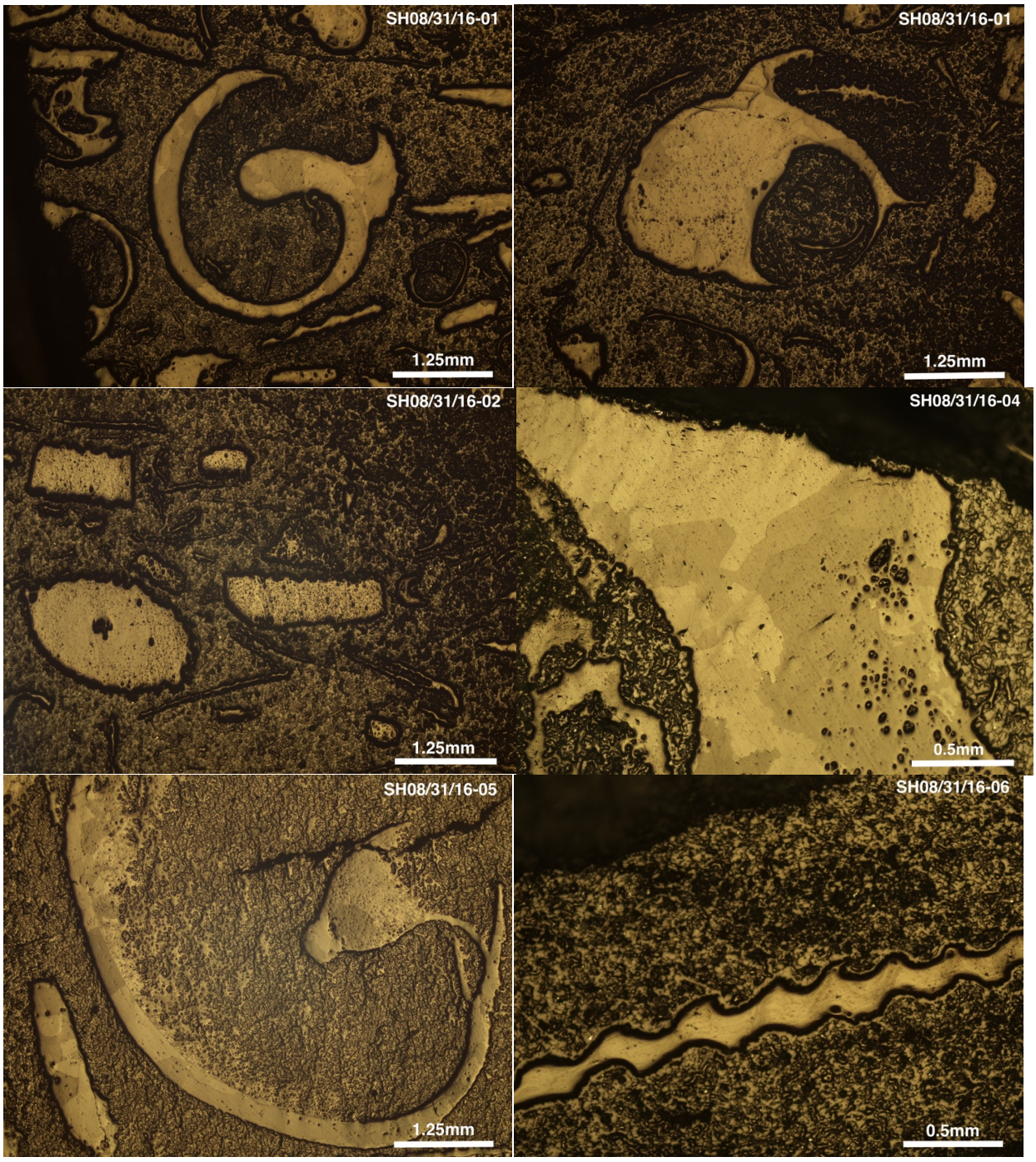
SH08/31/16-01
1.25mm
SH08/31/16-01
1.25mm
SH08/31/16-02
1.25mm
SH08/31/16-04
0.5mm
SH08/31/16-05
1.25mm
SH08/31/16-06
0.5mm

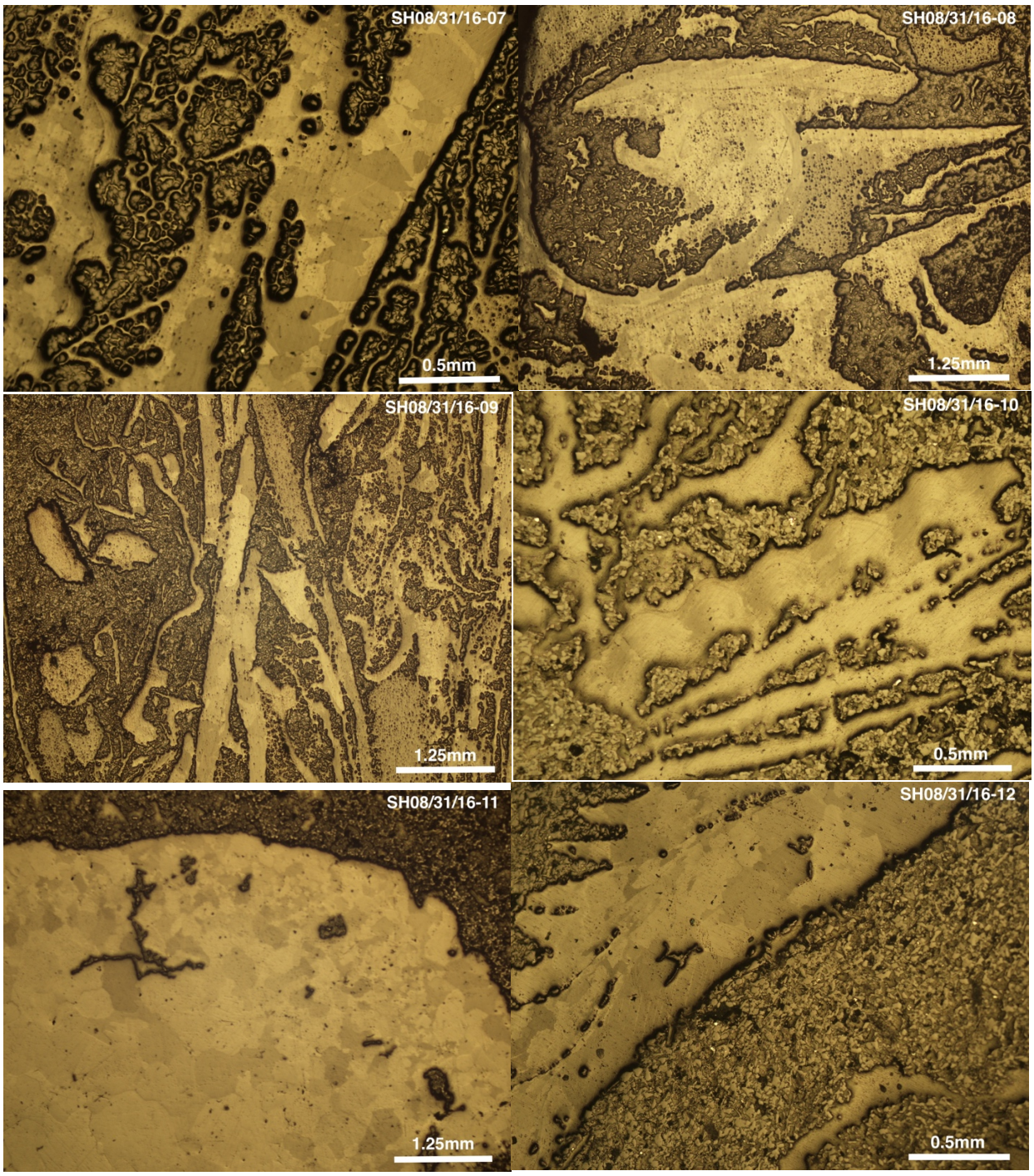
SH08/31/16-07
0.5mm
SH08/31/16-08
1.25mm
SH08/31/16-09
1.25mm
SH08/31/16-10
0.5mm
SH08/31/16-11
1.25mm
SH08/31/16-12
0.5mm

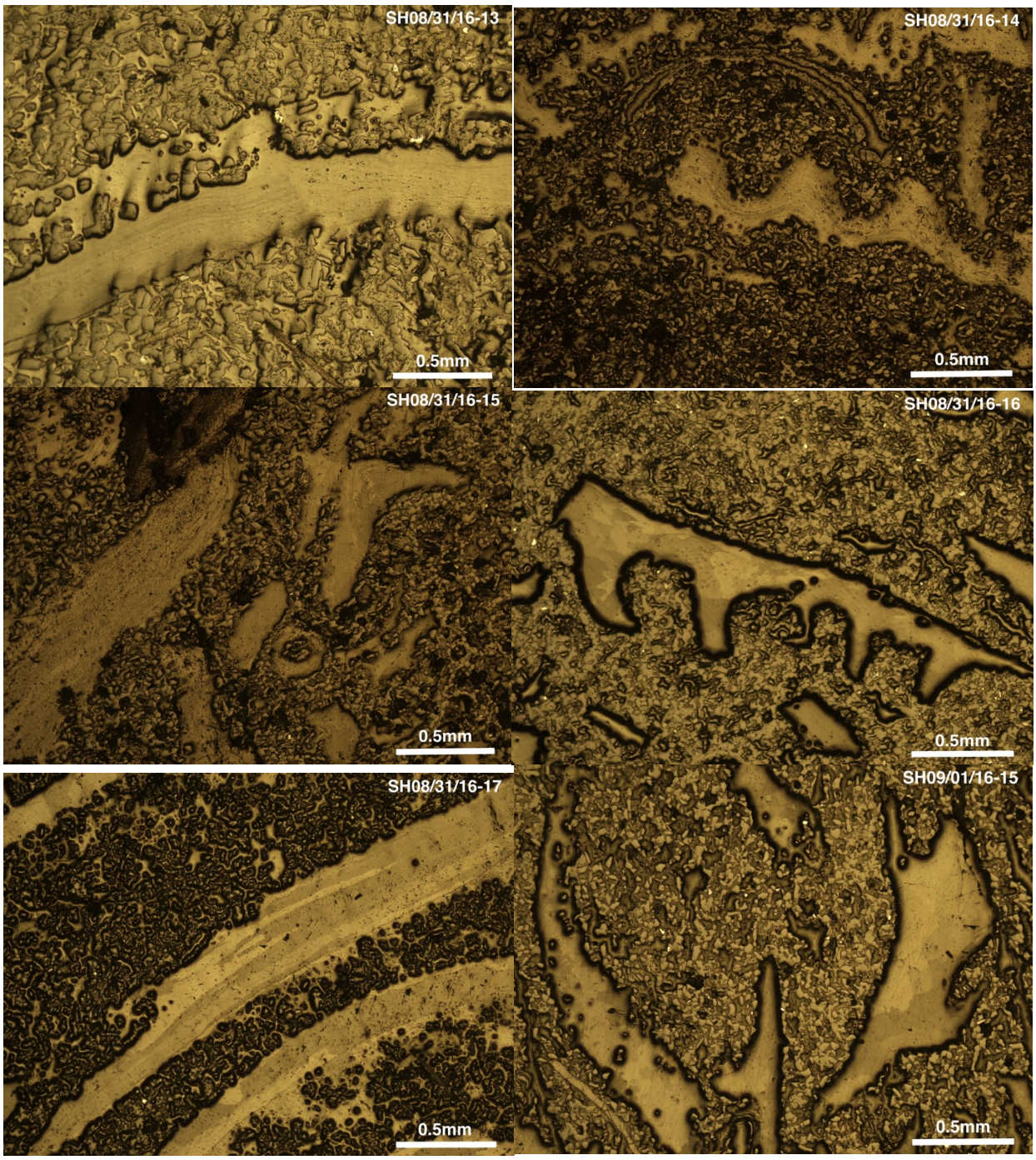
SH08/31/16-13
0.5mm
SH08/31/16-14
0.5mm
SH08/31/16-15
0.5mm
SH08/31/16-16
0.5mm
SH08/31/16-17
0.5mm
SH09/01/16-15
0.5mm

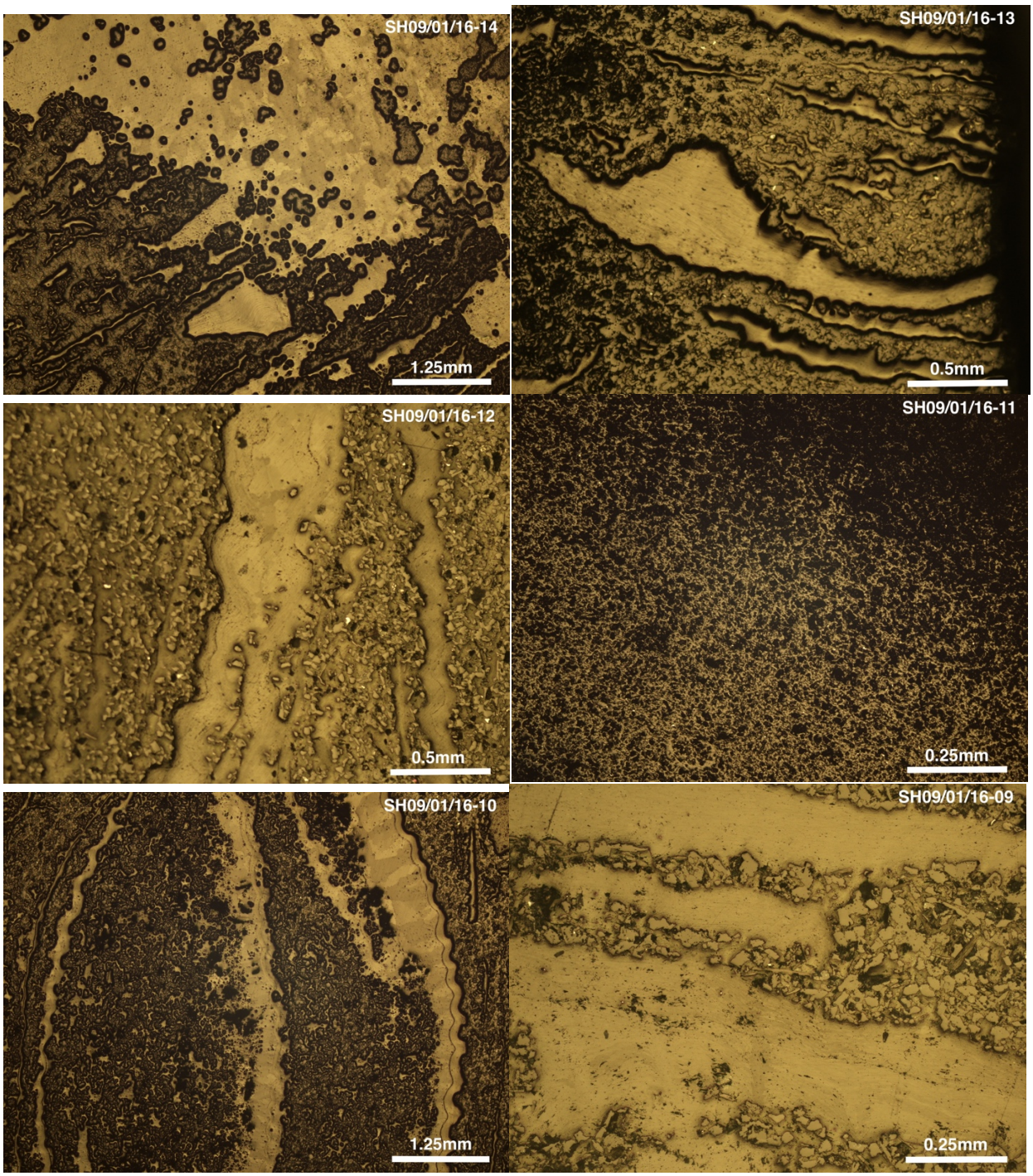
SH09/01/16-14
1.25mm
SH09/01/16-13
0.5mm
SH09/01/16-12
0.5mm
SH09/01/16-11
0.25mm
SH09/01/16-10
1.25mm
SH09/01/16-09
0.25mm

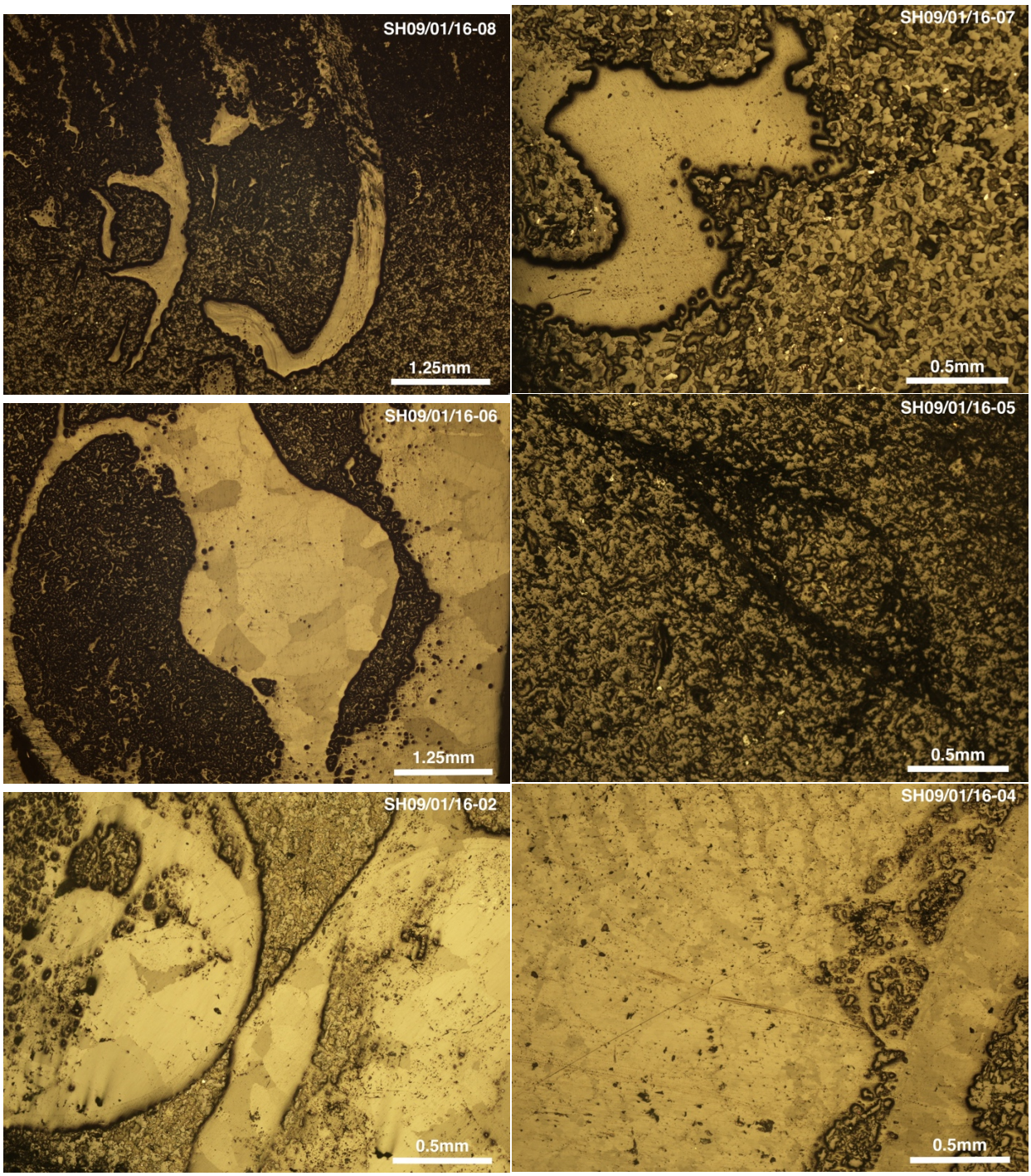
SH09/01/16-08
1.25mm
SH09/01/16-07
0.5mm
SH09/01/16-06
1.25mm
SH09/01/16-05
0.5mm
SH09/01/16-02
0.5mm
SH09/01/16-04
0.5mm

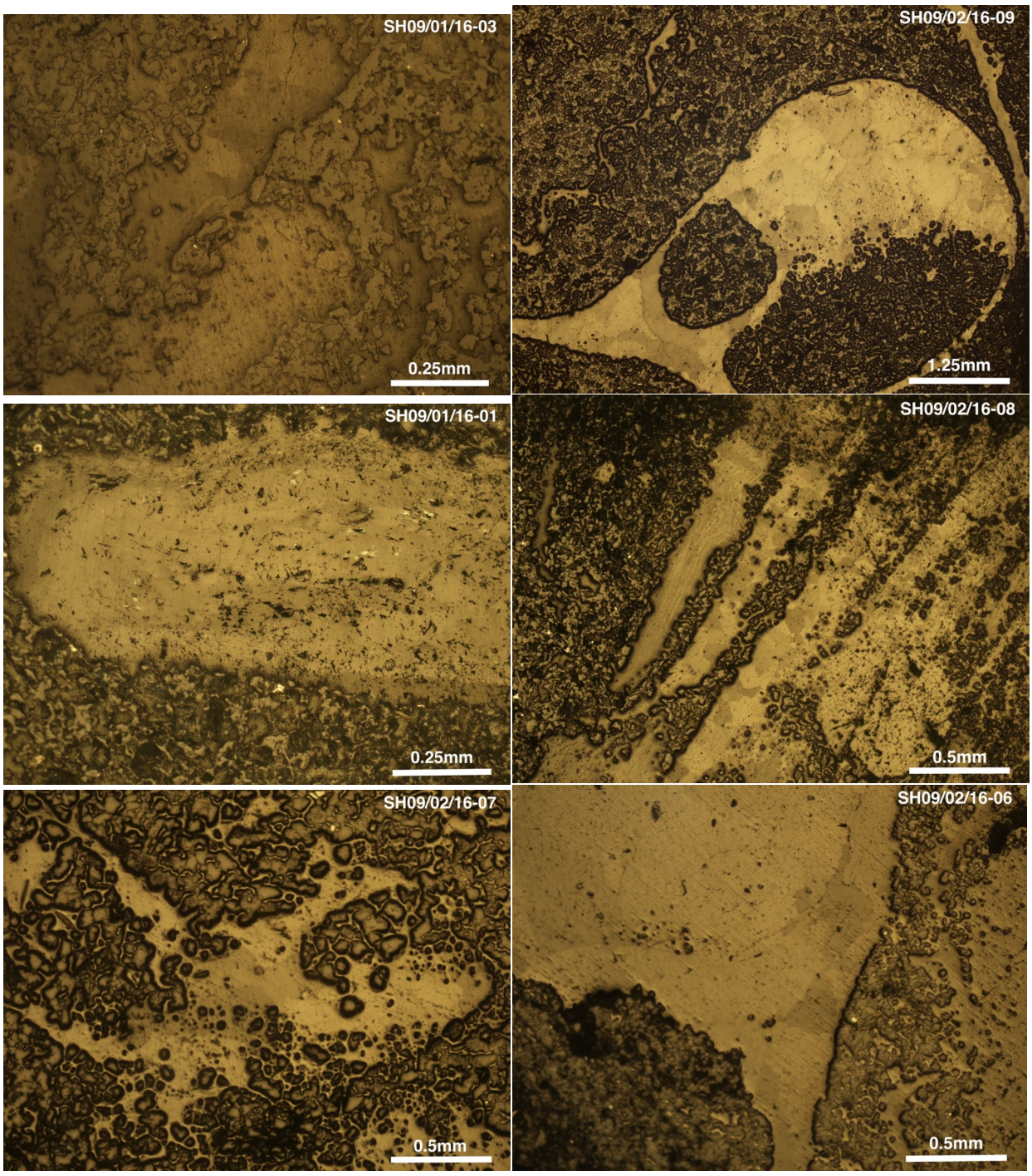
SH09/01/16-03
0.25mm
SH09/02/16-09
1.25mm
SH09/01/16-01
0.25mm
SH09/02/16-08
0.5mm
SH09/02/16-07
0.5mm
SH09/02/16-06
0.5mm

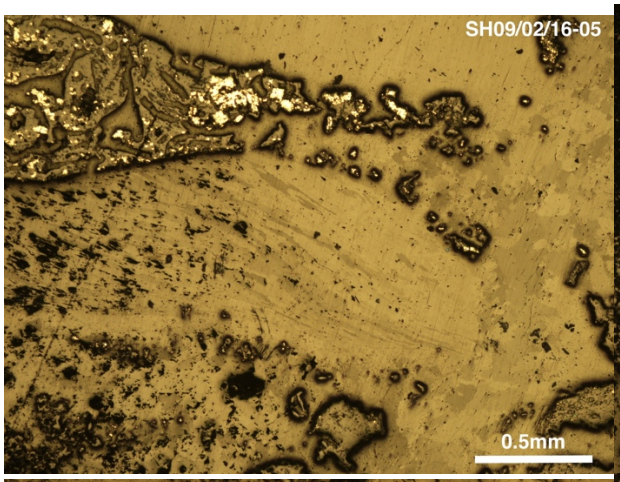
SH09/02/16-05
0.5mm

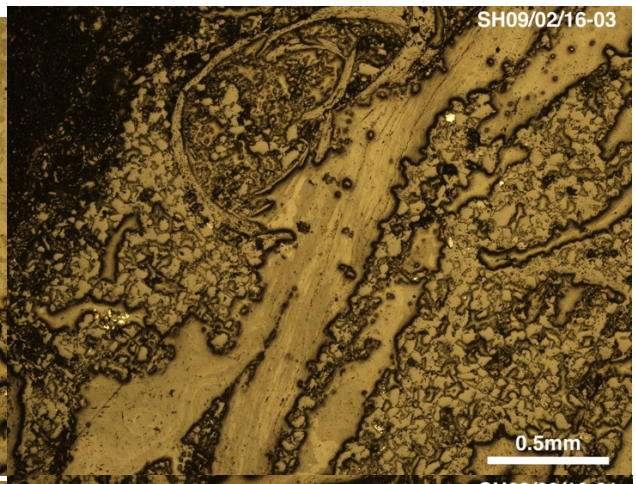
SH09/02/16-03
0.5mm

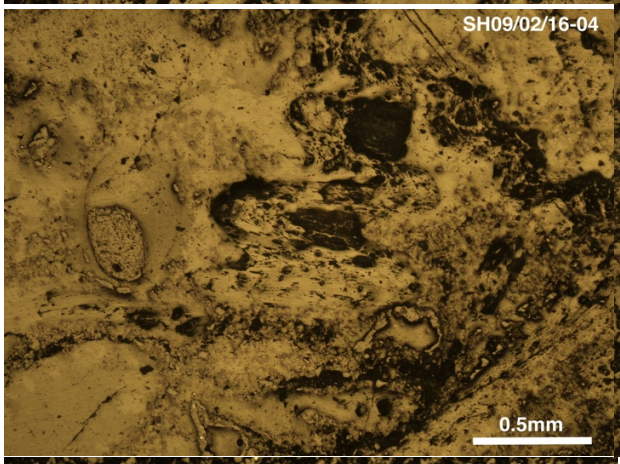
SH09/02/16-04
0.5mm

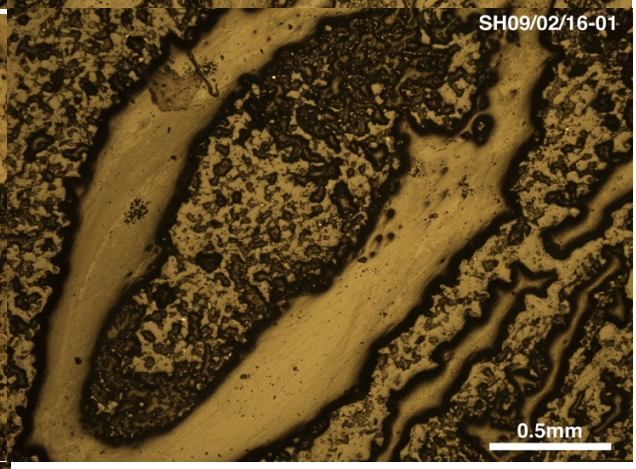
SH09/02/16-01
0.5mm

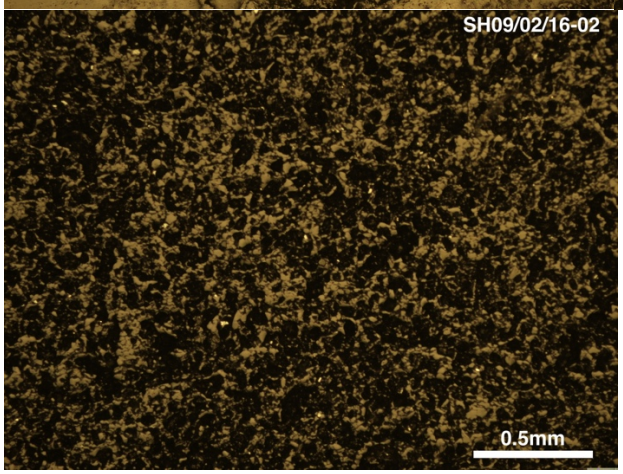
SH09/02/16-02
0.5mm

Appendix C

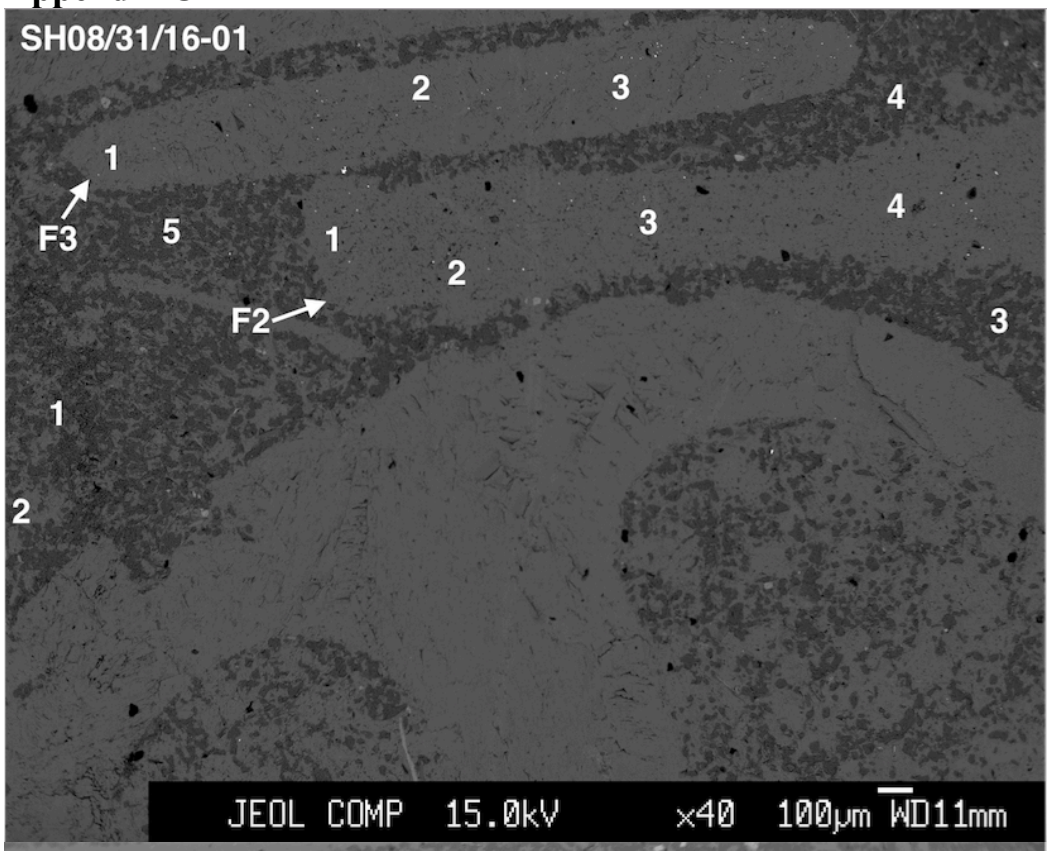
SH08/31/16-01
1
2
3
4
F3
5
1
2
3
4
F2
3
1
2
JEOL COMP 15.0kV x40 100µm WD11mm

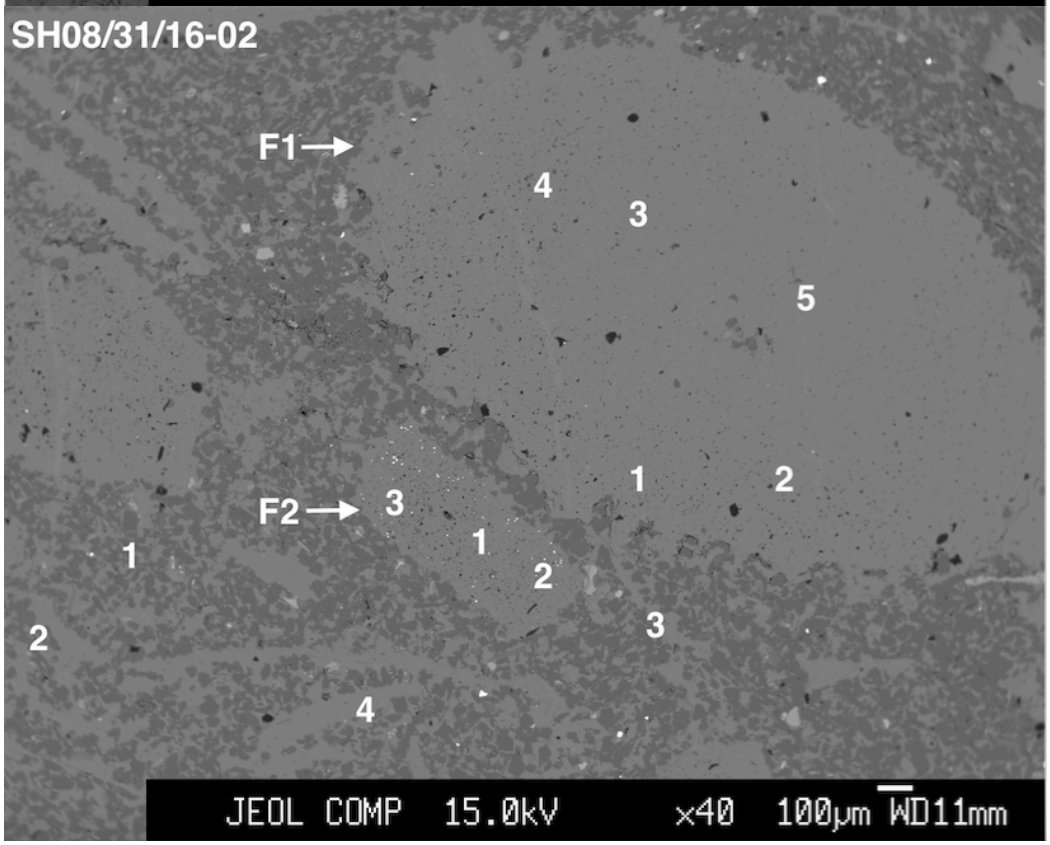
SH08/31/16-02
F1
4
3
5
1
2
F2
3
1
1
2
3
2
4
JEOL COMP 15.0kV x40 100µm WD11mm

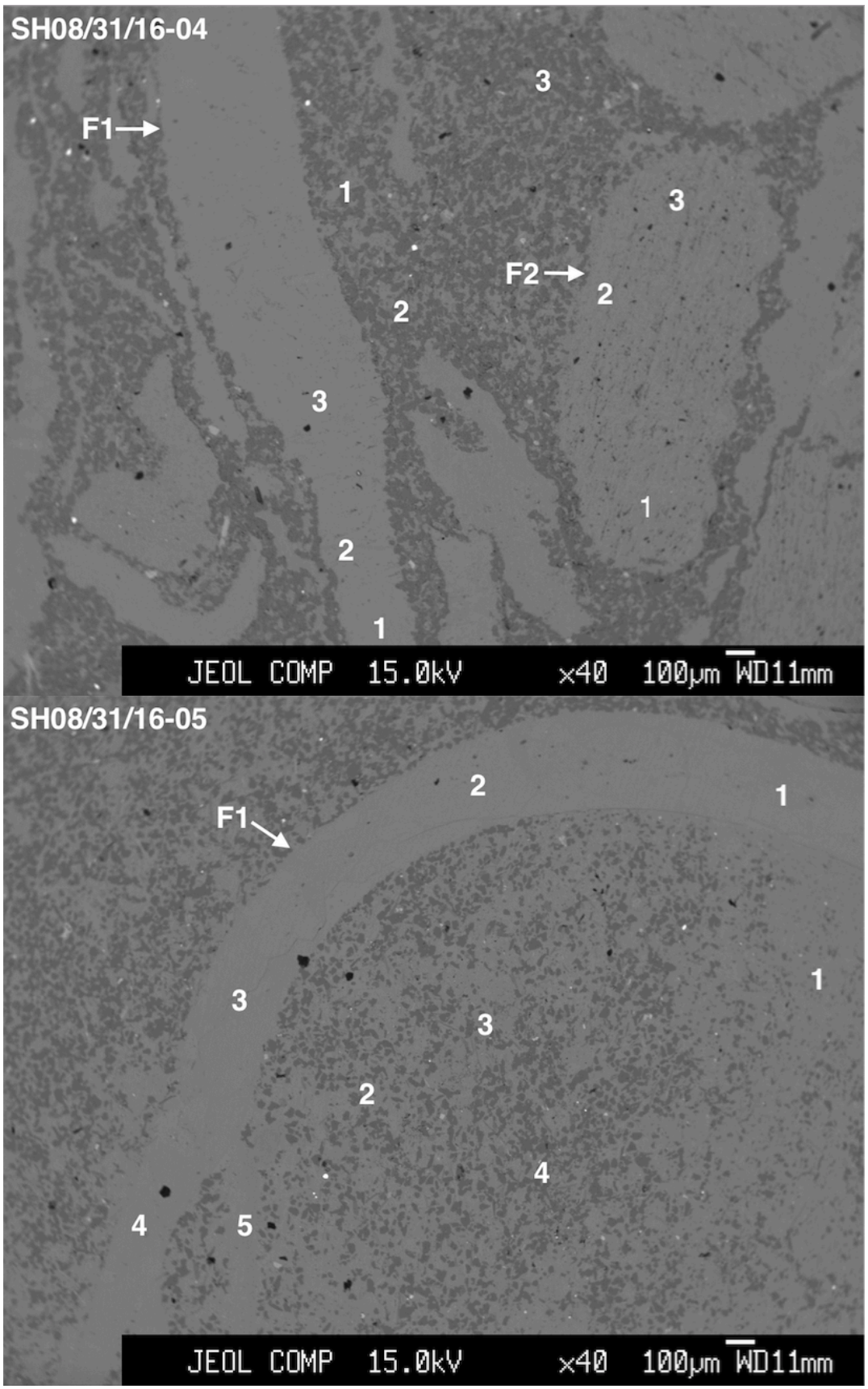
SH08/31/16-04
F1
F2
JEOL COMP 15.0kV x40 100µm WD11mm
SH08/31/16-05
F1
JEOL COMP 15.0kV x40 100µm WD11mm

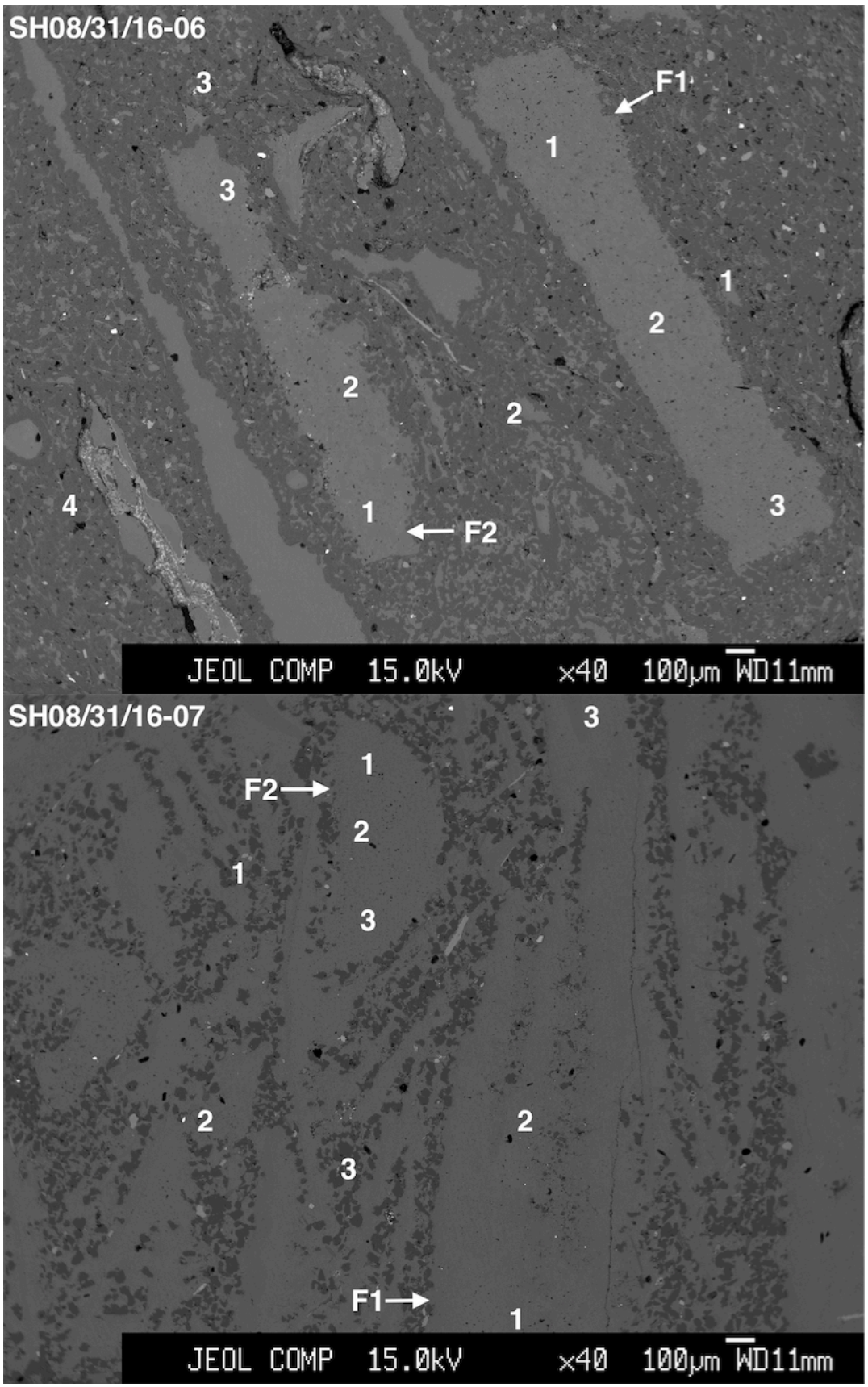
SH08/31/16-06
3
F1
1
3
1
2
2
2
4
1
F2
3
JEOL COMP 15.0kV ×40 100µm WD11mm
SH08/31/16-07
3
1
F2
2
1
3
2
2
3
F1
1
JEOL COMP 15.0kV ×40 100µm WD11mm

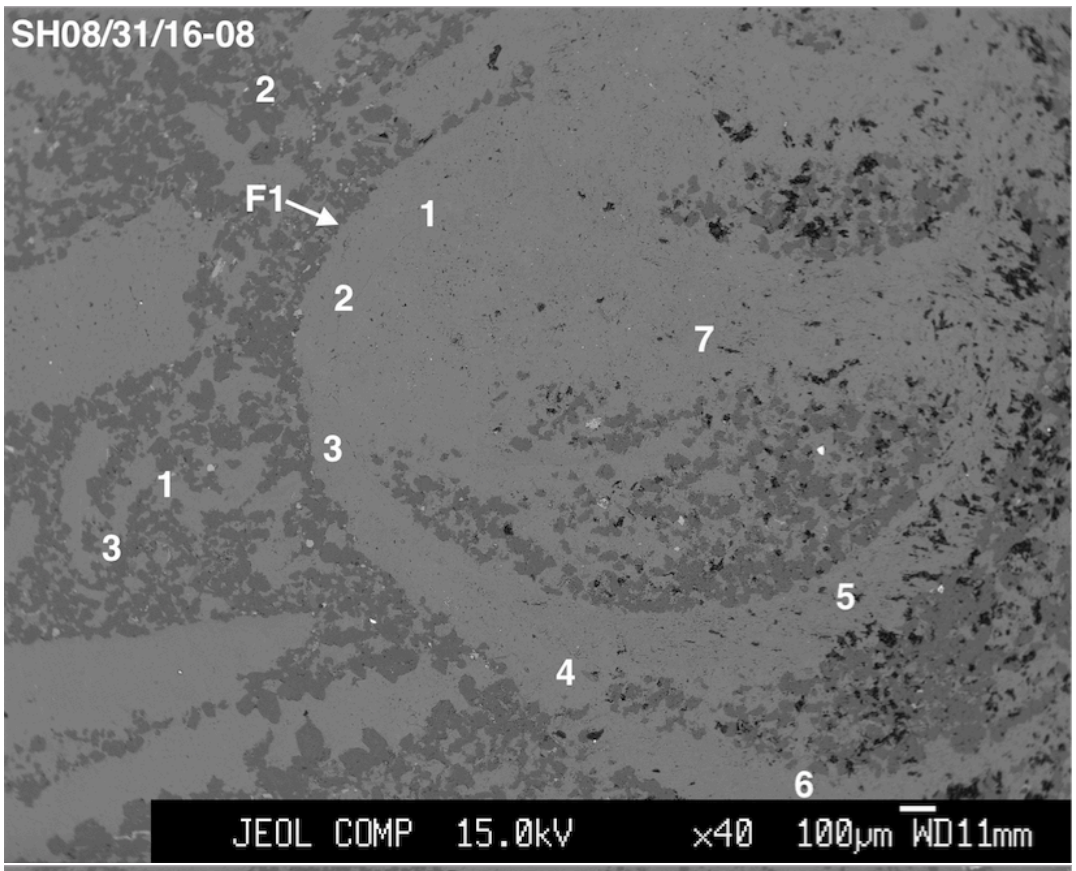
SH08/31/16-08
2
F1
1
2
7
3
1
3
5
4
6
JEOL COMP 15.0kV ×40 100µm WD11mm

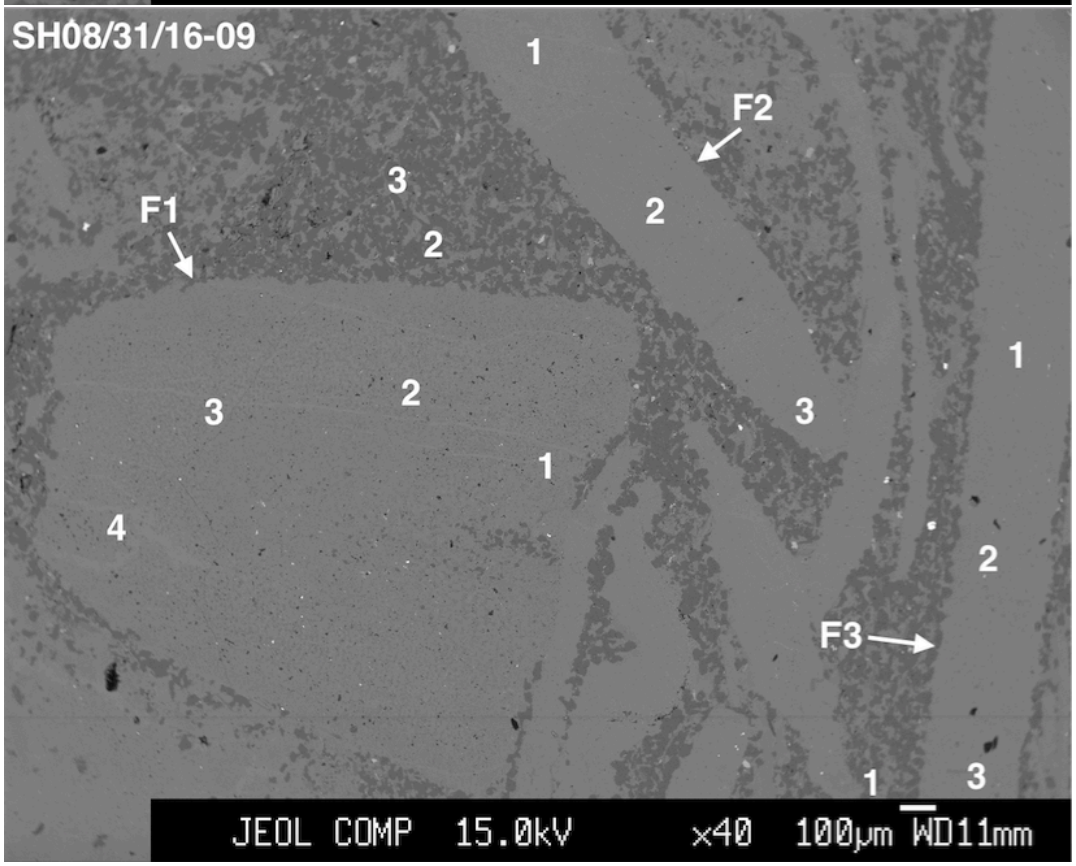
SH08/31/16-09
1
F2
3
F1
2
2
1
2
3
3
1
4
2
F3
1
3
JEOL COMP 15.0kV ×40 100µm WD11mm

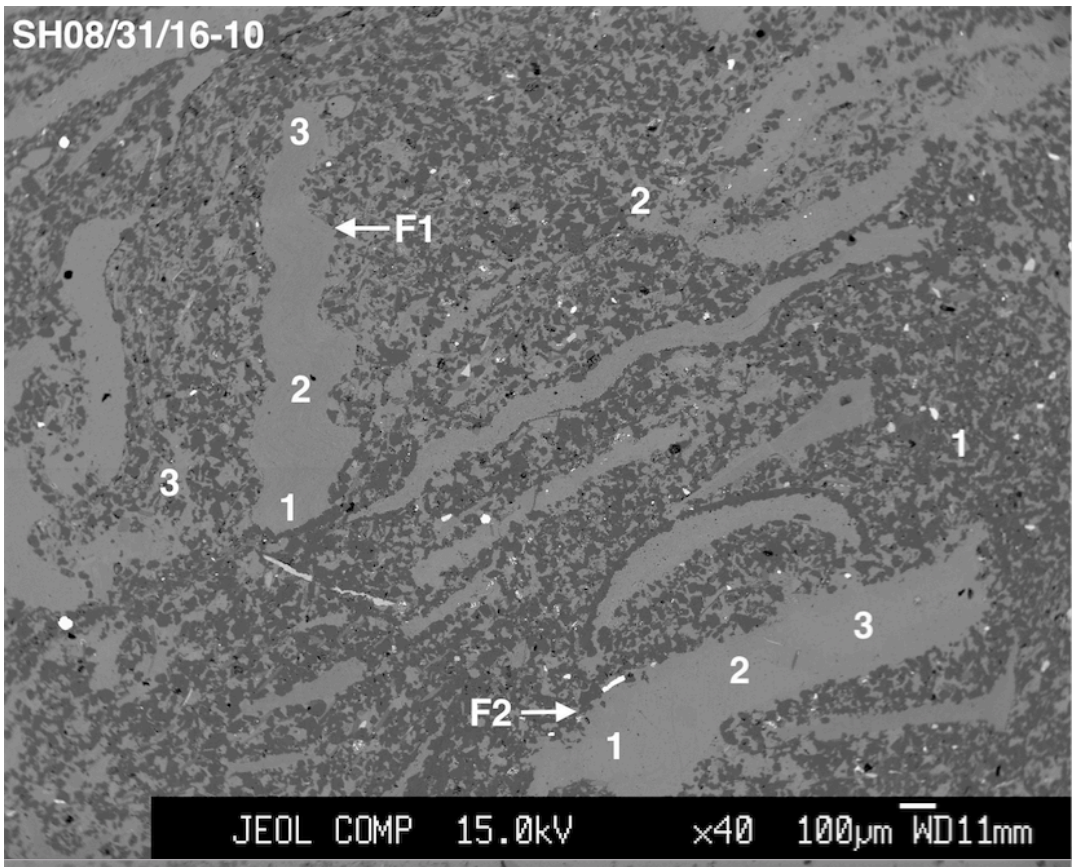
SH08/31/16-10
3
2
F1
2
1
3
1
3
2
F2
1
JEOL COMP 15.0kV x40 100µm WD11mm

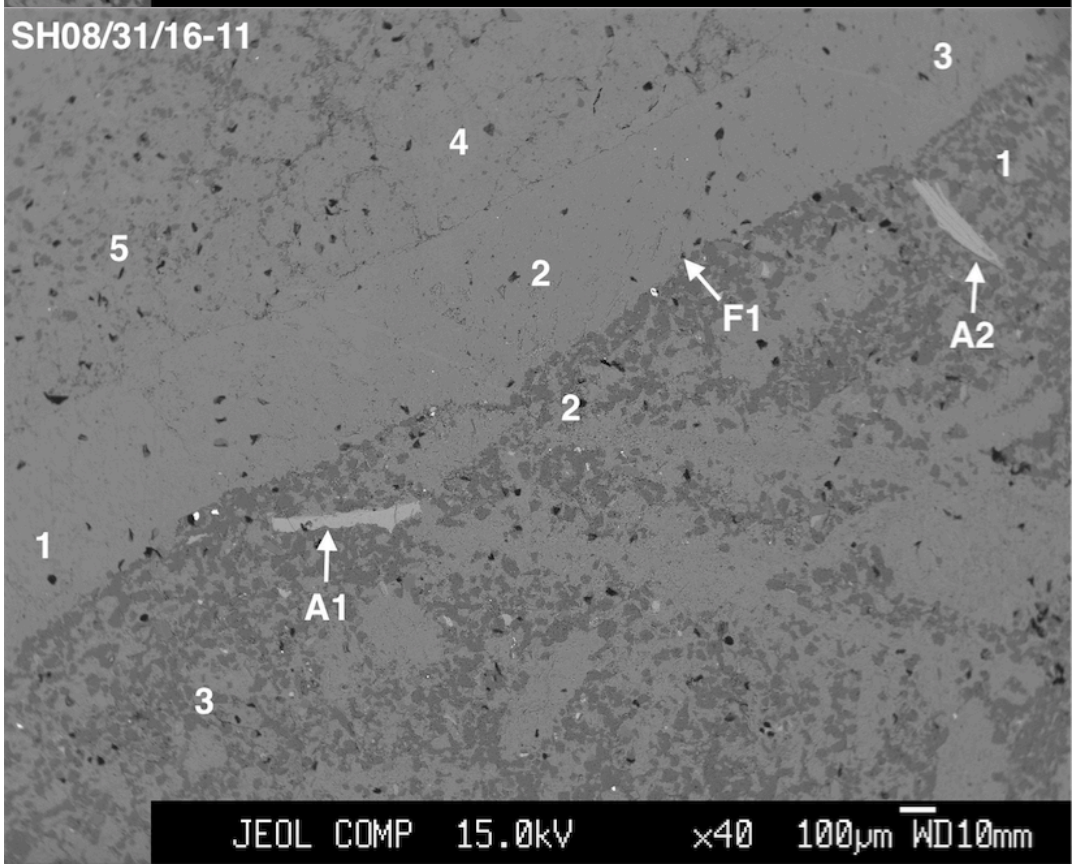
SH08/31/16-11
3
4
1
5
2
F1
A2
2
1
A1
3
JEOL COMP 15.0kV x40 100µm WD10mm

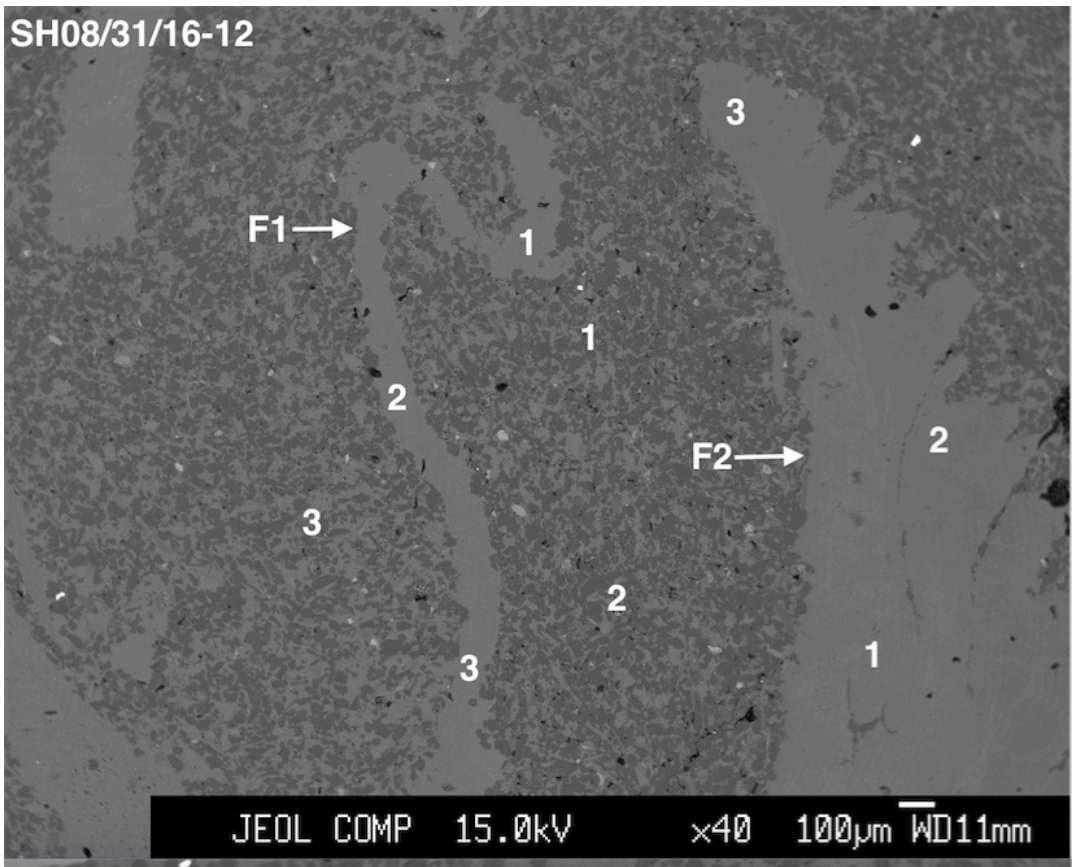
SH08/31/16-12
3
F1
1
1
2
F2
2
3
2
1
3
JEOL COMP 15.0kV ×40 100µm WD11mm

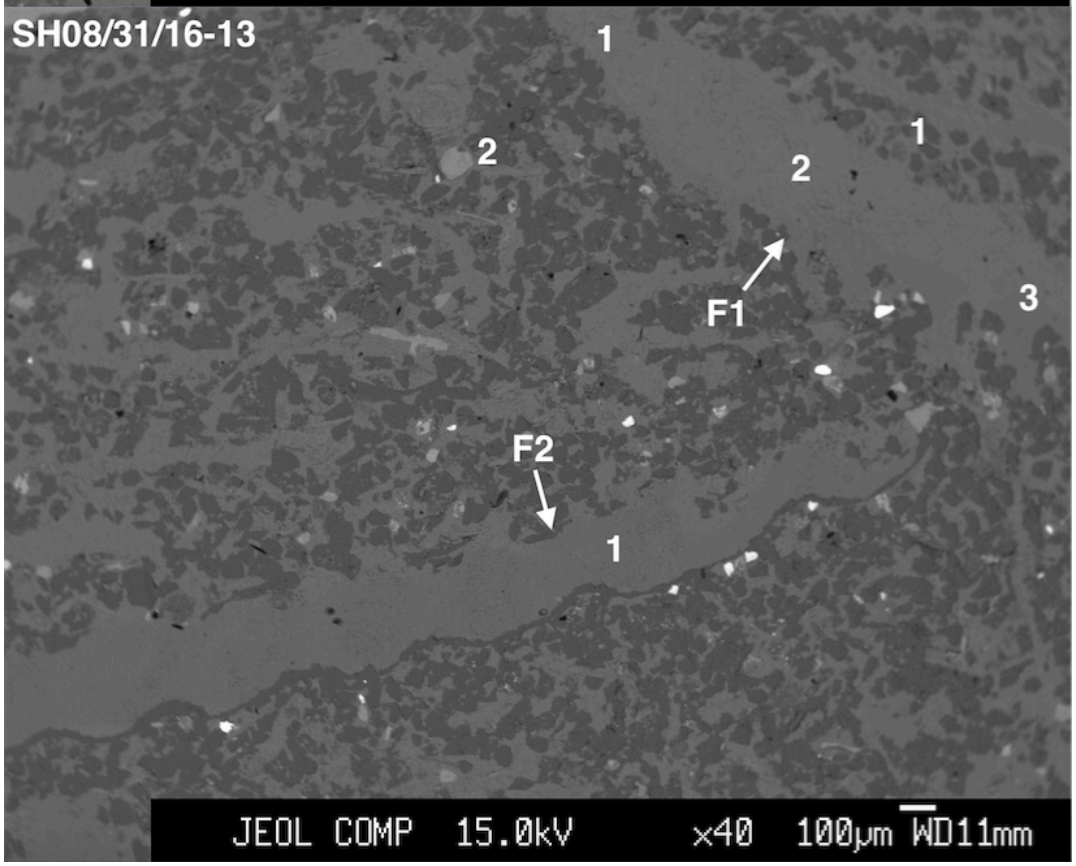
SH08/31/16-13
1
1
2
2
F1
3
F2
1
JEOL COMP 15.0kV ×40 100µm WD11mm

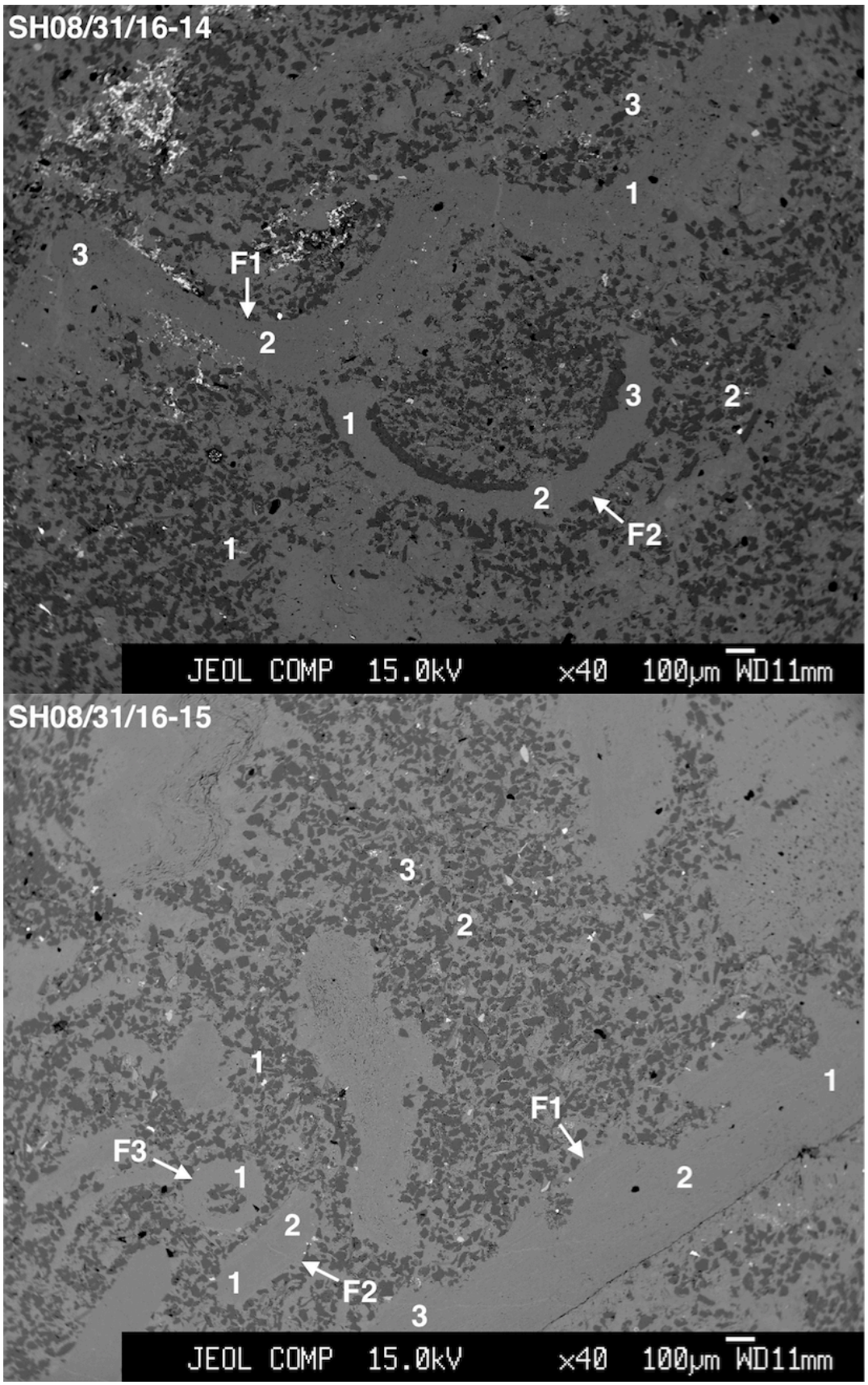
SH08/31/16-14
3
1
3
F1
2
3
2
1
2
F2
1
JEOL COMP 15.0kV ×40 100µm WD11mm
SH08/31/16-15
3
2
1
1
F1
F3
1
2
2
1
F2
3
JEOL COMP 15.0kV ×40 100µm WD11mm

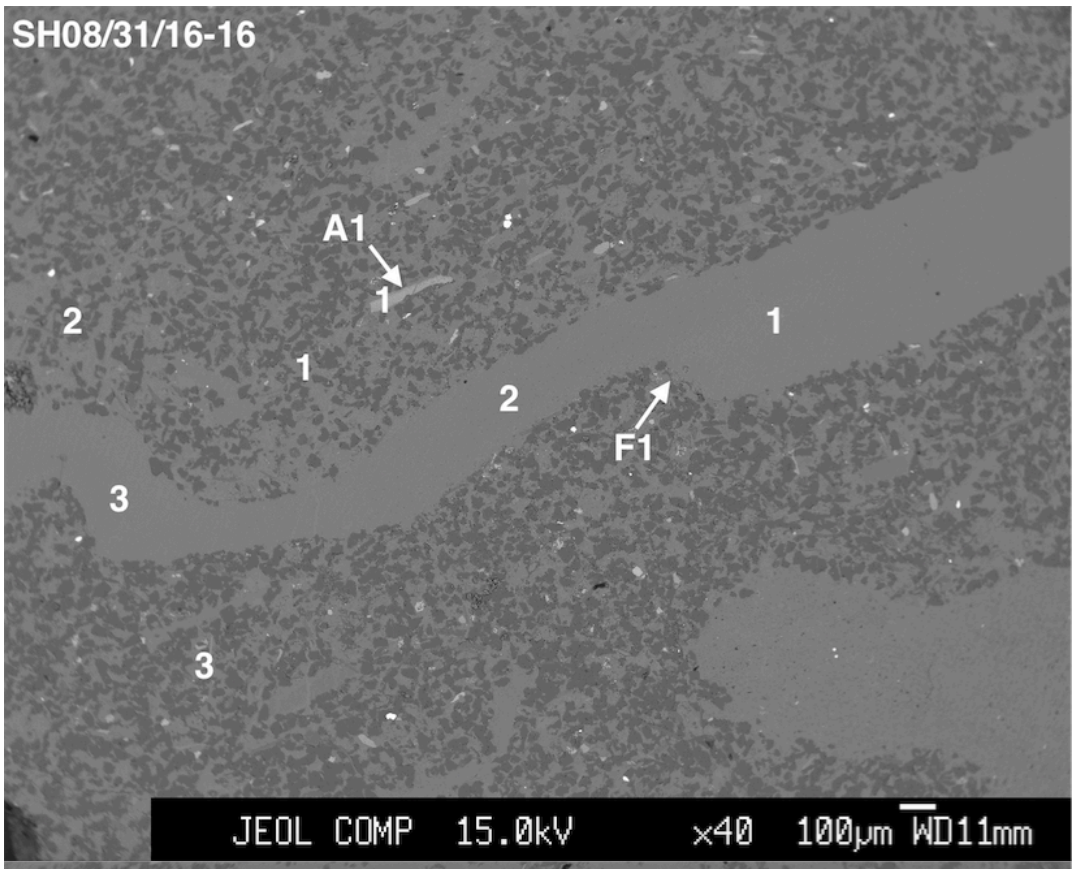
SH08/31/16-16
A1
1
2
1
1
2
F1
3
3
JEOL COMP 15.0kV x40 100µm WD11mm


SH08/31/16-17
1
3
2
2
3
F1
1
3
F2
2
1
JEOL COMP 15.0kV x40 100µm WD11mm

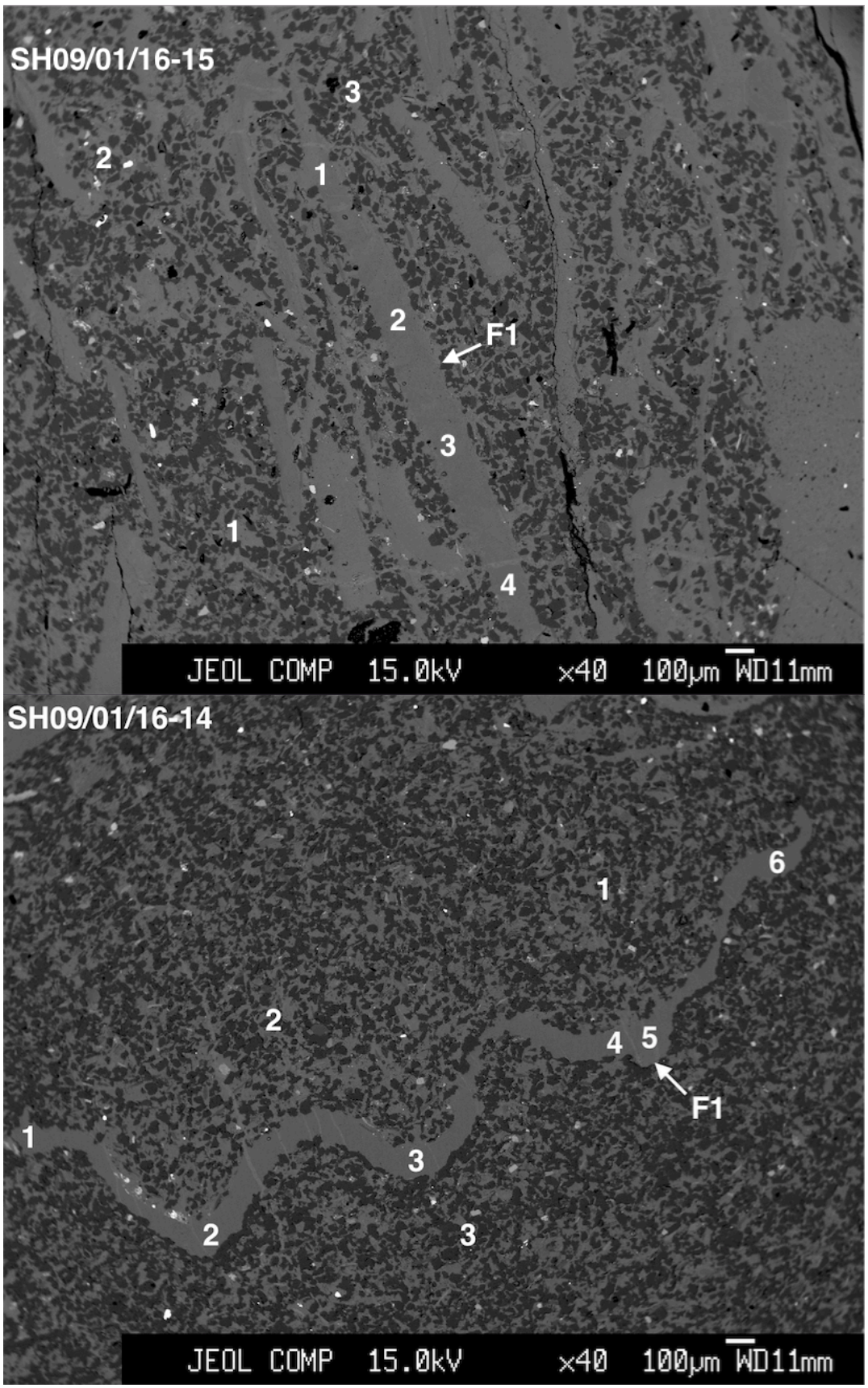
SH09/01/16-15
3
2
1
2
F1
3
1
4
JEOL COMP 15.0kV x40 100µm WD11mm
SH09/01/16-14
6
1
2
4
5
F1
1
3
2
3
JEOL COMP 15.0kV x40 100µm WD11mm

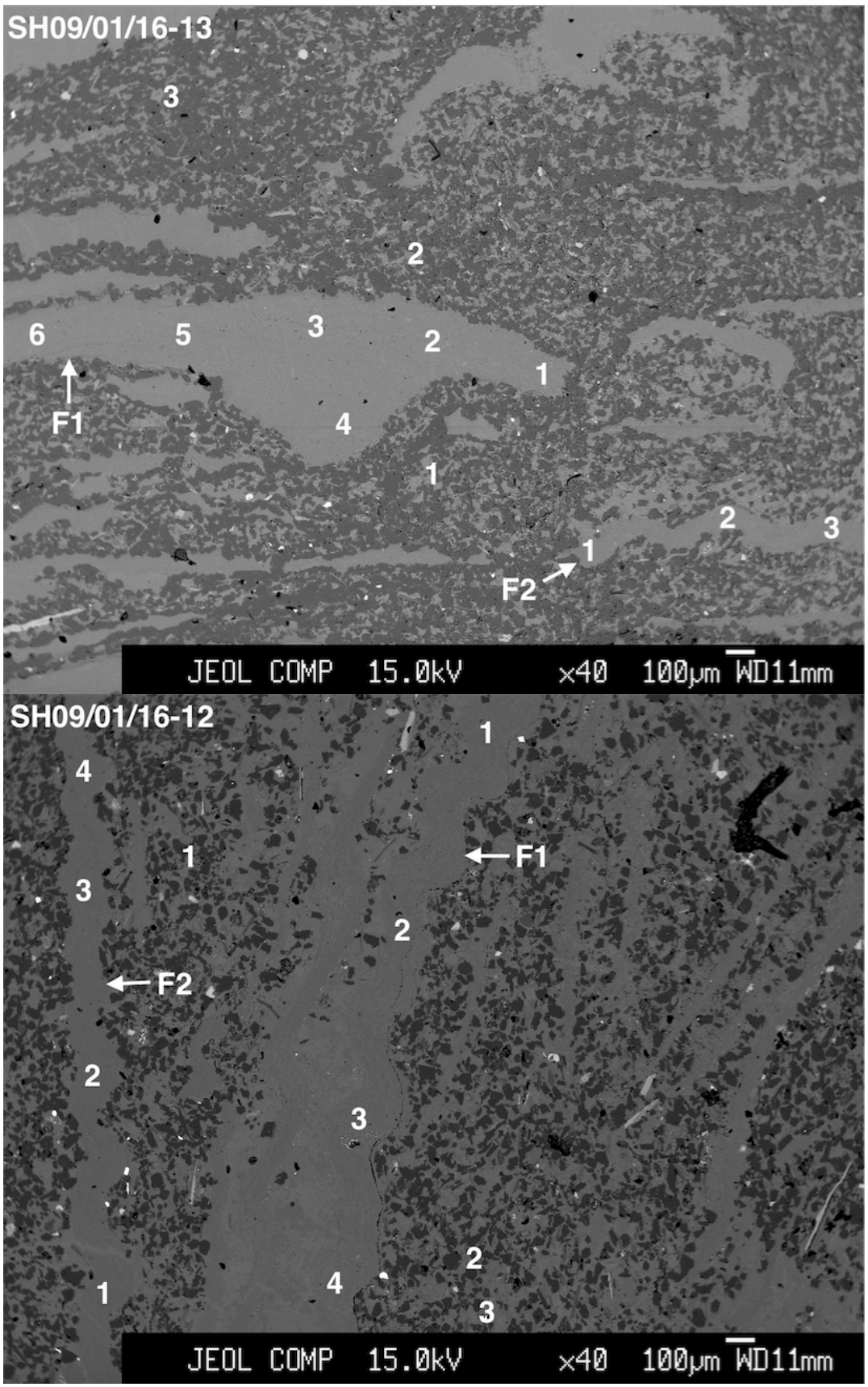
SH09/01/16-13
3
2
6
5
3
2
1
F1
4
1
2
3
1
F2
JEOL COMP 15.0kV x40 100µm WD11mm
SH09/01/16-12
1
4
1
F1
3
2
F2
2
3
2
4
1
3
JEOL COMP 15.0kV x40 100µm WD11mm


SH09/01/16-11
3
1
2
JEOL COMP 15.0kV x40 100µm WD11mm

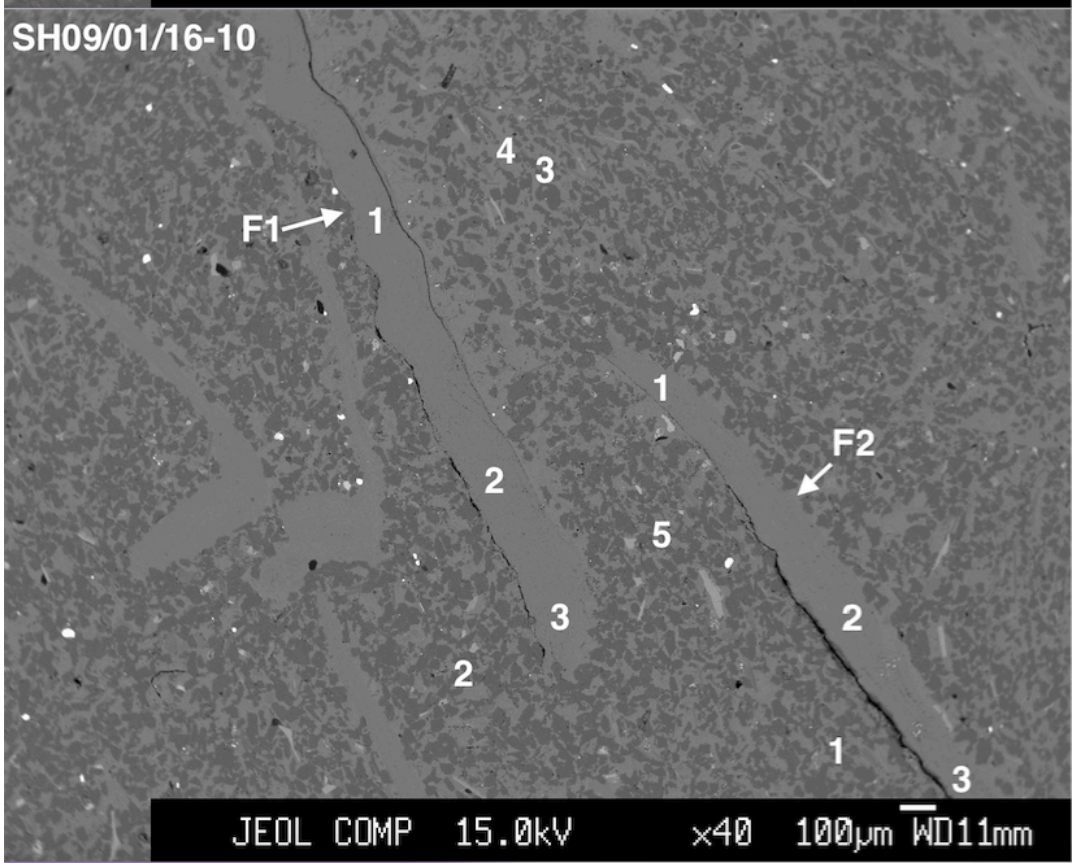
SH09/01/16-10
4
3
F1
1
1
F2
2
5
3
2
2
1
3
JEOL COMP 15.0kV x40 100µm WD11mm

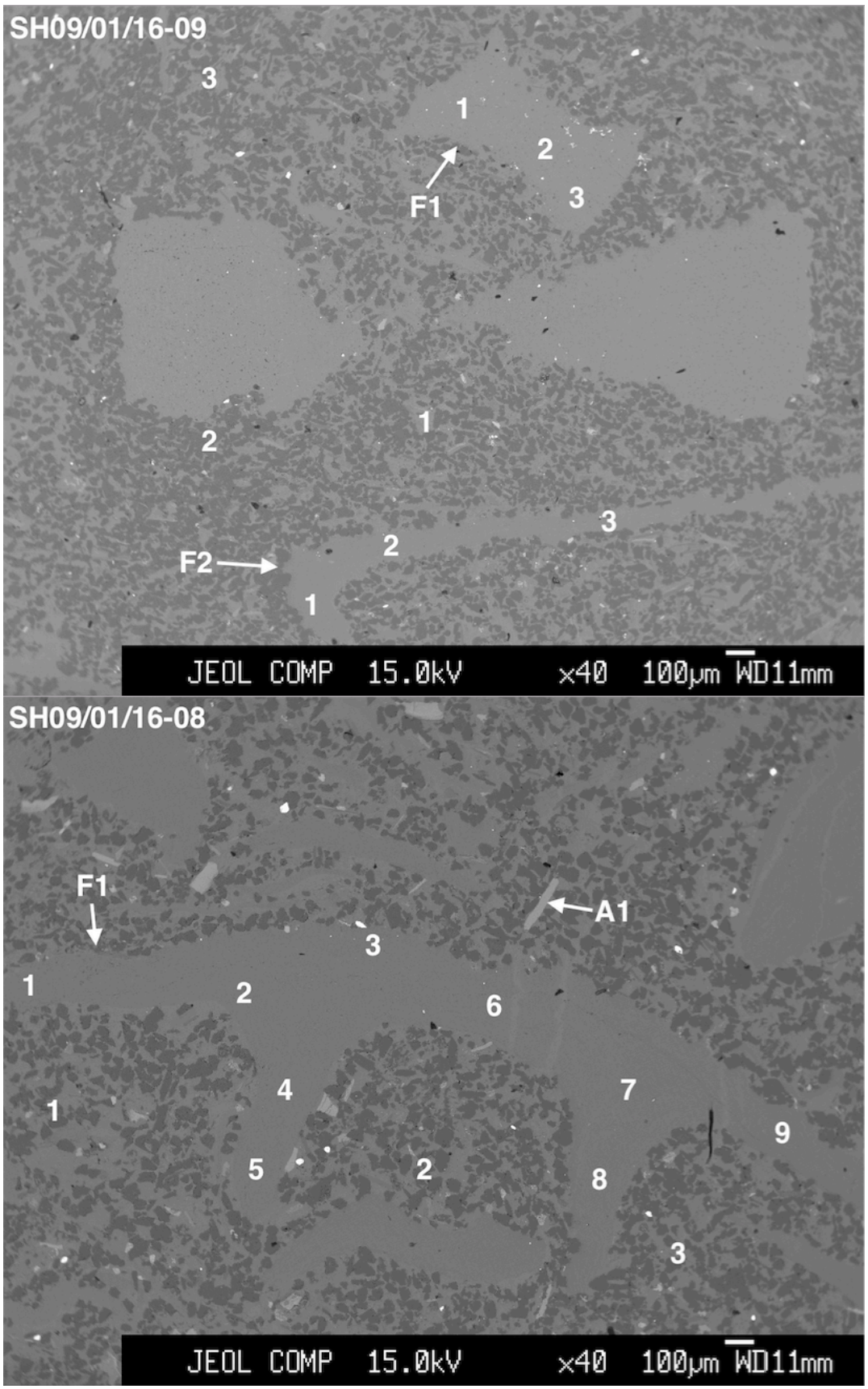
SH09/01/16-09
3
1
2
F1
3
2
1
3
2
F2
2
1
JEOL COMP 15.0kV ×40 100µm WD11mm
SH09/01/16-08
F1
A1
3
1
2
6
4
7
1
9
5
2
8
3
JEOL COMP 15.0kV ×40 100µm WD11mm

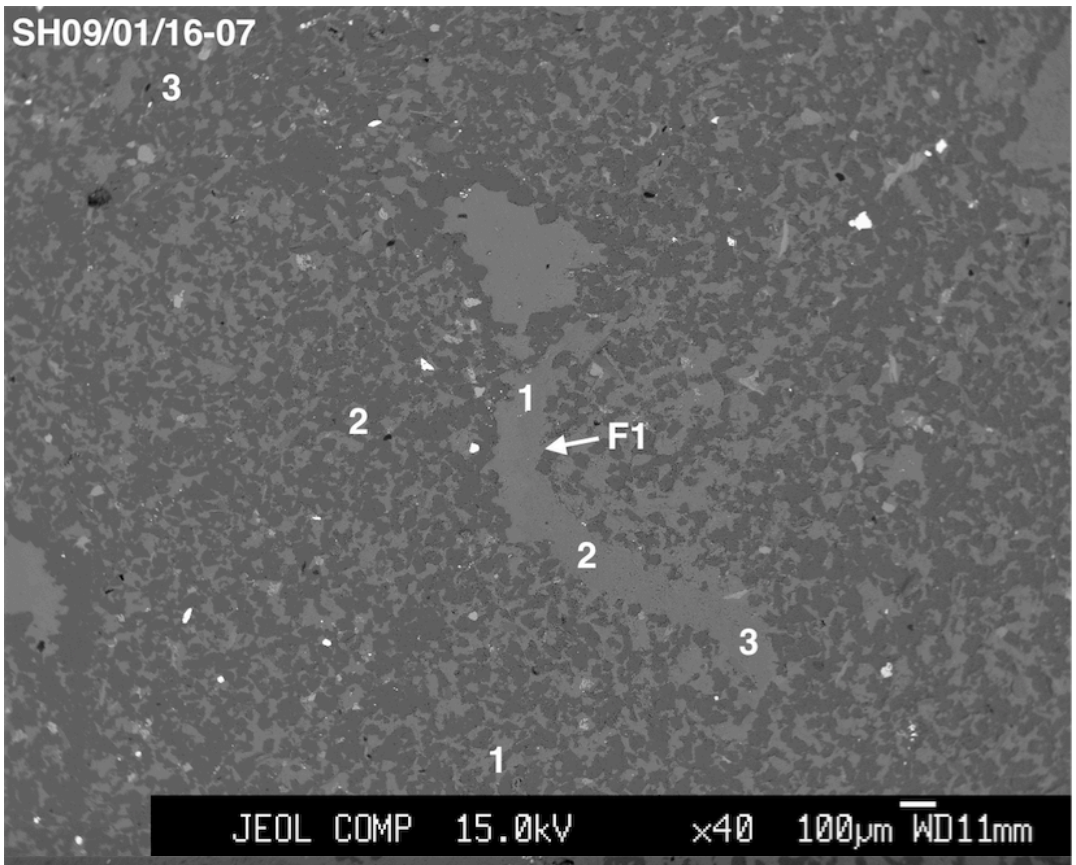
SH09/01/16-07
3
1
2
F1
2
3
1
JEOL COMP 15.0kV x40 100µm WD11mm

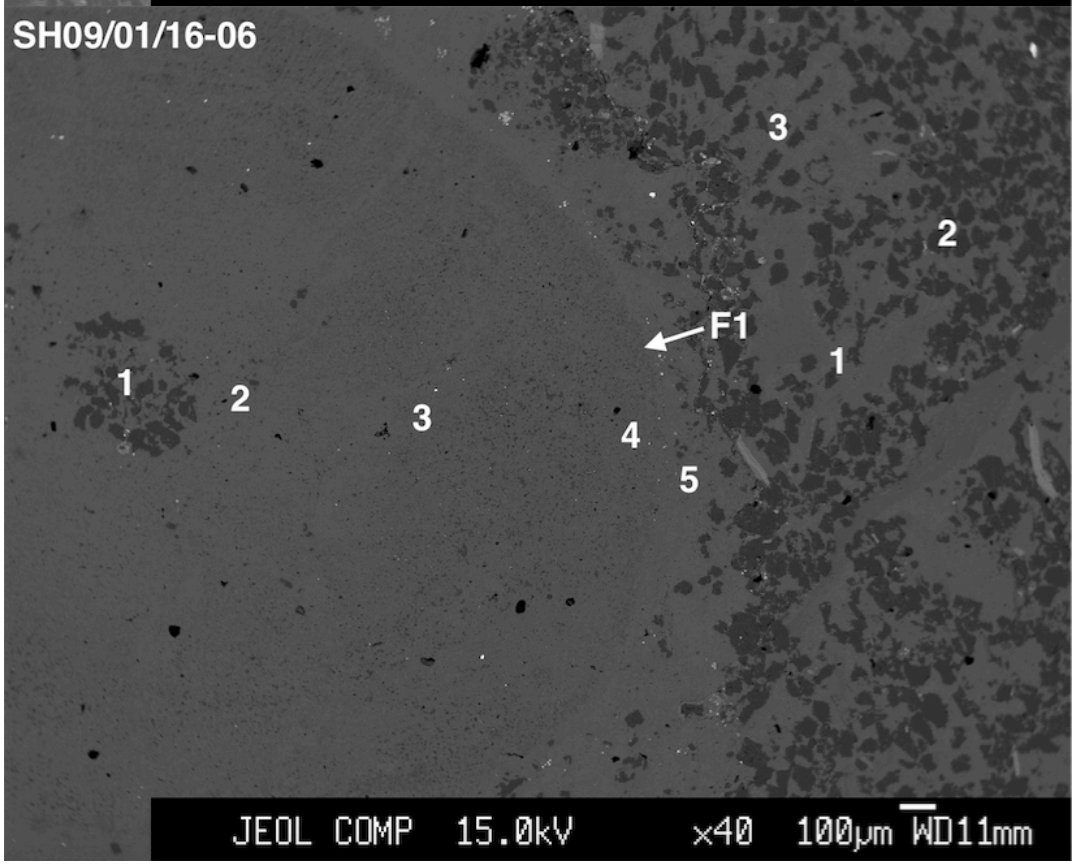
SH09/01/16-06
3
2
F1
1
1
2
3
4
5
JEOL COMP 15.0kV x40 100µm WD11mm

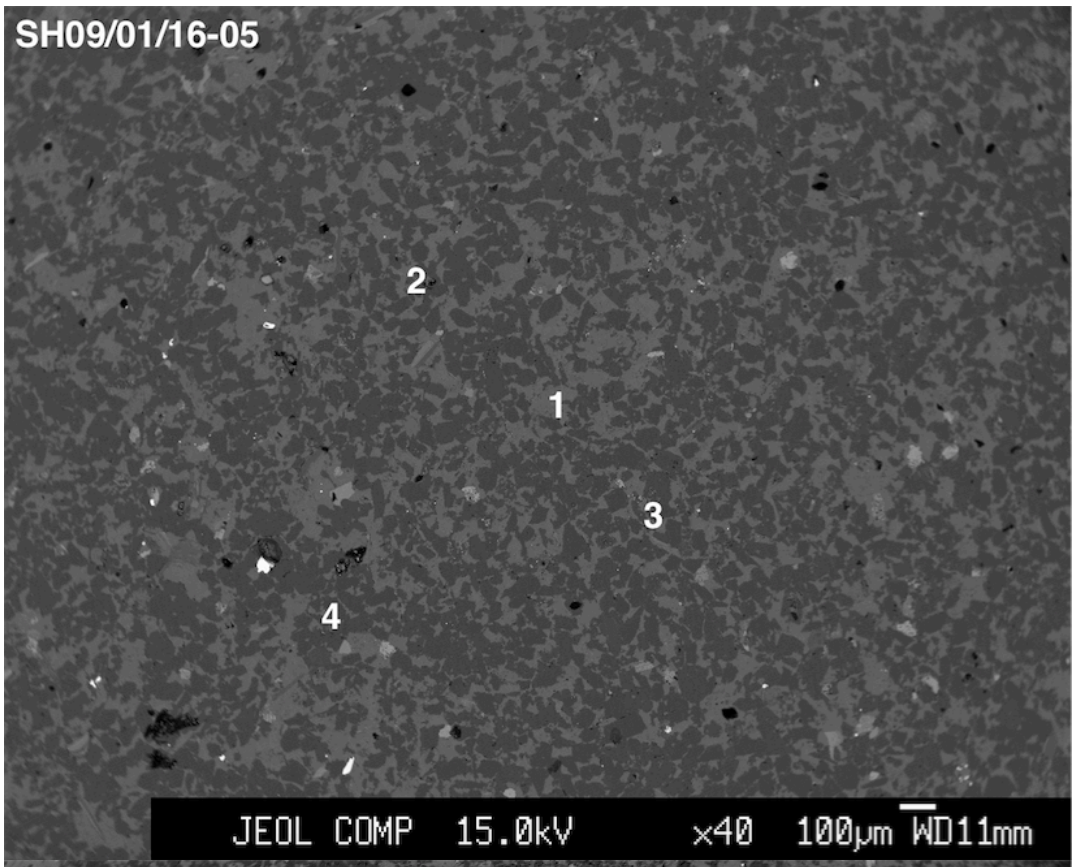
SH09/01/16-05
2
1
3
4
JEOL COMP 15.0kV x40 100µm WD11mm

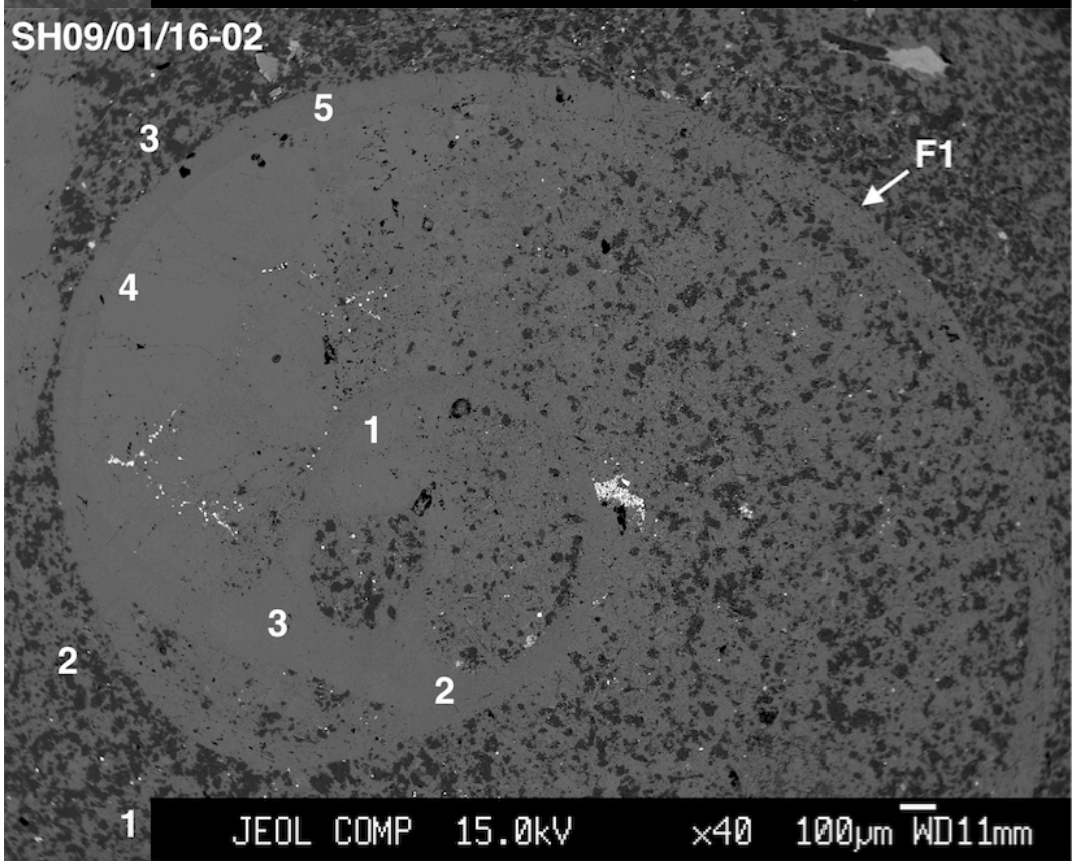
SH09/01/16-02
5
3
F1
4
1
3
2
2
1
JEOL COMP 15.0kV x40 100µm WD11mm

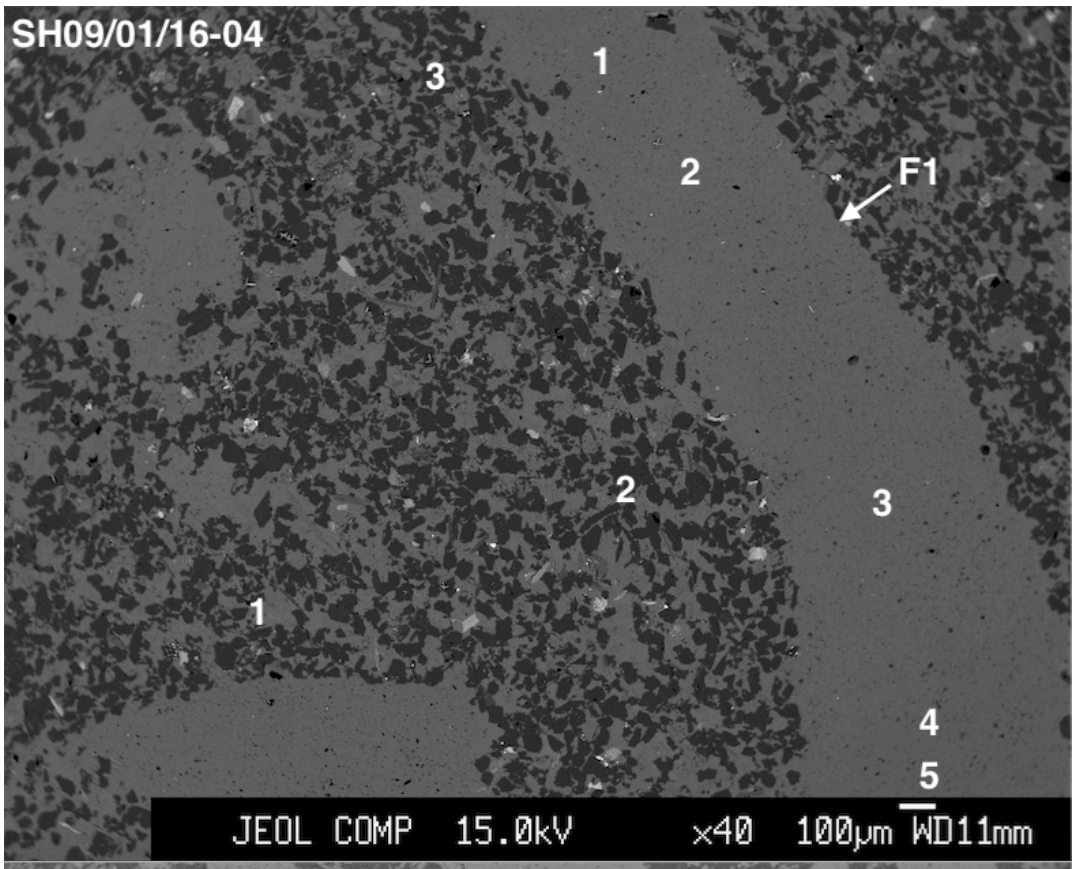
SH09/01/16-04
3
1
2
F1
2
3
1
4
5
JEOL COMP 15.0kV x40 100µm WD11mm

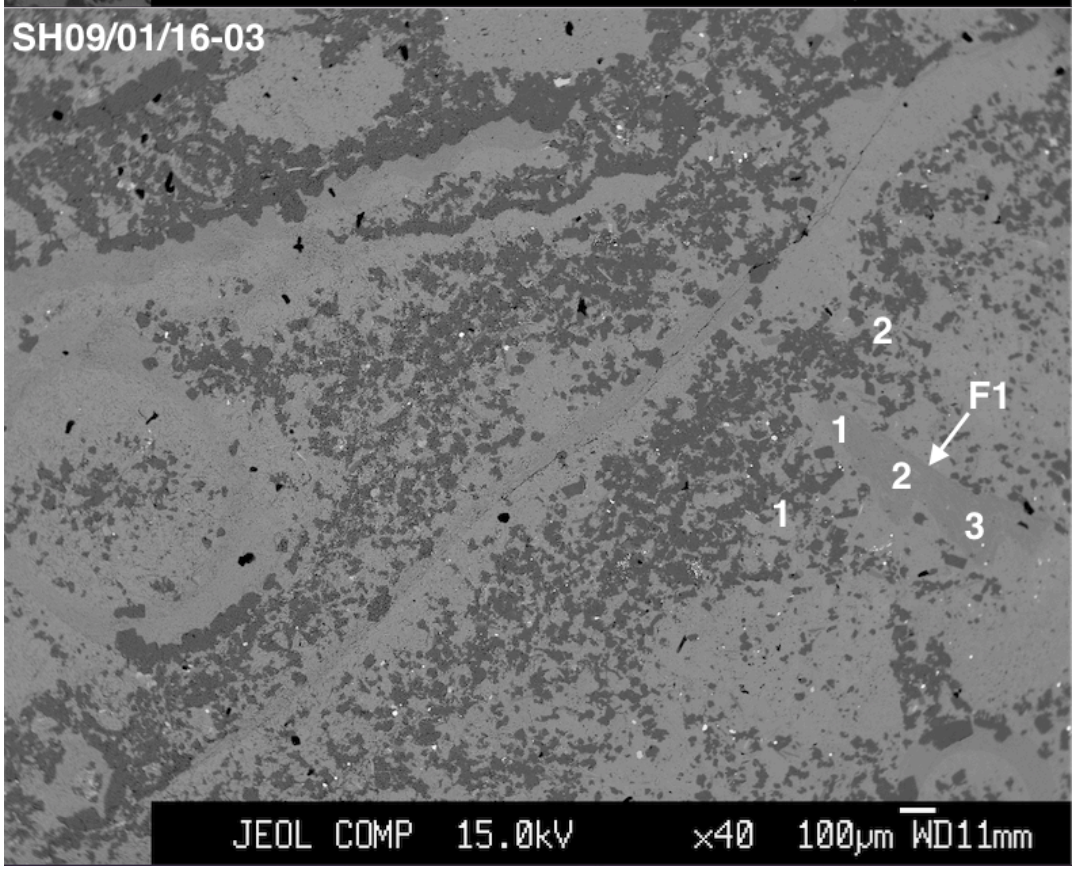
SH09/01/16-03
2
F1
1
2
1
3
JEOL COMP 15.0kV x40 100µm WD11mm

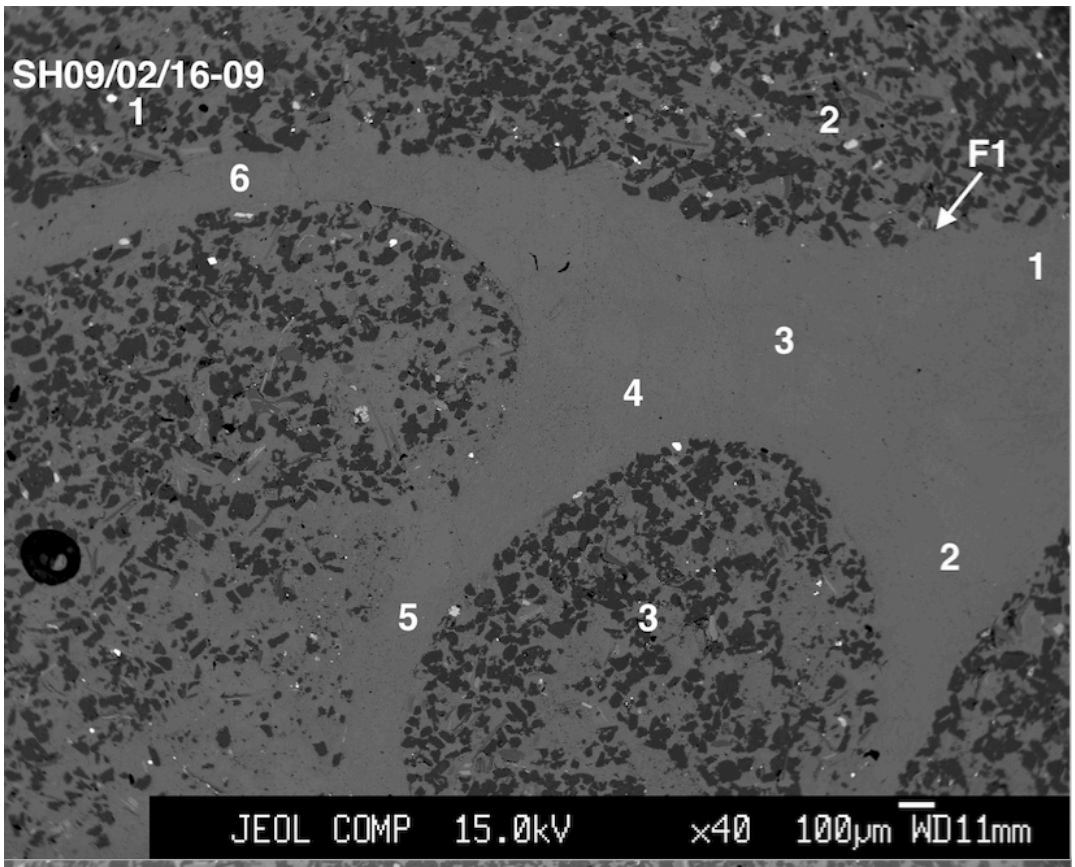
SH09/02/16-09
1
2
F1
6
1
3
4
2
5
3
JEOL COMP 15.0kV ×40 100µm WD11mm

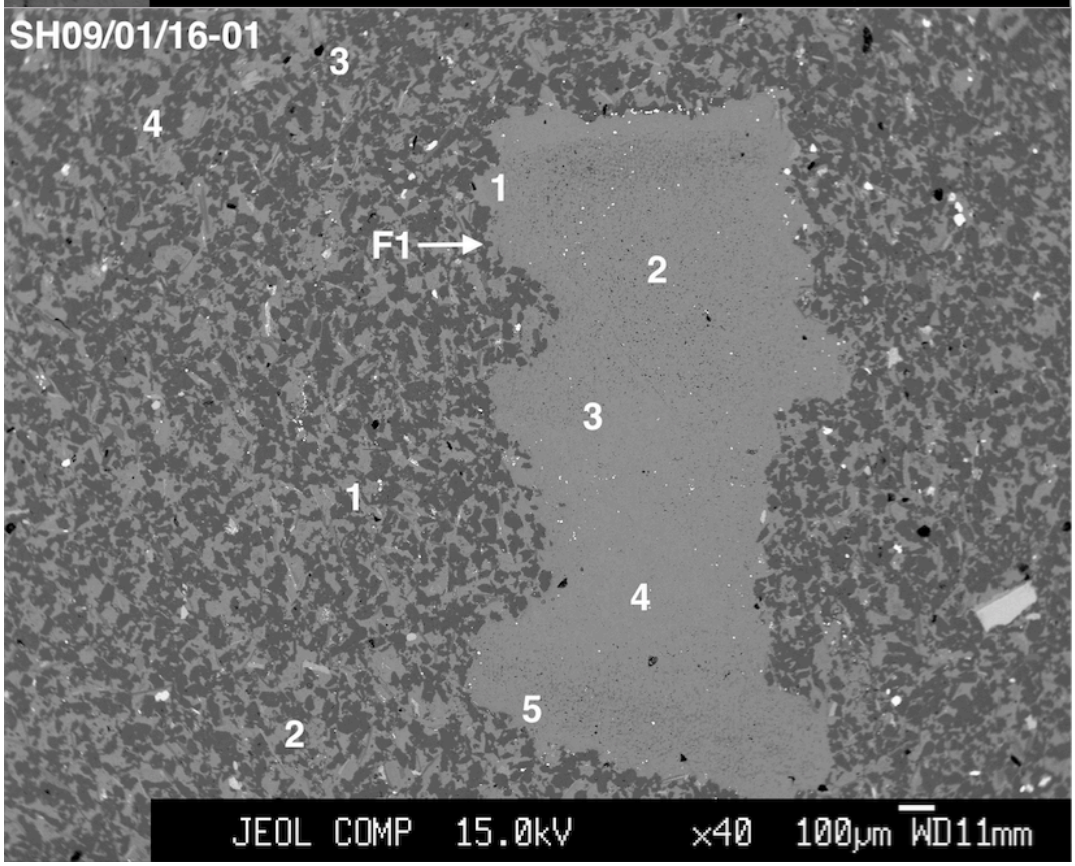
SH09/01/16-01
3
4
1
F1
2
3
1
4
5
2
JEOL COMP 15.0kV ×40 100µm WD11mm

Appendix D

Sample	SH08-31-16-01F2	SH08-31-16-01F2	SH08-31-16-01F2	SH08-31-16-01F2	SH08-31-16-01F3	SH08-31-16-01F3	SH08-31-16-01F3	SH08-31-16-01M	SH08-31-16-01M	SH08-31-16-01M	SH08-31-16-01M
Microprobe Data											
CaO	51.56	52.68	51.90	51.84	51.57	51.21	52.84	51.99	51.55	51.32	50.72
MgO	0.32	0.18	0.29	0.64	0.26	0.34	0.29	0.34	0.35	0.15	0.22
FeO	0.26	0.29	0.32	0.26	0.21	0.38	0.26	0.35	0.32	0.09	0.22
MnO	0.78	1.24	0.68	0.69	0.71	0.77	0.73	0.84	1.06	2.48	0.81
SiO2	0.00	0.00	0.02	0.01	0.02	0.00	-0.02	0.06	0.07	0.47	0.06
P2O5	0.01	-0.03	0.05	0.05	0.03	0.07	0.00	0.06	0.07	0.02	0.01
SrO	0.11	0.18	0.18	0.12	0.17	0.21	0.18	0.15	0.08	0.03	0.06
Total	53.04	54.55	53.44	53.62	52.96	52.97	54.29	53.79	53.50	54.56	52.11
Metal Cations											
CaO	0.97	0.97	0.97	0.97	0.98	0.97	0.98	0.97	0.96	0.94	0.98
MgO	0.01	0.00	0.01	0.02	0.01	0.01	0.01	0.01	0.01	0.00	0.01
FeO	0.00	0.00	0.00	0.00	0.00	0.01	0.00	0.01	0.00	0.00	0.00
MnO	0.01	0.02	0.01	0.01	0.01	0.01	0.01	0.01	0.02	0.04	0.01
SiO2	0.00	0.00	0.00	0.00	0.00	0.00	0.00	0.00	0.00	0.02	0.00
P2O5	0.00	0.00	0.00	0.00	0.00	0.00	0.00	0.00	0.00	0.00	0.00
SrO	0.00	0.00	0.00	0.00	0.00	0.00	0.00	0.00	0.00	0.00	0.00
Total	1.00	1.00	1.00	1.00	1.00	1.00	1.00	1.00	1.00	1.00	1.00
Proportion of End-Members											
Dolomite	1.66	0.95	1.52	3.34	1.34	1.80	1.50	1.75	1.83	0.78	1.19
Calcite	96.62	96.75	96.58	94.91	96.92	96.03	96.93	95.92	95.53	93.77	96.91
Siderite	0.39	0.41	0.46	0.38	0.31	0.56	0.38	0.51	0.46	0.13	0.33
Rhodochrosite	1.17	1.82	1.02	1.02	1.07	1.16	1.07	1.23	1.57	3.60	1.24
Strontianite	0.11	0.18	0.19	0.12	0.17	0.21	0.18	0.15	0.08	0.03	0.07
Total	99.94	100.10	99.76	99.77	99.81	99.75	100.06	99.55	99.47	98.31	99.73

Sample	SH08-31-16-01M	SH08-31-16-02F1	SH08-31-16-02F1	SH08-31-16-02F1	SH08-31-16-02F1	SH08-31-16-02F1	SH08-31-16-02F2	SH08-31-16-02F2	SH08-31-16-02F2	SH08-31-16-02M	SH08-31-16-02M
Microprobe Data											
CaO	49.35	54.56	53.83	53.89	53.47	53.44	53.23	52.98	54.05	50.83	53.62
MgO	0.21	0.54	0.30	0.42	0.43	0.41	0.58	0.34	0.28	0.10	0.12
FeO	0.17	0.33	0.35	0.41	0.31	0.25	0.21	0.21	0.24	0.03	0.01
MnO	0.55	0.69	0.71	0.76	0.59	0.61	0.58	0.61	0.64	4.03	0.97
SiO2	0.23	0.03	-0.01	0.02	-0.02	-0.02	-0.01	0.03	-0.03	0.15	0.10
P2O5	0.02	0.05	0.09	0.05	0.07	0.03	0.02	0.06	0.05	0.06	0.03
SrO	0.10	0.10	0.02	0.07	0.13	0.06	0.10	0.08	0.07	-0.01	0.00
Total	50.64	56.30	55.31	55.62	54.98	54.78	54.72	54.31	55.30	55.18	54.85
Metal Cations											
CaO	0.97	0.97	0.97	0.97	0.97	0.98	0.97	0.98	0.98	0.93	0.98
MgO	0.01	0.01	0.01	0.01	0.01	0.01	0.01	0.01	0.01	0.00	0.00
FeO	0.00	0.00	0.00	0.01	0.00	0.00	0.00	0.00	0.00	0.00	0.00
MnO	0.01	0.01	0.01	0.01	0.01	0.01	0.01	0.01	0.01	0.06	0.01
SiO2	0.01	0.00	0.00	0.00	0.00	0.00	0.00	0.00	0.00	0.01	0.00
P2O5	0.00	0.00	0.00	0.00	0.00	0.00	0.00	0.00	0.00	0.00	0.00
SrO	0.00	0.00	0.00	0.00	0.00	0.00	0.00	0.00	0.00	0.00	0.00
Total	1.00	1.00	1.00	1.00	1.00	1.00	1.00	1.00	1.00	1.00	1.00
Proportion of End-Members											
Dolomite	1.17	2.66	1.52	2.10	2.18	2.10	2.97	1.75	1.40	0.49	0.60
Calcite	96.69	95.55	96.63	95.91	96.23	96.58	95.76	96.66	97.19	92.92	97.54
Siderite	0.26	0.46	0.49	0.58	0.44	0.36	0.30	0.30	0.34	0.04	0.01
Rhodochrosite	0.86	0.97	1.02	1.08	0.85	0.88	0.84	0.89	0.91	5.83	1.40
Strontianite	0.11	0.10	0.02	0.06	0.13	0.06	0.09	0.08	0.07	-0.01	0.00
Total	99.09	99.73	99.68	99.73	99.84	99.96	99.97	99.68	99.91	99.27	99.55

Sample	SH08-31-16-02M	SH08-31-16-02M	SH08-31-16-04F1	SH08-31-16-04F1	SH08-31-16-04F1	SH08-31-16-04F2	SH08-31-16-04F2	SH08-31-16-04F2	SH08-31-16-04M	SH08-31-16-04M	SH08-31-16-04M
Microprobe Data											
CaO	53.15	52.28	52.57	54.93	52.41	51.95	50.83	51.95	53.57	50.00	51.83
MgO	0.08	0.12	0.27	0.19	0.05	0.59	0.37	0.38	0.37	0.13	0.12
FeO	-0.02	0.28	0.19	0.20	0.08	0.31	0.21	0.26	0.35	0.06	0.07
MnO	1.27	1.00	0.90	0.30	1.49	0.37	0.34	0.31	0.85	1.58	0.48
SiO2	0.10	0.41	-0.03	0.00	-0.01	0.01	0.04	0.03	0.22	1.00	0.09
P2O5	0.00	0.03	0.04	0.01	0.07	0.04	0.06	0.10	0.03	0.07	0.07
SrO	-0.06	0.16	0.08	0.22	0.11	0.13	0.11	0.18	0.13	0.08	0.08
Total	54.53	54.29	54.03	55.84	54.19	53.39	51.97	53.19	55.52	52.92	52.75
Metal Cations											
CaO	0.98	0.96	0.98	0.99	0.97	0.97	0.98	0.98	0.96	0.93	0.98
MgO	0.00	0.00	0.01	0.00	0.00	0.02	0.01	0.01	0.01	0.00	0.00
FeO	0.00	0.00	0.00	0.00	0.00	0.00	0.00	0.00	0.00	0.00	0.00
MnO	0.02	0.01	0.01	0.00	0.02	0.01	0.01	0.00	0.01	0.02	0.01
SiO2	0.00	0.01	0.00	0.00	0.00	0.00	0.00	0.00	0.01	0.03	0.00
P2O5	0.00	0.00	0.00	0.00	0.00	0.00	0.00	0.00	0.00	0.00	0.00
SrO	0.00	0.00	0.00	0.00	0.00	0.00	0.00	0.00	0.00	0.00	0.00
Total	1.00	1.00	1.00	1.00	1.00	1.00	1.00	1.00	1.00	1.00	1.00
Proportion of End-Members											
Dolomite	0.43	0.63	1.41	0.97	0.27	3.05	1.97	1.97	1.85	0.67	0.66
Calcite	97.47	95.82	96.86	98.08	97.12	95.63	96.68	96.56	95.49	93.07	97.84
Siderite	-0.03	0.41	0.27	0.28	0.11	0.45	0.31	0.38	0.50	0.09	0.11
Rhodochrosite	1.85	1.46	1.32	0.42	2.18	0.54	0.52	0.45	1.21	2.33	0.72
Strontianite	-0.06	0.16	0.09	0.21	0.11	0.13	0.12	0.18	0.13	0.08	0.08
Total	99.67	98.47	99.95	99.97	99.79	99.81	99.60	99.55	99.17	96.25	99.41

Sample	SH08-31-16-05M	SH08-31-16-05M	SH08-31-16-05M	SH08-31-16-05M	SH08-31-16-05F1	SH08-31-16-05F1	SH08-31-16-05F1	SH08-31-16-05F1	SH08-31-16-05F1	SH08-31-16-06F1	SH08-31-16-06F1
Microprobe Data											
CaO	53.84	50.23	51.58	48.83	52.27	54.88	52.46	53.89	52.48	42.39	52.94
MgO	0.30	0.36	0.30	1.03	0.30	0.32	0.30	0.33	0.21	0.80	0.16
FeO	0.32	0.29	0.26	0.98	0.27	0.28	0.27	0.24	0.06	0.89	0.08
MnO	1.12	0.99	0.96	1.65	1.19	1.20	1.09	0.95	0.88	0.65	0.01
SiO2	-0.01	0.01	0.01	1.35	0.01	0.01	0.03	0.03	0.02	8.59	-0.01
P2O5	0.03	0.04	0.04	0.03	0.03	0.09	0.07	0.06	0.02	0.04	0.01
SrO	0.13	0.23	0.14	0.09	-0.03	0.06	0.03	0.04	0.04	0.05	-0.02
Total	55.75	52.15	53.29	53.96	54.04	56.84	54.24	55.55	53.71	53.40	53.18
Metal Cations											
CaO	0.97	0.97	0.97	0.89	0.97	0.97	0.97	0.97	0.98	0.70	0.99
MgO	0.01	0.01	0.01	0.03	0.01	0.01	0.01	0.01	0.01	0.02	0.00
FeO	0.00	0.00	0.00	0.01	0.00	0.00	0.00	0.00	0.00	0.01	0.00
MnO	0.02	0.02	0.01	0.02	0.02	0.02	0.02	0.01	0.01	0.01	0.00
SiO2	0.00	0.00	0.00	0.05	0.00	0.00	0.00	0.00	0.00	0.26	0.00
P2O5	0.00	0.00	0.00	0.00	0.00	0.00	0.00	0.00	0.00	0.00	0.00
SrO	0.00	0.00	0.00	0.00	0.00	0.00	0.00	0.00	0.00	0.00	0.00
Total	1.00	1.00	1.00	1.00	1.00	1.00	1.00	1.00	1.00	1.00	1.00
Proportion of End-Members											
Dolomite	1.53	1.91	1.59	5.22	1.56	1.58	1.52	1.67	1.09	3.67	0.85
Calcite	96.21	95.72	96.28	86.24	96.20	95.94	96.12	96.28	97.34	67.83	99.02
Siderite	0.46	0.44	0.38	1.39	0.39	0.38	0.39	0.33	0.08	1.14	0.11
Rhodochrosite	1.60	1.51	1.43	2.37	1.75	1.67	1.59	1.36	1.29	0.84	0.02
Strontianite	0.13	0.24	0.15	0.09	-0.03	0.05	0.03	0.04	0.04	0.05	-0.02
Total	99.92	99.81	99.81	95.32	99.86	99.64	99.64	99.67	99.86	73.52	99.98

Sample	SH08-31-16-06F1	SH08-31-16-06F2	SH08-31-16-06F2	SH08-31-16-06F2	SH08-31-16-06M	SH08-31-16-06M	SH08-31-16-06M	SH08-31-16-06M	SH08-31-16-07F1	SH08-31-16-07F1	SH08-31-16-07F1
Microprobe Data											
CaO	52.11	51.82	51.71	52.33	53.50	51.97	52.50	50.55	53.97	51.26	53.82
MgO	0.14	0.32	0.05	0.09	0.19	0.39	0.07	0.21	0.32	0.11	0.10
FeO	0.11	0.18	0.08	0.01	0.15	0.11	0.12	0.30	0.01	0.08	0.01
MnO	1.28	0.30	1.21	-0.02	0.07	0.37	1.81	2.56	0.21	1.30	1.18
SiO2	0.17	0.08	0.04	0.07	0.07	0.14	0.24	0.17	-0.02	-0.02	0.05
P2O5	0.03	0.09	0.03	0.03	0.08	0.03	0.08	0.04	-0.03	0.02	-0.01
SrO	0.00	0.07	0.06	-0.05	0.28	0.21	0.01	-0.01	0.03	0.02	-0.04
Total	53.85	52.86	53.17	52.46	54.34	53.22	54.84	53.82	54.50	52.77	55.11
Metal Cations											
CaO	0.97	0.98	0.98	0.99	0.98	0.97	0.96	0.95	0.99	0.98	0.98
MgO	0.00	0.01	0.00	0.00	0.00	0.01	0.00	0.01	0.01	0.00	0.00
FeO	0.00	0.00	0.00	0.00	0.00	0.00	0.00	0.00	0.00	0.00	0.00
MnO	0.02	0.00	0.02	0.00	0.00	0.01	0.03	0.04	0.00	0.02	0.02
SiO2	0.01	0.00	0.00	0.00	0.00	0.01	0.01	0.01	0.00	0.00	0.00
P2O5	0.00	0.00	0.00	0.00	0.00	0.00	0.00	0.00	0.00	0.00	0.00
SrO	0.00	0.00	0.00	0.00	0.00	0.00	0.00	0.00	0.00	0.00	0.00
Total	1.00	1.00	1.00	1.00	1.00	1.00	1.00	1.00	1.00	1.00	1.00
Proportion of End-Members											
Dolomite	0.74	1.70	0.25	0.46	0.98	2.06	0.38	1.11	1.66	0.56	0.49
Calcite	96.49	96.90	97.53	99.25	97.90	96.41	95.73	93.95	98.15	97.34	97.70
Siderite	0.16	0.26	0.12	0.02	0.22	0.16	0.18	0.43	0.01	0.12	0.01
Rhodochrosite	1.88	0.45	1.80	-0.03	0.11	0.55	2.62	3.78	0.31	1.95	1.69
Strontianite	0.00	0.07	0.06	-0.05	0.28	0.22	0.01	-0.01	0.03	0.02	-0.04
Total	99.28	99.38	99.76	99.66	99.48	99.40	98.91	99.27	100.15	100.00	99.86

Sample	SH08-31-16-07F2	SH08-31-16-07F2	SH08-31-16-07F2	SH08-31-16-07M	SH08-31-16-07M	SH08-31-16-07M	SH08-31-16-08F1	SH08-31-16-08F1	SH08-31-16-08F1	SH08-31-16-08F1	SH08-31-16-08F1
Microprobe Data											
CaO	52.16	52.06	53.41	48.06	51.47	51.74	54.54	54.49	56.59	55.61	54.06
MgO	0.09	0.10	0.17	0.57	0.22	0.28	0.52	0.20	0.30	0.08	0.15
FeO	0.07	0.03	0.06	0.53	0.06	0.28	0.28	0.23	0.23	0.05	0.11
MnO	1.78	0.77	1.43	0.56	0.41	0.64	0.81	0.82	0.83	1.72	0.20
SiO2	0.06	0.66	-0.02	2.99	0.08	0.03	0.01	0.02	0.01	-0.02	0.00
P2O5	0.05	0.07	0.01	0.02	0.09	0.05	0.01	0.12	0.03	0.04	0.06
SrO	-0.04	-0.02	0.04	0.05	0.31	0.07	0.09	0.11	0.19	0.04	0.09
Total	54.16	53.67	55.10	52.78	52.64	53.10	56.25	55.99	58.18	57.52	54.68
Metal Cations											
CaO	0.97	0.96	0.97	0.87	0.98	0.98	0.97	0.97	0.98	0.97	0.99
MgO	0.00	0.00	0.00	0.01	0.01	0.01	0.01	0.00	0.01	0.00	0.00
FeO	0.00	0.00	0.00	0.01	0.00	0.00	0.00	0.00	0.00	0.00	0.00
MnO	0.03	0.01	0.02	0.01	0.01	0.01	0.01	0.01	0.01	0.02	0.00
SiO2	0.00	0.02	0.00	0.10	0.00	0.00	0.00	0.00	0.00	0.00	0.00
P2O5	0.00	0.00	0.00	0.00	0.00	0.00	0.00	0.00	0.00	0.00	0.00
SrO	0.00	0.00	0.00	0.00	0.00	0.00	0.00	0.00	0.00	0.00	0.00
Total	1.00	1.00	1.00	1.00	1.00	1.00	1.00	1.00	1.00	1.00	1.00
Proportion of End-Members											
Dolomite	0.45	0.52	0.84	2.88	1.15	1.48	2.55	0.98	1.42	0.38	0.78
Calcite	96.49	95.81	97.00	85.37	97.19	96.78	95.76	96.95	96.83	97.04	98.46
Siderite	0.10	0.04	0.08	0.75	0.08	0.42	0.39	0.32	0.31	0.07	0.15
Rhodochrosite	2.61	1.12	2.06	0.79	0.62	0.95	1.14	1.16	1.13	2.38	0.29
Strontianite	-0.04	-0.02	0.04	0.05	0.32	0.08	0.08	0.11	0.18	0.04	0.09
Total	99.61	97.47	100.02	89.84	99.37	99.71	99.93	99.52	99.87	99.91	99.78

Sample	SH08-01-16-08F1	SH08-01-16-08F1	SH08-31-16-08M	SH08-31-16-08M	SH08-31-16-08M	SH08-31-16-09F1	SH08-31-16-09F1	SH08-31-16-09F1	SH08-31-16-09F1	SH08-31-16-09F2	SH08-01-16-09F2
Microprobe Data											
CaO	52.92	52.45	53.22	53.19	52.75	55.47	53.12	39.66	53.92	55.65	53.16
MgO	0.13	0.24	0.04	0.22	0.08	0.16	0.30	6.80	1.06	0.13	0.38
FeO	0.02	0.35	0.02	0.24	0.02	0.08	0.09	3.46	0.14	0.17	0.39
MnO	0.96	0.78	1.72	0.66	2.02	1.23	1.45	4.16	0.80	0.32	0.98
SiO2	0.01	0.03	-0.01	-0.02	0.01	0.03	1.00	0.23	-0.01	0.00	-0.01
P2O5	0.09	0.04	0.09	0.07	0.03	0.02	0.07	0.07	-0.01	0.08	0.04
SrO	0.07	0.58	0.01	0.25	0.06	0.03	0.01	0.10	0.07	0.07	0.08
Total	54.19	54.47	55.10	54.62	54.97	57.02	56.05	54.48	55.98	56.41	55.03
Metal Cations											
CaO	0.98	0.97	0.97	0.98	0.97	0.98	0.94	0.71	0.96	0.99	0.97
MgO	0.00	0.01	0.00	0.01	0.00	0.00	0.01	0.17	0.03	0.00	0.01
FeO	0.00	0.01	0.00	0.00	0.00	0.00	0.00	0.05	0.00	0.00	0.01
MnO	0.01	0.01	0.02	0.01	0.03	0.02	0.02	0.06	0.01	0.00	0.01
SiO2	0.00	0.00	0.00	0.00	0.00	0.00	0.03	0.01	0.00	0.00	0.00
P2O5	0.00	0.00	0.00	0.00	0.00	0.00	0.00	0.00	0.00	0.00	0.00
SrO	0.00	0.01	0.00	0.00	0.00	0.00	0.00	0.00	0.00	0.00	0.00
Total	1.00	1.00	1.00	1.00	1.00	1.00	1.00	1.00	1.00	1.00	1.00
Proportion of End-Members											
Dolomite	0.66	1.23	0.22	1.13	0.43	0.79	1.46	33.95	5.25	0.63	1.92
Calcite	97.49	96.30	96.96	97.11	96.42	97.20	92.84	54.19	93.43	98.34	95.91
Siderite	0.02	0.51	0.03	0.34	0.03	0.11	0.13	4.84	0.19	0.24	0.55
Rhodochrosite	1.41	1.14	2.48	0.96	2.93	1.70	2.02	5.90	1.13	0.44	1.41
Strontianite	0.07	0.58	0.01	0.25	0.06	0.03	0.01	0.09	0.07	0.06	0.08
Total	99.65	99.77	99.71	99.80	99.86	99.84	96.46	98.97	100.08	99.72	99.88

Sample	SH08-31-16-09F2	SH08-31-16-09F3	SH08-31-16-09F3	SH08-31-16-09F3	SH08-31-16-09M	SH08-31-16-09M	SH08-31-16-09M	SH08-31-16-10F1	SH08-31-16-10F1	SH08-31-16-10F1	SH08-31-16-10F2
Microprobe Data											
CaO	53.29	53.59	54.47	53.72	54.65	52.86	56.33	55.35	54.69	55.48	55.26
MgO	0.44	0.46	0.27	0.40	0.31	0.31	0.27	0.65	0.39	0.63	0.30
FeO	0.41	0.38	0.29	0.32	0.04	0.00	0.28	-0.02	0.06	-0.01	0.21
MnO	1.11	1.16	1.86	0.93	0.03	0.69	1.64	0.07	0.67	0.07	1.25
SiO2	0.00	0.11	-0.01	0.02	0.12	0.19	0.06	0.02	0.00	0.01	0.03
P2O5	0.04	0.08	-0.03	0.06	0.06	-0.02	0.04	0.04	0.07	0.04	-0.02
SrO	0.08	0.08	0.05	0.03	0.01	0.03	0.05	0.23	0.20	0.35	0.07
Total	55.36	55.85	56.90	55.49	55.21	54.05	58.68	56.34	56.08	56.57	57.09
Metal Cations											
CaO	0.97	0.96	0.96	0.97	0.99	0.98	0.96	0.98	0.98	0.98	0.97
MgO	0.01	0.01	0.01	0.01	0.01	0.01	0.01	0.02	0.01	0.02	0.01
FeO	0.01	0.01	0.00	0.00	0.00	0.00	0.00	0.00	0.00	0.00	0.00
MnO	0.02	0.02	0.03	0.01	0.00	0.01	0.02	0.00	0.01	0.00	0.02
SiO2	0.00	0.00	0.00	0.00	0.00	0.01	0.00	0.00	0.00	0.00	0.00
P2O5	0.00	0.00	0.00	0.00	0.00	0.00	0.00	0.00	0.00	0.00	0.00
SrO	0.00	0.00	0.00	0.00	0.00	0.00	0.00	0.00	0.00	0.00	0.00
Total	1.00	1.00	1.00	1.00	1.00	1.00	1.00	1.00	1.00	1.00	1.00
Proportion of End-Members											
Dolomite	2.21	2.28	1.33	2.00	1.55	1.57	1.26	3.19	1.95	3.10	1.45
Calcite	95.42	94.83	95.75	95.90	97.74	96.83	95.74	96.31	96.60	96.32	96.45
Siderite	0.58	0.53	0.40	0.45	0.06	0.00	0.38	-0.03	0.08	-0.01	0.28
Rhodochrosite	1.59	1.64	2.61	1.33	0.04	1.00	2.21	0.09	0.94	0.10	1.74
Strontianite	0.07	0.08	0.04	0.03	0.01	0.03	0.05	0.22	0.19	0.33	0.07
Total	99.88	99.35	100.13	99.71	99.40	99.44	99.64	99.79	99.77	99.85	99.99

Sample	SH08-31-16-12M	SH08-31-16-12M	SH08-31-16-13F1	SH08-31-16-13F1	SH08-31-16-13F1	SH08-31-16-13F2	SH08-31-16-13M	SH08-31-16-13M	SH08-31-16-13M	SH08-31-16-13M	SH08/31/16-14F1
Microprobe Data											
CaO	51.52	51.67	52.21	50.51	52.97	51.40	51.60	50.99	51.06	50.15	53.94
MgO	0.36	0.41	0.37	0.43	0.53	0.39	0.15	0.23	0.57	0.40	0.24
FeO	0.42	0.45	0.38	0.30	-0.02	0.02	0.10	0.03	0.03	0.32	0.00
MnO	0.50	0.41	0.84	0.86	0.07	0.19	0.18	1.04	0.47	0.43	0.49
SiO2	0.07	0.84	-0.02	-0.01	0.03	0.02	0.06	0.05	0.01	0.18	0.00
P2O5	0.05	0.07	0.02	0.06	0.14	-0.01	0.05	0.02	0.02	0.03	0.04
SrO	0.04	0.12	0.15	0.06	0.32	0.23	0.06	0.20	0.22	0.08	0.02
Total	52.96	53.97	53.95	52.20	54.03	52.24	52.20	52.57	52.38	51.59	54.73
Metal Cations											
CaO	0.97	0.94	0.97	0.97	0.98	0.98	0.99	0.97	0.97	0.97	0.99
MgO	0.01	0.01	0.01	0.01	0.01	0.01	0.00	0.01	0.02	0.01	0.01
FeO	0.01	0.01	0.01	0.00	0.00	0.00	0.00	0.00	0.00	0.00	0.00
MnO	0.01	0.01	0.01	0.01	0.00	0.00	0.00	0.02	0.01	0.01	0.01
SiO2	0.00	0.03	0.00	0.00	0.00	0.00	0.00	0.00	0.00	0.01	0.00
P2O5	0.00	0.00	0.00	0.00	0.01	0.00	0.00	0.00	0.00	0.00	0.00
SrO	0.00	0.00	0.00	0.00	0.00	0.00	0.00	0.00	0.00	0.00	0.00
Total	1.00	1.00	1.00	1.00	1.00	1.00	1.00	1.00	1.00	1.00	1.00
Proportion of End-Members											
Dolomite	1.88	2.10	1.94	2.29	2.69	2.10	0.78	1.24	3.02	2.14	1.20
Calcite	96.28	93.43	96.13	95.72	96.31	97.31	98.34	96.69	95.88	95.85	97.91
Siderite	0.62	0.65	0.55	0.44	-0.03	0.03	0.15	0.04	0.05	0.49	0.00
Rhodochrosite	0.74	0.59	1.23	1.30	0.10	0.28	0.27	1.57	0.71	0.66	0.70
Strontianite	0.04	0.12	0.15	0.06	0.32	0.24	0.06	0.20	0.23	0.08	0.02
Total	99.56	96.89	100.00	99.82	99.39	99.96	99.61	99.73	99.88	99.22	99.84

Sample	SH08/31/16-14F1	SH08/31/16-14F1	SH08/31/16-14F2	SH08/31/16-14F2	SH08/31/16-14F2	SH08/31/16-14M	SH08/31/16-14M	SH08/31/16-14M	SH08/31/16-15F1	SH08/31/16-15F1	SH08/31/16-15F1
Microprobe Data											
CaO	53.96	53.04	56.08	55.84	56.43	52.95	54.34	52.65	52.75	53.13	53.15
MgO	0.34	0.18	0.47	0.38	0.21	0.27	0.16	0.67	0.37	0.72	0.31
FeO	0.06	0.29	-0.01	0.07	0.11	0.63	0.12	0.60	0.28	-0.01	0.01
MnO	0.40	0.74	0.01	0.09	0.55	0.30	0.46	1.17	0.33	0.06	0.03
SiO2	0.03	0.03	0.00	0.00	0.02	0.44	0.05	-0.02	0.01	0.02	0.01
P2O5	0.05	0.07	0.08	0.05	0.04	0.05	0.03	0.04	0.03	0.11	0.03
SrO	0.16	0.09	0.22	0.30	0.05	0.21	0.03	0.05	0.07	0.28	0.19
Total	54.99	54.44	56.84	56.74	57.40	54.84	55.19	55.15	53.84	54.31	53.73
Metal Cations											
CaO	0.98	0.98	0.98	0.98	0.98	0.96	0.98	0.96	0.98	0.97	0.99
MgO	0.01	0.00	0.01	0.01	0.00	0.01	0.00	0.02	0.01	0.02	0.01
FeO	0.00	0.00	0.00	0.00	0.00	0.01	0.00	0.01	0.00	0.00	0.00
MnO	0.01	0.01	0.00	0.00	0.01	0.00	0.01	0.02	0.00	0.00	0.00
SiO2	0.00	0.00	0.00	0.00	0.00	0.01	0.00	0.00	0.00	0.00	0.00
P2O5	0.00	0.00	0.00	0.00	0.00	0.00	0.00	0.00	0.00	0.00	0.00
SrO	0.00	0.00	0.00	0.00	0.00	0.00	0.00	0.00	0.00	0.00	0.00
Total	1.00	1.00	1.00	1.00	1.00	1.00	1.00	1.00	1.00	1.00	1.00
Proportion of End-Members											
Dolomite	1.71	0.94	2.27	1.89	0.99	1.37	0.81	3.38	1.93	3.65	1.61
Calcite	97.20	97.12	97.23	97.44	97.87	95.46	98.06	93.99	96.96	95.54	98.01
Siderite	0.09	0.42	-0.02	0.10	0.15	0.90	0.17	0.85	0.41	-0.01	0.02
Rhodochrosite	0.57	1.07	0.02	0.12	0.75	0.42	0.65	1.68	0.48	0.09	0.05
Strontianite	0.16	0.09	0.21	0.29	0.05	0.21	0.03	0.05	0.07	0.28	0.19
Total	99.72	99.63	99.70	99.84	99.82	98.36	99.72	99.94	99.86	99.56	99.88

Sample	SH08/31/16-15F2	SH08/31/16-15F2	SH08/31/16-15F3	SH08/31/16-15M	SH08/31/16-15M	SH08/31/16-15M	SH08/31/16-16F1	SH08/31/16-16F1	SH08/31/16-16F1	SH08/31/16-16A1	SH08/31/16-16M
Microprobe Data											
CaO	53.20	53.90	53.57	53.56	56.50	52.85	55.87	53.87	53.89	52.96	50.81
MgO	0.51	0.52	0.16	0.43	0.45	0.36	0.38	0.29	0.43	0.09	0.18
FeO	-0.01	0.01	0.05	0.37	0.39	0.27	0.10	0.07	0.12	0.16	0.39
MnO	0.01	0.00	0.55	0.37	0.42	0.30	1.12	0.74	0.62	0.06	0.56
SiO2	-0.01	-0.01	0.03	0.12	0.24	0.16	0.00	-0.02	0.01	0.05	3.16
P2O5	0.23	0.26	0.04	0.05	0.10	0.08	0.06	0.05	0.05	36.43	0.02
SrO	0.39	0.33	0.28	0.06	0.01	0.01	0.03	0.12	0.04	0.03	0.21
Total	54.33	55.01	54.68	54.96	58.10	54.04	57.56	55.13	55.16	89.79	55.34
Metal Cations											
CaO	0.97	0.97	0.98	0.97	0.97	0.97	0.97	0.98	0.98	0.42	0.88
MgO	0.01	0.01	0.00	0.01	0.01	0.01	0.01	0.01	0.01	0.00	0.00
FeO	0.00	0.00	0.00	0.01	0.01	0.00	0.00	0.00	0.00	0.00	0.01
MnO	0.00	0.00	0.01	0.01	0.01	0.00	0.02	0.01	0.01	0.00	0.01
SiO2	0.00	0.00	0.00	0.00	0.01	0.01	0.00	0.00	0.00	0.00	0.10
P2O5	0.01	0.01	0.00	0.00	0.00	0.00	0.00	0.00	0.00	0.57	0.00
SrO	0.00	0.00	0.00	0.00	0.00	0.00	0.00	0.00	0.00	0.00	0.00
Total	1.00	1.00	1.00	1.00	1.00	1.00	1.00	1.00	1.00	1.00	1.00
Proportion of End-Members											
Dolomite	2.63	2.61	0.83	2.16	2.14	1.85	1.85	1.48	2.16	0.20	0.87
Calcite	96.19	96.17	97.77	96.14	95.68	96.44	96.24	97.11	96.53	42.15	87.36
Siderite	-0.01	0.01	0.07	0.53	0.52	0.39	0.14	0.11	0.16	0.10	0.52
Rhodochrosite	0.01	0.01	0.80	0.54	0.57	0.44	1.55	1.06	0.89	0.04	0.77
Strontianite	0.39	0.33	0.27	0.06	0.01	0.01	0.02	0.12	0.04	0.01	0.20
Total	99.20	99.13	99.75	99.42	98.92	99.14	99.80	99.88	99.77	42.51	89.73

Sample	SH08/31/16-16M	SH08/31/16-16M	SH08/31/16-17F1	SH08/31/16-17F1	SH08/31/16-17F1	SH08/31/16-17F2	SH08/31/16-17F2	SH08/31/16-17F2	SH08/31/16-17M	SH08/31/16-17M	SH08/31/16-17M
Microprobe Data											
CaO	52.99	45.22	54.27	53.55	53.93	54.47	53.05	52.84	55.85	53.51	53.59
MgO	0.62	0.65	0.43	0.59	0.60	0.53	0.41	0.52	0.43	0.54	0.46
FeO	0.66	0.63	0.37	0.35	0.30	0.37	0.28	0.36	0.45	0.49	0.33
MnO	1.55	1.19	0.99	0.63	0.44	0.61	0.66	0.63	0.74	1.12	0.82
SiO2	0.08	7.30	0.01	0.02	-0.03	0.05	0.01	0.02	0.01	0.05	0.06
P2O5	0.01	0.01	0.08	0.03	0.04	0.05	0.02	0.02	0.05	0.05	0.01
SrO	0.02	0.07	0.09	0.12	0.18	0.13	0.14	0.15	0.21	0.10	0.15
Total	55.93	55.08	56.25	55.29	55.46	56.20	54.57	54.53	57.73	55.86	55.43
Metal Cations											
CaO	0.95	0.74	0.97	0.97	0.97	0.97	0.97	0.97	0.97	0.96	0.97
MgO	0.02	0.01	0.01	0.01	0.02	0.01	0.01	0.01	0.01	0.01	0.01
FeO	0.01	0.01	0.01	0.00	0.00	0.01	0.00	0.01	0.01	0.01	0.00
MnO	0.02	0.02	0.01	0.01	0.01	0.01	0.01	0.01	0.01	0.02	0.01
SiO2	0.00	0.22	0.00	0.00	0.00	0.00	0.00	0.00	0.00	0.00	0.00
P2O5	0.00	0.00	0.00	0.00	0.00	0.00	0.00	0.00	0.00	0.00	0.00
SrO	0.00	0.00	0.00	0.00	0.00	0.00	0.00	0.00	0.00	0.00	0.00
Total	1.00	1.00	1.00	1.00	1.00	1.00	1.00	1.00	1.00	1.00	1.00
Proportion of End-Members											
Dolomite	3.11	2.96	2.13	2.99	3.03	2.62	2.10	2.65	2.08	2.69	2.32
Calcite	93.47	72.35	95.55	95.34	95.70	95.55	96.28	95.64	95.92	94.58	95.64
Siderite	0.92	0.80	0.52	0.49	0.42	0.52	0.40	0.51	0.61	0.68	0.47
Rhodochrosite	2.19	1.53	1.40	0.90	0.62	0.85	0.95	0.91	1.01	1.59	1.18
Strontianite	0.02	0.06	0.09	0.12	0.18	0.13	0.14	0.15	0.20	0.10	0.15
Total	99.72	77.71	99.68	99.83	99.94	99.67	99.87	99.86	99.81	99.64	99.75

Sample	SH09/01/16-15F1	SH09/01/16-15F1	SH09/01/16-15F1	SH09/01/16-15F1	SH09/01/16-15M	SH09/01/16-15M	SH09/01/16-15M	SH09/01/16-14F1	SH09/01/16-14F1	SH09/01/16-14F1	SH09/01/16-14F1
Microprobe Data											
CaO	53.66	53.76	53.07	53.04	54.26	51.21	54.51	52.93	53.65	52.94	52.67
MgO	0.61	0.59	0.78	0.52	0.46	0.18	0.35	0.38	0.79	0.68	0.42
FeO	0.02	0.01	0.02	0.17	0.38	0.13	0.23	0.02	0.08	0.09	0.08
MnO	0.11	0.15	0.07	0.14	0.70	4.40	1.33	0.35	0.70	0.48	0.57
SiO2	-0.01	-0.02	0.01	0.04	0.06	0.06	0.15	-0.01	0.01	0.03	0.03
P2O5	0.06	0.03	0.03	0.06	0.01	0.05	0.07	0.05	0.07	0.00	0.03
SrO	0.25	0.30	0.28	0.25	0.15	0.00	0.03	0.50	0.42	0.54	0.54
Total	54.70	54.83	54.27	54.23	56.01	56.03	56.67	54.22	55.72	54.76	54.35
Metal Cations											
CaO	0.98	0.98	0.97	0.98	0.97	0.93	0.96	0.98	0.96	0.97	0.97
MgO	0.02	0.02	0.02	0.01	0.01	0.00	0.01	0.01	0.02	0.02	0.01
FeO	0.00	0.00	0.00	0.00	0.01	0.00	0.00	0.00	0.00	0.00	0.00
MnO	0.00	0.00	0.00	0.00	0.01	0.06	0.02	0.01	0.01	0.01	0.01
SiO2	0.00	0.00	0.00	0.00	0.00	0.00	0.01	0.00	0.00	0.00	0.00
P2O5	0.00	0.00	0.00	0.00	0.00	0.00	0.00	0.00	0.00	0.00	0.00
SrO	0.00	0.00	0.00	0.00	0.00	0.00	0.00	0.00	0.00	0.01	0.01
Total	1.00	1.00	1.00	1.00	1.00	1.00	1.00	1.00	1.00	1.00	1.00
Proportion of End-Members											
Dolomite	3.10	3.01	3.97	2.66	2.26	0.89	1.70	1.94	3.95	3.47	2.15
Calcite	96.30	96.42	95.47	96.28	95.84	92.25	95.33	96.87	94.24	95.08	96.14
Siderite	0.02	0.02	0.03	0.24	0.53	0.18	0.31	0.02	0.11	0.13	0.12
Rhodochrosite	0.16	0.22	0.11	0.21	0.99	6.29	1.86	0.51	0.99	0.70	0.83
Strontianite	0.25	0.29	0.28	0.25	0.14	0.00	0.03	0.50	0.41	0.53	0.54
Total	99.83	99.96	99.85	99.64	99.77	99.61	99.24	99.85	99.71	99.91	99.79

Sample	SH09/01/16-14F1	SH09/01/16-14F1	SH09/01/16-14FM	SH09/01/16-14FM	SH09/01/16-14FM	SH09/01/16-13F1	SH09/01/16-13F1	SH09/01/16-13F1	SH09/01/16-13F1	SH09/01/16-13F1	SH09/01/16-13F1
Microprobe Data											
CaO	54.45	52.66	52.71	54.77	52.76	53.43	53.61	54.23	53.65	55.99	54.41
MgO	0.56	0.52	0.42	0.22	0.40	0.47	0.29	0.43	0.51	0.45	0.37
FeO	0.13	0.10	0.41	0.33	0.35	0.09	0.06	0.01	0.02	0.00	-0.02
MnO	0.60	0.31	0.81	1.17	0.70	0.37	0.61	0.06	0.08	0.00	0.04
SiO2	0.03	0.03	0.09	0.07	0.09	0.03	0.00	0.00	-0.02	0.01	0.00
P2O5	0.03	0.05	0.02	0.00	0.06	0.05	0.10	0.01	0.03	0.04	0.05
SrO	0.54	0.57	0.01	0.68	-0.05	0.17	0.10	0.12	0.19	0.07	0.22
Total	56.33	54.26	54.48	57.23	54.32	54.60	54.77	54.86	54.45	56.56	55.07
Metal Cations											
CaO	0.97	0.97	0.97	0.97	0.97	0.98	0.98	0.99	0.98	0.99	0.99
MgO	0.01	0.01	0.01	0.01	0.01	0.01	0.01	0.01	0.01	0.01	0.01
FeO	0.00	0.00	0.01	0.00	0.00	0.00	0.00	0.00	0.00	0.00	0.00
MnO	0.01	0.00	0.01	0.02	0.01	0.01	0.01	0.00	0.00	0.00	0.00
SiO2	0.00	0.00	0.00	0.00	0.00	0.00	0.00	0.00	0.00	0.00	0.00
P2O5	0.00	0.00	0.00	0.00	0.00	0.00	0.00	0.00	0.00	0.00	0.00
SrO	0.01	0.01	0.00	0.01	0.00	0.00	0.00	0.00	0.00	0.00	0.00
Total	1.00	1.00	1.00	1.00	1.00	1.00	1.00	1.00	1.00	1.00	1.00
Proportion of End-Members											
Dolomite	2.75	2.65	2.16	1.09	2.05	2.41	1.46	2.16	2.59	2.19	1.88
Calcite	95.52	95.87	95.67	95.98	95.94	96.50	97.12	97.56	97.06	97.58	97.69
Siderite	0.18	0.15	0.59	0.45	0.50	0.13	0.08	0.02	0.03	-0.01	-0.03
Rhodochrosite	0.84	0.46	1.17	1.62	1.02	0.53	0.88	0.08	0.11	0.00	0.05
Strontianite	0.52	0.57	0.01	0.65	-0.04	0.17	0.10	0.12	0.19	0.07	0.22
Total	99.82	99.69	99.61	99.79	99.47	99.75	99.65	99.94	99.98	99.84	99.81

Sample	SH09/01/16-13F2	SH09/01/16-13F2	SH09/01/16-13F2	SH09/01/16-13M	SH09/01/16-13M	SH09/01/16-13M	SH09/01/16-12F1	SH09/01/16-12F1	SH09/01/16-12F1	SH09/01/16-12F1	SH09/01/16-12F2
Microprobe Data											
CaO	52.85	54.98	53.11	51.80	51.93	54.01	58.11	53.98	55.00	53.84	53.69
MgO	0.54	0.54	0.26	0.37	0.68	0.06	0.64	0.24	0.41	0.27	0.16
FeO	0.08	0.02	0.15	0.30	0.10	0.18	0.04	0.04	0.32	0.04	0.03
MnO	0.48	0.47	0.84	1.04	0.15	1.91	0.25	0.91	0.55	0.97	1.38
SiO2	0.00	0.00	0.03	0.39	0.10	0.20	0.00	-0.02	-0.02	-0.04	0.00
P2O5	-0.01	0.07	0.06	0.02	0.05	0.04	0.11	0.08	0.08	0.05	0.05
SrO	0.17	0.19	0.14	0.13	0.16	-0.03	0.30	0.16	0.08	0.14	0.06
Total	54.11	56.27	54.59	54.04	53.17	56.37	59.44	55.40	56.42	55.27	55.36
Metal Cations											
CaO	0.98	0.98	0.97	0.96	0.97	0.96	0.97	0.98	0.97	0.98	0.97
MgO	0.01	0.01	0.01	0.01	0.02	0.00	0.01	0.01	0.01	0.01	0.00
FeO	0.00	0.00	0.00	0.00	0.00	0.00	0.00	0.00	0.00	0.00	0.00
MnO	0.01	0.01	0.01	0.02	0.00	0.03	0.00	0.01	0.01	0.01	0.02
SiO2	0.00	0.00	0.00	0.01	0.00	0.01	0.00	0.00	0.00	0.00	0.00
P2O5	0.00	0.00	0.00	0.00	0.00	0.00	0.00	0.00	0.00	0.00	0.00
SrO	0.00	0.00	0.00	0.00	0.00	0.00	0.00	0.00	0.00	0.00	0.00
Total	1.00	1.00	1.00	1.00	1.00	1.00	1.00	1.00	1.00	1.00	1.00
Proportion of End-Members											
Dolomite	2.77	2.65	1.35	1.88	3.54	0.28	2.99	1.21	2.01	1.36	0.79
Calcite	96.28	96.22	96.77	94.62	95.41	96.01	96.00	97.03	96.47	96.99	96.97
Siderite	0.12	0.03	0.22	0.43	0.14	0.25	0.05	0.06	0.44	0.05	0.04
Rhodochrosite	0.70	0.67	1.22	1.51	0.22	2.69	0.33	1.30	0.78	1.39	1.97
Strontianite	0.17	0.18	0.14	0.13	0.17	-0.03	0.27	0.15	0.08	0.14	0.06
Total	100.04	99.75	99.69	98.57	99.47	99.20	99.65	99.76	99.77	99.94	99.83

Sample	SH09/01/16-12F2	SH09/01/16-12F2	SH09/01/16-12F2	SH09/01/16-12M	SH09/01/16-12M	SH09/01/16-12M	SH09/01/16-11M	SH09/01/16-11M	SH09/01/16-11M	SH09/01/16-10F1	SH09/01/16-10F1
Microprobe Data											
CaO	56.08	53.36	54.71	53.54	53.86	54.63	54.40	0.00	54.79	53.17	53.23
MgO	0.49	0.49	0.60	0.16	0.27	0.17	0.12	2.44	0.13	0.58	0.45
FeO	-0.03	0.03	0.03	0.10	0.15	0.00	0.24	3.02	0.32	0.01	0.04
MnO	0.75	0.68	0.13	1.32	0.89	-0.02	0.46	0.01	0.89	0.99	0.71
SiO2	-0.01	0.00	-0.01	0.01	0.04	-0.01	0.70	42.88	0.13	-0.01	0.00
P2O5	0.05	0.03	0.04	0.02	0.04	0.01	0.06	0.03	0.02	0.02	0.05
SrO	0.15	0.19	0.26	0.10	0.40	-0.03	0.11	0.04	0.24	0.28	0.17
Total	57.49	54.79	55.76	55.25	55.65	54.76	56.10	48.42	56.53	55.04	54.64
Metal Cations											
CaO	0.98	0.97	0.98	0.97	0.97	1.00	0.96	0.00	0.97	0.97	0.97
MgO	0.01	0.01	0.01	0.00	0.01	0.00	0.00	0.04	0.00	0.01	0.01
FeO	0.00	0.00	0.00	0.00	0.00	0.00	0.00	0.03	0.00	0.00	0.00
MnO	0.01	0.01	0.00	0.02	0.01	0.00	0.01	0.00	0.01	0.01	0.01
SiO2	0.00	0.00	0.00	0.00	0.00	0.00	0.02	0.93	0.00	0.00	0.00
P2O5	0.00	0.00	0.00	0.00	0.00	0.00	0.00	0.00	0.00	0.00	0.00
SrO	0.00	0.00	0.00	0.00	0.00	0.00	0.00	0.00	0.00	0.00	0.00
Total	1.00	1.00	1.00	1.00	1.00	1.00	1.00	1.00	1.00	1.00	1.00
Proportion of End-Members											
Dolomite	2.37	2.48	2.96	0.81	1.36	0.88	0.61	7.91	0.66	2.95	2.27
Calcite	96.35	96.19	96.43	96.95	96.48	99.15	95.78	-3.95	96.91	95.30	96.31
Siderite	-0.04	0.05	0.05	0.14	0.21	0.00	0.33	2.75	0.45	0.01	0.06
Rhodochrosite	1.04	0.99	0.19	1.90	1.27	-0.03	0.64	0.01	1.25	1.42	1.02
Strontianite	0.15	0.19	0.25	0.10	0.39	-0.03	0.10	0.02	0.23	0.28	0.17
Total	99.86	99.90	99.87	99.89	99.71	99.98	97.47	6.74	99.50	99.96	99.82

Sample	SH09/01/16-10F1	SH09/01/16-10F2	SH09/01/16-10F2	SH09/01/16-10F2	SH09/01/16-10M	SH09/01/16-10M	SH09/01/16-10M	SH09/01/16-10M	SH09/01/16-10M	SH09/01/16-09F1	SH09/01/16-09F1
Microprobe Data											
CaO	53.50	53.64	55.62	53.98	53.07	50.82	50.91	52.82	54.00	52.01	53.46
MgO	0.74	0.49	0.67	0.69	0.32	0.21	0.91	0.19	0.01	0.57	0.41
FeO	0.02	0.01	0.09	0.05	0.16	0.24	0.80	0.71	0.11	0.50	0.41
MnO	0.20	0.28	0.27	0.27	0.81	0.59	2.72	0.15	0.07	1.80	1.79
SiO2	0.02	0.00	0.00	0.01	0.12	3.40	1.25	0.13	0.01	0.01	0.03
P2O5	0.05	0.02	0.01	0.03	0.09	0.07	0.03	36.39	37.83	0.02	0.05
SrO	0.28	0.26	0.30	0.25	0.19	0.08	0.01	-0.04	-0.10	0.08	0.02
Total	54.81	54.70	56.97	55.26	54.76	55.41	56.62	90.34	91.93	54.99	56.17
Metal Cations											
CaO	0.97	0.98	0.98	0.97	0.97	0.87	0.89	0.42	0.42	0.95	0.96
MgO	0.02	0.01	0.02	0.02	0.01	0.01	0.02	0.00	0.00	0.01	0.01
FeO	0.00	0.00	0.00	0.00	0.00	0.00	0.01	0.00	0.00	0.01	0.01
MnO	0.00	0.00	0.00	0.00	0.01	0.01	0.04	0.00	0.00	0.03	0.03
SiO2	0.00	0.00	0.00	0.00	0.00	0.11	0.04	0.00	0.00	0.00	0.00
P2O5	0.00	0.00	0.00	0.00	0.00	0.00	0.00	0.57	0.58	0.00	0.00
SrO	0.00	0.00	0.00	0.00	0.00	0.00	0.00	0.00	0.00	0.00	0.00
Total	1.00	1.00	1.00	1.00	1.00	1.00	1.00	1.00	1.00	1.00	1.00
Proportion of End-Members											
Dolomite	3.77	2.51	3.27	3.47	1.60	1.00	4.43	0.41	0.03	2.92	2.04
Calcite	95.38	96.76	95.90	95.72	96.08	86.66	86.56	41.76	41.89	93.60	94.57
Siderite	0.02	0.01	0.13	0.07	0.23	0.32	1.08	0.44	0.07	0.71	0.57
Rhodochrosite	0.29	0.41	0.38	0.38	1.17	0.80	3.75	0.09	0.04	2.60	2.53
Strontianite	0.28	0.26	0.29	0.24	0.18	0.08	0.01	-0.02	-0.04	0.08	0.02
Total	99.74	99.95	99.96	99.88	99.27	88.86	95.83	42.69	41.98	99.90	99.72

Sample	SH09/01/16-09F1	SH09/01/16-09F2	SH09/01/16-09F2	SH09/01/16-09F2	SH09/01/16-09M	SH09/01/16-09M	SH09/01/16-09M	SH09/01/16-08F1	SH09/01/16-08F1	SH09/01/16-08F1	SH09/01/16-08F1
Microprobe Data											
CaO	53.14	55.46	53.57	53.22	48.63	54.31	53.46	53.85	54.79	54.49	55.94
MgO	0.72	0.81	0.58	0.41	1.08	0.50	0.39	0.54	0.66	0.32	0.39
FeO	0.57	0.04	0.08	0.10	0.72	0.40	0.20	0.02	-0.02	0.00	0.01
MnO	2.22	0.03	0.17	0.88	0.57	0.67	0.98	0.05	0.01	0.02	0.01
SiO2	0.03	0.03	-0.04	0.02	1.88	0.25	0.13	0.01	0.00	-0.02	0.00
P2O5	0.06	0.03	0.08	0.06	0.01	0.06	0.06	0.06	-0.01	-0.01	0.05
SrO	-0.02	0.27	0.26	0.15	0.05	0.08	0.37	0.21	0.27	0.21	0.31
Total	56.71	56.67	54.71	54.84	52.93	56.28	55.58	54.75	55.70	55.02	56.69
Metal Cations											
CaO	0.94	0.97	0.98	0.97	0.89	0.96	0.96	0.98	0.98	0.99	0.99
MgO	0.02	0.02	0.01	0.01	0.03	0.01	0.01	0.01	0.02	0.01	0.01
FeO	0.01	0.00	0.00	0.00	0.01	0.01	0.00	0.00	0.00	0.00	0.00
MnO	0.03	0.00	0.00	0.01	0.01	0.01	0.01	0.00	0.00	0.00	0.00
SiO2	0.00	0.00	0.00	0.00	0.06	0.01	0.00	0.00	0.00	0.00	0.00
P2O5	0.00	0.00	0.00	0.00	0.00	0.00	0.00	0.00	0.00	0.00	0.00
SrO	0.00	0.00	0.00	0.00	0.00	0.00	0.00	0.00	0.00	0.00	0.00
Total	1.00	1.00	1.00	1.00	1.00	1.00	1.00	1.00	1.00	1.00	1.00
Proportion of End-Members											
Dolomite	3.53	3.98	2.96	2.07	5.49	2.48	1.94	2.74	3.29	1.63	1.90
Calcite	92.30	95.47	96.26	96.08	86.17	94.90	95.38	96.70	96.50	98.23	97.62
Siderite	0.79	0.05	0.11	0.14	1.03	0.55	0.27	0.03	-0.03	0.01	0.01
Rhodochrosite	3.10	0.04	0.25	1.27	0.82	0.94	1.40	0.08	0.01	0.03	0.01
Strontianite	-0.02	0.26	0.26	0.15	0.05	0.08	0.36	0.21	0.26	0.21	0.29
Total	99.70	99.80	99.84	99.71	93.56	98.96	99.35	99.76	100.03	100.10	99.83

Sample	SH09/01/16-08F1	SH09/01/16-08F1	SH09/01/16-08F1	SH09/01/16-08F1	SH09/01/16-08F1	SH09/01/16-08A	SH09/01/16-08A	SH09/01/16-08A	SH09/01/16-08M	SH09/01/16-08M	SH09/01/16-08M
Microprobe Data											
CaO	54.93	53.81	54.33	54.48	53.77	53.15	52.55	52.99	56.29	52.49	54.27
MgO	0.43	0.42	0.20	0.24	0.42	0.15	0.37	0.13	0.17	0.34	0.09
FeO	0.01	-0.02	0.00	0.02	-0.01	0.22	0.66	0.11	0.18	0.30	0.22
MnO	0.04	0.07	0.05	0.03	0.02	0.12	0.08	0.11	1.11	0.89	1.73
SiO2	0.02	-0.03	-0.02	0.00	0.02	0.07	0.71	0.00	0.06	0.03	0.38
P2O5	0.05	0.08	0.02	0.00	0.02	34.03	35.28	33.80	0.06	0.00	0.02
SrO	0.19	0.26	0.33	0.21	0.20	-0.04	-0.05	-0.06	0.01	0.02	0.19
Total	55.67	54.60	54.90	54.98	54.43	87.70	89.61	87.08	57.88	54.06	56.90
Metal Cations											
CaO	0.98	0.98	0.99	0.99	0.99	0.44	0.42	0.44	0.97	0.97	0.96
MgO	0.01	0.01	0.01	0.01	0.01	0.00	0.00	0.00	0.00	0.01	0.00
FeO	0.00	0.00	0.00	0.00	0.00	0.00	0.00	0.00	0.00	0.00	0.00
MnO	0.00	0.00	0.00	0.00	0.00	0.00	0.00	0.00	0.02	0.01	0.02
SiO2	0.00	0.00	0.00	0.00	0.00	0.00	0.01	0.00	0.00	0.00	0.01
P2O5	0.00	0.00	0.00	0.00	0.00	0.56	0.56	0.56	0.00	0.00	0.00
SrO	0.00	0.00	0.00	0.00	0.00	0.00	0.00	0.00	0.00	0.00	0.00
Total	1.00	1.00	1.00	1.00	1.00	1.00	1.00	1.00	1.00	1.00	1.00
Proportion of End-Members											
Dolomite	2.16	2.14	1.03	1.24	2.12	0.35	0.83	0.29	0.81	1.74	0.42
Calcite	97.34	97.32	98.58	98.50	97.54	43.76	41.74	43.98	97.01	96.42	95.34
Siderite	0.02	-0.03	-0.01	0.03	-0.01	0.14	0.41	0.07	0.24	0.43	0.30
Rhodochrosite	0.05	0.10	0.07	0.05	0.02	0.08	0.05	0.07	1.52	1.30	2.41
Strontianite	0.18	0.26	0.33	0.20	0.20	-0.02	-0.02	-0.03	0.01	0.02	0.18
Total	99.75	99.79	100.01	100.02	99.87	44.31	43.01	44.39	99.60	99.91	98.66

Sample	SH09/01/16-07F1	SH09/01/16-07F1	SH09/01/16-07F1	SH09/01/16-07M	SH09/01/16-07M	SH09/01/16-07M	SH09/01/16-06F1	SH09/01/16-06F1	SH09/01/16-06F1	SH09/01/16-06F1	SH09/01/16-06F1
Microprobe Data											
CaO	54.89	53.71	55.57	50.09	52.92	54.24	54.21	54.94	53.59	56.01	50.86
MgO	0.13	0.23	0.17	0.05	0.20	0.51	0.05	0.18	0.17	0.35	0.31
FeO	0.32	0.50	0.04	0.05	0.21	0.04	0.22	0.17	0.30	0.22	0.59
MnO	1.29	0.32	0.22	0.44	1.23	0.40	1.02	2.05	3.42	1.80	4.02
SiO2	0.03	0.04	0.00	3.79	0.39	0.11	0.64	0.03	0.03	-0.01	1.24
P2O5	0.01	0.06	0.05	0.04	0.07	0.08	0.04	0.05	0.04	0.05	0.06
SrO	0.43	0.21	0.22	0.08	0.04	0.20	0.12	0.05	0.13	0.18	0.03
Total	57.11	55.07	56.27	54.54	55.07	55.58	56.29	57.47	57.68	58.61	57.11
Metal Cations											
CaO	0.97	0.98	0.99	0.87	0.96	0.97	0.96	0.96	0.94	0.96	0.89
MgO	0.00	0.01	0.00	0.00	0.00	0.01	0.00	0.00	0.00	0.01	0.01
FeO	0.00	0.01	0.00	0.00	0.00	0.00	0.00	0.00	0.00	0.00	0.01
MnO	0.02	0.00	0.00	0.01	0.02	0.01	0.01	0.03	0.05	0.02	0.06
SiO2	0.00	0.00	0.00	0.12	0.01	0.00	0.02	0.00	0.00	0.00	0.04
P2O5	0.00	0.00	0.00	0.00	0.00	0.00	0.00	0.00	0.00	0.00	0.00
SrO	0.00	0.00	0.00	0.00	0.00	0.00	0.00	0.00	0.00	0.00	0.00
Total	1.00	1.00	1.00	1.00	1.00	1.00	1.00	1.00	1.00	1.00	1.00
Proportion of End-Members											
Dolomite	0.65	1.14	0.82	0.26	1.00	2.55	0.22	0.85	0.83	1.68	1.52
Calcite	96.53	97.10	98.42	86.61	95.33	95.99	95.70	95.75	93.67	95.26	87.88
Siderite	0.44	0.71	0.06	0.06	0.30	0.06	0.31	0.24	0.42	0.30	0.80
Rhodochrosite	1.80	0.46	0.31	0.60	1.76	0.57	1.43	2.84	4.74	2.44	5.54
Strontianite	0.41	0.20	0.22	0.07	0.04	0.20	0.11	0.05	0.12	0.17	0.03
Total	99.84	99.61	99.83	87.61	98.42	99.37	97.77	99.73	99.79	99.85	95.77

Sample	SH09/01/16-06M	SH09/01/16-06M	SH09/01/16-06M	SH09/01/16-06A	SH09/01/16-06A	SH09/01/16-06A	SH09/01/16-05M	SH09/01/16-05M	SH09/01/16-05M	SH09/01/16-05M	SH09/01/16-02F1
Microprobe Data											
CaO	54.60	53.87	53.74	26.49	54.18	53.99	55.54	54.45	55.38	51.45	53.63
MgO	0.25	0.37	0.26	6.01	0.06	0.05	0.05	0.18	0.20	0.05	1.20
FeO	0.34	0.54	0.40	15.95	0.16	0.08	0.13	0.31	0.35	0.18	2.36
MnO	3.00	2.49	3.55	0.31	0.21	0.12	0.80	1.81	2.21	1.05	3.96
SiO2	0.03	0.06	-0.01	11.87	0.00	0.05	0.08	0.09	0.06	2.41	-0.01
P2O5	-0.01	0.05	0.08	19.10	36.56	36.51	0.02	0.05	0.04	0.02	0.15
SrO	0.10	0.21	0.06	-0.21	-0.19	-0.16	0.04	0.07	0.15	0.15	0.03
Total	58.30	57.58	58.08	79.52	90.98	90.65	56.66	56.96	58.39	55.32	61.32
Metal Cations											
CaO	0.95	0.94	0.94	0.25	0.43	0.43	0.98	0.96	0.96	0.90	0.89
MgO	0.01	0.01	0.01	0.08	0.00	0.00	0.00	0.00	0.00	0.00	0.03
FeO	0.00	0.01	0.01	0.12	0.00	0.00	0.00	0.00	0.00	0.00	0.03
MnO	0.04	0.03	0.05	0.00	0.00	0.00	0.01	0.03	0.03	0.01	0.05
SiO2	0.00	0.00	0.00	0.21	0.00	0.00	0.00	0.00	0.00	0.08	0.00
P2O5	0.00	0.00	0.00	0.35	0.57	0.57	0.00	0.00	0.00	0.00	0.00
SrO	0.00	0.00	0.00	0.00	0.00	0.00	0.00	0.00	0.00	0.00	0.00
Total	1.00	1.00	1.00	1.00	1.00	1.00	1.00	1.00	1.00	1.00	1.00
Proportion of End-Members											
Dolomite	1.22	1.82	1.28	15.58	0.13	0.11	0.24	0.90	0.98	0.26	5.52
Calcite	94.06	93.45	93.00	16.89	42.71	42.67	98.09	95.61	95.06	89.93	85.79
Siderite	0.46	0.74	0.54	11.60	0.10	0.05	0.18	0.43	0.47	0.25	3.04
Rhodochrosite	4.11	3.44	4.89	0.23	0.13	0.08	1.12	2.52	3.01	1.46	5.17
Strontianite	0.09	0.20	0.05	-0.11	-0.08	-0.07	0.04	0.06	0.14	0.15	0.03
Total	99.93	99.65	99.76	44.19	42.99	42.84	99.66	99.52	99.67	92.04	99.54

Sample	SH09/01/16-02F1	SH09/01/16-02F1	SH09/01/16-02F1	SH09/01/16-02F1	SH09/01/16-02M	SH09/01/16-02M	SH09/01/16-02M	SH09/01/16-04F1	SH09/01/16-04F1	SH09/01/16-04F1	SH09/01/16-04F1
Microprobe Data											
CaO	53.62	53.66	53.31	52.05	56.06	51.00	53.02	52.64	55.09	55.84	52.89
MgO	1.05	1.13	1.41	1.04	0.10	0.15	0.29	0.37	0.75	0.25	0.26
FeO	1.71	1.54	2.30	1.73	0.15	0.45	0.35	0.70	1.23	0.33	0.29
MnO	2.92	2.70	3.82	3.03	1.26	0.99	2.65	0.50	0.57	1.11	1.06
SiO2	-0.01	0.04	0.01	-0.05	0.00	1.45	0.12	3.34	-0.01	0.04	0.00
P2O5	0.14	0.11	0.14	0.08	0.07	0.08	0.11	0.11	0.10	0.03	0.09
SrO	0.11	0.16	0.04	0.05	0.07	0.18	0.03	0.05	0.08	0.06	-0.01
Total	59.54	59.34	61.03	57.94	57.71	54.30	56.56	57.69	57.80	57.66	54.59
Metal Cations											
CaO	0.91	0.91	0.88	0.91	0.98	0.92	0.94	0.87	0.95	0.97	0.97
MgO	0.02	0.03	0.03	0.03	0.00	0.00	0.01	0.01	0.02	0.01	0.01
FeO	0.02	0.02	0.03	0.02	0.00	0.01	0.00	0.01	0.02	0.00	0.00
MnO	0.04	0.04	0.05	0.04	0.02	0.01	0.04	0.01	0.01	0.02	0.02
SiO2	0.00	0.00	0.00	0.00	0.00	0.05	0.00	0.10	0.00	0.00	0.00
P2O5	0.00	0.00	0.00	0.00	0.00	0.00	0.00	0.00	0.00	0.00	0.00
SrO	0.00	0.00	0.00	0.00	0.00	0.00	0.00	0.00	0.00	0.00	0.00
Total	1.00	1.00	1.00	1.00	1.00	1.00	1.00	1.00	1.00	1.00	1.00
Proportion of End-Members											
Dolomite	4.93	5.32	6.49	5.03	0.47	0.75	1.43	1.68	3.59	1.22	1.33
Calcite	88.36	88.38	85.02	88.27	97.29	91.83	93.57	86.08	93.59	96.52	96.38
Siderite	2.26	2.04	2.98	2.36	0.20	0.64	0.49	0.90	1.66	0.45	0.42
Rhodochrosite	3.91	3.62	5.01	4.18	1.73	1.41	3.72	0.65	0.78	1.53	1.53
Strontianite	0.10	0.15	0.04	0.05	0.06	0.18	0.02	0.04	0.08	0.05	-0.01
Total	99.57	99.51	99.52	99.89	99.76	94.82	99.23	89.36	99.71	99.77	99.65

Sample	SH09/01/16-04F1	SH09/01/16-04M	SH09/01/16-04M	SH09/01/16-04M	SH09/01/16-03F1	SH09/01/16-03F1	SH09/01/16-03F1	SH09/01/16-03M	SH09/01/16-03M	SH09/02/16-09F1	SH09/02/16-09F1
Microprobe Data											
CaO	51.99	54.32	53.23	53.02	52.27	56.15	54.20	52.67	53.32	52.15	54.13
MgO	0.54	0.73	0.53	0.31	0.55	0.77	0.21	0.45	0.31	0.65	0.56
FeO	0.97	0.70	0.54	0.37	0.20	0.03	0.06	1.19	0.41	1.14	1.16
MnO	0.71	1.59	2.15	1.23	0.94	0.06	1.46	1.81	1.72	1.60	1.84
SiO2	0.98	0.07	0.04	0.07	0.69	0.02	0.02	0.07	-0.01	-0.01	0.00
P2O5	0.09	0.00	0.01	0.05	0.04	0.10	0.03	0.08	0.03	0.09	0.16
SrO	0.03	0.00	-0.03	0.03	0.17	0.27	0.08	0.04	-0.01	0.00	0.06
Total	55.31	57.42	56.48	55.09	54.85	57.40	56.04	56.31	55.78	55.62	57.92
Metal Cations											
CaO	0.93	0.95	0.95	0.96	0.94	0.97	0.97	0.94	0.96	0.94	0.94
MgO	0.01	0.02	0.01	0.01	0.01	0.02	0.01	0.01	0.01	0.02	0.01
FeO	0.01	0.01	0.01	0.01	0.00	0.00	0.00	0.02	0.01	0.02	0.02
MnO	0.01	0.02	0.03	0.02	0.01	0.00	0.02	0.03	0.02	0.02	0.03
SiO2	0.03	0.00	0.00	0.00	0.02	0.00	0.00	0.00	0.00	0.00	0.00
P2O5	0.00	0.00	0.00	0.00	0.00	0.00	0.00	0.00	0.00	0.00	0.01
SrO	0.00	0.00	0.00	0.00	0.00	0.00	0.00	0.00	0.00	0.00	0.00
Total	1.00	1.00	1.00	1.00	1.00	1.00	1.00	1.00	1.00	1.00	1.00
Proportion of End-Members											
Dolomite	2.66	3.54	2.62	1.57	2.79	3.72	1.03	2.26	1.56	3.27	2.71
Calcite	91.39	93.08	93.43	95.68	92.98	95.47	96.59	92.98	95.33	92.55	92.57
Siderite	1.35	0.96	0.75	0.53	0.28	0.04	0.08	1.66	0.58	1.61	1.57
Rhodochrosite	1.00	2.20	3.03	1.77	1.34	0.08	2.06	2.55	2.46	2.28	2.52
Strontianite	0.02	0.00	-0.03	0.03	0.16	0.25	0.08	0.04	-0.01	0.00	0.06
Total	96.43	99.78	99.81	99.58	97.55	99.56	99.84	99.50	99.91	99.71	99.43

Sample	SH09/02/16-09F1	SH09/02/16-09F1	SH09/02/16-09F1	SH09/02/16-09F1	SH09/02/16-09M	SH09/02/16-09M	SH09/02/16-09M	SH09/01/16-01F1	SH09/01/16-01F1	SH09/01/16-01F1	SH09/01/16-01F1
Microprobe Data											
CaO	52.20	53.39	54.85	53.77	53.33	54.37	52.18	52.62	51.61	54.53	52.69
MgO	0.72	0.59	0.44	0.89	0.34	0.06	0.37	0.19	0.63	0.51	0.43
FeO	1.11	0.82	0.86	1.66	0.47	0.12	0.50	0.60	0.79	0.62	0.48
MnO	2.24	1.82	1.26	2.14	1.40	1.06	2.75	1.57	1.52	1.65	1.35
SiO2	0.00	0.02	-0.01	0.02	0.04	0.14	0.06	0.03	0.00	-0.01	0.00
P2O5	0.02	0.02	-0.01	0.12	0.08	0.04	0.04	0.01	0.03	0.08	0.08
SrO	0.02	0.03	0.06	0.05	0.05	0.04	-0.02	0.19	0.00	0.05	0.02
Total	56.31	56.70	57.45	58.65	55.72	55.83	55.88	55.21	54.58	57.42	55.06
Metal Cations											
CaO	0.93	0.95	0.96	0.92	0.96	0.98	0.94	0.96	0.95	0.95	0.96
MgO	0.02	0.01	0.01	0.02	0.01	0.00	0.01	0.00	0.02	0.01	0.01
FeO	0.02	0.01	0.01	0.02	0.01	0.00	0.01	0.01	0.01	0.01	0.01
MnO	0.03	0.03	0.02	0.03	0.02	0.01	0.04	0.02	0.02	0.02	0.02
SiO2	0.00	0.00	0.00	0.00	0.00	0.00	0.00	0.00	0.00	0.00	0.00
P2O5	0.00	0.00	0.00	0.00	0.00	0.00	0.00	0.00	0.00	0.00	0.00
SrO	0.00	0.00	0.00	0.00	0.00	0.00	0.00	0.00	0.00	0.00	0.00
Total	1.00	1.00	1.00	1.00	1.00	1.00	1.00	1.00	1.00	1.00	1.00
Proportion of End-Members											
Dolomite	3.59	2.93	2.16	4.26	1.70	0.32	1.84	0.94	3.23	2.50	2.18
Calcite	91.62	93.21	94.94	90.11	95.16	97.38	93.20	95.62	93.30	94.09	94.87
Siderite	1.55	1.14	1.17	2.22	0.66	0.16	0.71	0.86	1.13	0.84	0.69
Rhodochrosite	3.17	2.56	1.75	2.91	1.99	1.50	3.92	2.26	2.21	2.27	1.94
Strontianite	0.02	0.03	0.05	0.05	0.05	0.04	-0.02	0.19	0.00	0.04	0.02
Total	99.94	99.86	100.07	99.54	99.57	99.39	99.65	99.87	99.88	99.75	99.69

Sample	SH09/01/16-01F1	SH09/01/16-01M	SH09/01/16-01M	SH09/01/16-01M	SH09/01/16-01M
Microprobe Data					
CaO	53.78	50.32	51.96	52.59	53.65
MgO	0.06	0.59	0.08	0.50	0.63
FeO	0.13	0.82	0.17	0.56	0.69
MnO	1.39	1.53	1.15	1.94	2.43
SiO2	0.03	1.19	1.55	0.04	0.11
P2O5	0.00	0.01	0.04	0.11	0.11
SrO	0.10	-0.04	0.08	0.01	-0.01
Total	55.49	54.42	55.03	55.75	57.61
Metal Cations					
CaO	0.97	0.91	0.93	0.95	0.93
MgO	0.00	0.01	0.00	0.01	0.02
FeO	0.00	0.01	0.00	0.01	0.01
MnO	0.02	0.02	0.02	0.03	0.03
SiO2	0.00	0.04	0.05	0.00	0.00
P2O5	0.00	0.00	0.00	0.00	0.00
SrO	0.00	0.00	0.00	0.00	0.00
Total	1.00	1.00	1.00	1.00	1.00
Proportion of End-Members					
Dolomite	0.30	2.97	0.37	2.52	3.03
Calcite	97.32	89.68	92.40	93.41	91.94
Siderite	0.18	1.17	0.24	0.79	0.93
Rhodochrosite	1.99	2.19	1.62	2.76	3.34
Strontianite	0.10	-0.03	0.08	0.01	-0.01
Total	99.89	95.96	94.72	99.50	99.24